

Fermion mass hierarchies from vector-like families with an extended 2HDM and a possible explanation for the electron and muon anomalous magnetic moments

A. E. Cárcamo Hernández,^{1,*} S. F. King,^{2,†} and H. Lee^{2,‡}

¹*Departamento de Física, Universidad Técnica Federico Santa María,
Casilla 110-V, Valparaíso, Chile*

²*School of Physics and Astronomy, University of Southampton,
SO17 1BJ Southampton, United Kingdom*

(Dated: May 14, 2022)

We study an extended 2 Higgs doublet model (2HDM) in which the Standard Model (SM) Yukawa interactions are forbidden due to a global $U(1)'$ symmetry, but may arise via mixing with vector-like families. In this model, the hierarchical structure of Yukawa couplings of quarks and leptons in the SM arises from the heavy masses of the fourth and fifth vector-like families. Within this model, we consider various non-standard contributions to the electron and muon anomalous magnetic moments. We first consider the W exchange at one-loop level, consistent with the $\mu \rightarrow e\gamma$ constraint, and show that it yields a negligible contribution to both electron and muon anomalous magnetic moments. We then consider Higgs scalar exchange, together with vector-like leptons, at one-loop level and show that it is possible to have non-standard contributions to the electron and muon anomalous magnetic moments within the 1σ constraint of certain experiments. We present some benchmark points for both the muon and the electron anomalies, together with some numerical scans around these points, which indicate the mass regions of the Higgs scalars of the 2HDM in this scenario.

I. INTRODUCTION

The Standard Model (SM) has made many successful predictions for the phenomenology of both quark and lepton sectors with very high accuracy. However there are long-established anomalies which are not addressed by the SM such as muon and electron anomalous magnetic moments $a_\mu = (g-2)_\mu$, $a_e = (g-2)_e$. The muon anomalous magnetic moment reported by the Brookhaven E821 experiment at BNL[1] and the electron anomaly have confirmed $+3.5\sigma$ and -2.5σ deviations from the SM, respectively. The experimentally observed values for the muon and electron anomalies at 1σ of experimental error bars, respectively, read ¹:

$$\begin{aligned}\Delta a_\mu &= a_\mu^{\text{Exp}} - a_\mu^{\text{SM}} = (26.1 \pm 8.0) \times 10^{-10} \\ \Delta a_e &= a_e^{\text{Exp}} - a_e^{\text{SM}} = (-0.88 \pm 0.36) \times 10^{-12}.\end{aligned}\tag{1}$$

When trying to explain both anomalies to within 1σ , a main difficulty arises from the sign of each anomaly: the muon anomaly requires positive definite non-standard contributions, whereas the electron anomaly requires such contributions to contribute with a negative sign [3]. Without loss of generality, the Feynman diagrams corresponding to the contributions for the muon and electron anomalies take the same internal structure at one-loop except from the fact that the external particles are different. The similar structure of the one-loop level contributions to the muon and electron anomalous magnetic moments might be able to be explained by the same new physics, but accounting for the relative negative sign is challenging. For example, considering the one-loop exchange of W or Z' gauge bosons results in theoretical predictions for the muon and electron anomalies having the same sign.

In this paper we take the view that both anomalies should be explained to 1σ using the same internal structure at the one-loop level by some new physics which is capable of accounting for the correct signs of the anomalies. To

*Electronic address: antonio.carcamo@usm.cl

†Electronic address: king@soton.ac.uk

‡Electronic address: hl2n18@soton.ac.uk

¹ It is worth mentioning that the experimental value of the anomalous magnetic moment of the electron is sensitive to the measurement of the fine-structure constant α . The experimental value of $\Delta a_e = a_{e,\text{exp}} - a_e(\alpha_{\text{Berkeley}})$ used in this work and given in Equation 1 is obtained using α_{Berkeley} from caesium recoil measurements by the Berkeley 2018 experiment [2]. As this paper was being completed a different experiment [3] reported a result that implies $\Delta a_e = a_e^{\text{Exp}} - a_e^{\text{SM}} = (0.48 \pm 0.30) \times 10^{-12}$ which differs from the SM by $+1.6\sigma$. The two experiments appear to be inconsistent with each other, and our results here are based on the earlier result in Equation 1.

explain the muon and electron anomalies, we focus on a well motivated model which is also capable of accounting for origin of Yukawa couplings and hierarchies in the SM. The model we consider will account for the Yukawa coupling constant for the top quark being nearly 1 while that for the electron is around 10^{-6} , as well as all the other fermion hierarchies in between, as well as the neutrino masses and mixing. In order to achieve this we shall introduce vector-like particles, which are charged under a global $U(1)'$ symmetry. In a related previous work [4], with a gauged $U(1)'$ symmetry, the first family of quarks and leptons remained massless when only one vector-like family is included. Here we shall modify the model to include two vector-like families charged under a global $U(1)'$ to allow also the first family to be massive and avoid Z' constraints. Then we shall apply the resulting model to the problem of muon and electron anomalous magnetic moments. The considered model is based on a 2 Higgs doublet model (2HDM) extension of the SM, supplemented by a global $U(1)'$ symmetry, where the particle spectrum is enlarged by the inclusion of two vector-like fermion families, as well as one singlet Higgs to break the $U(1)'$ symmetry. The SM Yukawa interactions are forbidden, but the Yukawa interactions with vector-like families charged under the $U(1)'$ symmetry are allowed. Once the flavon develops a vev and the heavy vector-like fermions are integrated out, the effective SM Yukawa interactions are generated, as indicated in Figure 1. Furthermore, this model also highlights the shape of the 2HDM model type II, since in our proposed model, one Higgs doublet (which in the alignment limit corresponds to the SM Higgs doublet) couples with the up type quarks whereas the other one features Yukawa interactions with down type quarks and SM charged leptons. Regarding the neutrino sector, since we consider the SM neutrinos as Majorana particles, we have that this sector requires another approach relying on the inclusion of a new five dimensional Weinberg-like operator, which is allowed in this model and which requires both SM Higgs doublets to be present, namely the so called Type Ib seesaw model [5].

We shall show that the heavy vector-like leptons are useful and necessary to explain the anomalous electron and muon magnetic moment deviations from the SM, of magnitude and opposite signs given in Equation 1. A study of such $g - 2$ anomalies in terms of New Physics and a possible UV complete explanation via vector-like leptons was performed in [6], although the model presented here is quite different, since our model is motivated by the requirement of accounting also for the fermion mass hierarchies. Other theories with extended symmetries and particle spectrum have also been proposed to find an explanation for the muon and electron anomalous magnetic moments [6–48]. In the following we provide a brief comparison of our model to other works, starting with the model proposed in [41] where vector-like leptons are also present. The model of [41] corresponds to an extended type X lepton specific 2HDM model of [41] having a Z_2 discrete symmetry under which one of the scalar doublets and the leptonic fields are charged. In such model the vector-like leptons induces a one-loop level contribution to the electron anomalous magnetic moment whereas the muon anomalous magnetic moment is generated at two-loop via the exchange of a light pseudoscalar. On the other hand, in our proposed model a spontaneously broken global $U(1)'$ symmetry is considered instead of the Z_2 symmetry and the vector-like leptons generate one-loop level contributions to the muon and electron anomalous magnetic moments and at the same type produce the SM charged lepton masses, thus providing a connection of the charged lepton mass generation mechanism and the $g - 2$ anomalies, which is not given in the model of [41]. It is also worth emphasising that our model is very different from other models proposed in the literature based on the Universal Seesaw mechanism [49–66]. Universal Seesaw models are typically based on the left-right symmetric model with electroweak singlet fermions only, while our vector-like fermions involves complete families, including electroweak doublets which are typically the lightest ones. Some examples of theories relying on the Universal Seesaw mechanism to explain the SM charged fermion mass hierarchy are provided in [49–66].

Returning to our proposed model framework, we first consider the contribution of W boson exchange with neutrinos to the electron and muon anomalous magnetic moments at the one-loop level. Since this model involves the vector-like neutrinos, the sensitivity of the branching ratio of $\mu \rightarrow e\gamma$ decay can be enhanced with respect to the observable level and the muon and electron anomalous magnetic moments are studied while keeping the $\mu \rightarrow e\gamma$ constraint. As a result, we find that the impact of our predictions with W exchange at one-loop level is negligible when compared to their experimental bound. We then consider the contributions from the 2HDM scalar exchange. To study the implications of the one-loop level scalar exchange in the muon and electron anomalous magnetic moments, we first construct a scalar potential and derive the mass squared matrix for CP-even, CP-odd and charged Higgses assuming there is no mixing between the SM Higgs h and two non-SM physical scalars $H_{1,2}$. A diagonal Yukawa matrix for charged leptons implies the absence of mixing between charged leptons, resulting in vanishing branching ratio for the $\mu \rightarrow e\gamma$ decay, which in turn leads to a fulfillment of the charged lepton flavor violating constraints in this scenario. In such a framework we show that both anomalies can successfully explain both anomalies, including their opposite signs, at the 1σ level. We present some benchmark points for both the muon and the electron anomalies, together with some numerical scans around these points, which indicate the mass regions of the Higgs scalars of the 2HDM in this scenario. We also provide some analytic arguments to augment the numerical results.

The layout of the remainder of the paper is as follows. In Section II we discuss the origin of Yukawa couplings from

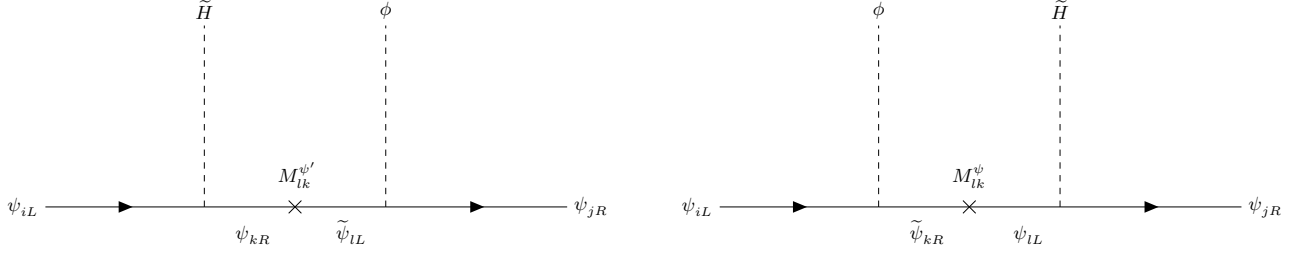


Figure 1: Diagrams in this model which lead to the effective Yukawa interactions, where $\psi, \psi' = Q, u, d, L, e$ (neutrinos will be treated separately) $i, j = 1, 2, 3$, $k, l = 4, 5$, M_{lk} is vector-like mass and $\tilde{H} = i\sigma_2 H^*$, $H = H_{u,d}$

a fourth and fifth vector-like family, within a mass insertion approximation. In Section III we construct the effective Yukawa matrices using a more detailed mixing formalism which goes beyond the mass insertion approximation. In Section IV we consider W exchange contributions to $(g-2)_\mu, (g-2)_e$ and $\text{BR}(\mu \rightarrow e\gamma)$ based on the type Ib seesaw mechanism within our model and show that the contributions are too small. In Section V we turn to Higgs scalar exchange contributions to $(g-2)_\mu, (g-2)_e$ and $\text{BR}(\mu \rightarrow e\gamma)$, focussing on analytical formulae. Then in Section VI we give a full numerical analysis of such contributions, showing that they can successfully explain the anomalies, presenting some benchmark points for both the muon and the electron anomalies, together with some numerical scans around these points, which indicate the mass regions of the Higgs scalars of the 2HDM in this scenario. Section VII concludes the main body of the paper. Appendix A provides a discussion of the quark mass matrices in two bases. Appendix B includes a brief discussion of heavy scalar production at a proton-proton collider.

II. THE ORIGIN OF YUKAWA COUPLINGS FROM A FOURTH AND FIFTH VECTOR-LIKE FAMILY

We start by asking a question: what is the origin of the SM Yukawa couplings? In addressing such question, we assume that the SM Yukawa Lagrangian is the low energy limit of an extended theory with enlarged symmetry and particle spectrum, and arises after the spontaneous breaking of an $U(1)'$ global symmetry at an energy scale as low as TeV. Therefore, understanding the origin of the Yukawa interaction naturally leads to the presence of another Higgses whose masses are higher than the mass of the SM Higgs. Furthermore, the SM Yukawa interactions are forbidden by the global $U(1)'$ symmetry, however the Yukawa interaction with the vector-like particles are allowed. With these considerations in place, the possible diagrams generating the Yukawa interactions can be drawn as indicated in Figure 1.

There are two key features in Figure 1, one of which is the presence of the assumed flavon ϕ and the other one is the vector-like mass M . Once the flavon ϕ develops its vev, the effective Yukawa interactions $\bar{\psi}_{iL} \tilde{H} \psi_{jR}$ are generated with a coupling constant proportional to $\langle \phi \rangle / M$, which takes place in front of the usual Yukawa constant. The proportional factor $\langle \phi \rangle / M$ plays a crucial role in explaining why one Yukawa constant can be relatively smaller or bigger than the other ones since the magnitude of each Yukawa constant is accompanied by the mass of the vector-like particles. The effective Lagrangian in this diagram reads:

$$\mathcal{L}_{\text{eff}}^{\text{Yukawa}} = \frac{x_{lj}^{\psi'} \langle \phi \rangle}{M_{lk}^{\psi'}} y_{ik}^{\psi} \bar{\psi}_{iL} \tilde{H} \psi_{jR} + \frac{x_{ik}^{\psi} \langle \phi \rangle}{M_{lk}^{\psi}} y_{lj}^{\psi} \bar{\psi}_{iL} \tilde{H} \psi_{jR} + \text{h.c.} \quad (2)$$

where $\psi, \psi' = Q, u, d, L, e$ (neutrinos will be treated separately) and x is a Yukawa constant in the interaction with ϕ and y is in the interaction with \tilde{H} as per Figure 1. Throughout this work, we take a view that the Yukawa constant y can be ideally of order unity while the x is small compared to the y .

A. The model with $U(1)'$ global symmetry

For an analysis of the phenomenology described above, we extend the SM fermion sector by adding two vector-like fermions, the SM gauge symmetry by including the global $U(1)'$ symmetry and the scalar sector of the 2HDM model is

Field	Q_{iL}	u_{iR}	d_{iR}	L_{iL}	e_{iR}	Q_{kL}	u_{kR}	d_{kR}	L_{kL}	e_{kR}	ν_{kR}	\tilde{Q}_{kR}	\tilde{u}_{kL}	\tilde{d}_{kL}	\tilde{L}_{kR}	\tilde{e}_{kL}	$\tilde{\nu}_{kR}$	ϕ	H_u	H_d
$SU(3)_C$	3	3	3	1	1	3	3	3	1	1	1	3	3	3	1	1	1	1	1	1
$SU(2)_L$	2	1	1	2	1	2	1	1	2	1	1	2	1	1	2	1	1	1	2	2
$U(1)_Y$	$\frac{1}{6}$	$\frac{2}{3}$	$-\frac{1}{3}$	$-\frac{1}{2}$	1	$\frac{1}{6}$	$\frac{2}{3}$	$-\frac{1}{3}$	$-\frac{1}{2}$	-1	0	$\frac{1}{6}$	$\frac{2}{3}$	$-\frac{1}{3}$	$-\frac{1}{2}$	-1	0	0	$\frac{1}{2}$	$-\frac{1}{2}$
$U(1)'$	0	0	0	0	0	1	-1	-1	1	-1	-1	1	-1	-1	1	-1	-1	1	-1	-1

Table I: This model is an extended 2HDM by the global $U(1)'$ symmetry with two vector-like families plus one flavon and reflects the property that the SM Yukawa interactions are forbidden. All SM particles $\psi_i (i = 1, 2, 3)$ are neutral under the $U(1)'$ symmetry and the right neutrinos ν_{iR} are not considered. Notice that this model involves two right-handed vector-like neutrinos $\nu_{kR}, \tilde{\nu}_{kR}$. The SM particles are extended by two vector-like families where $k = 4, 5$ and two SM Higgses $H_{u,d}$ are charged negatively under $U(1)'$ to forbid the renormalizable SM Yukawa interactions. The flavon field ϕ plays a role of braking the $U(1)'$ symmetry at TeV scale.

enlarged by considering a gauge scalar singlet, whose VEV triggers the spontaneous breaking of the $U(1)'$ symmetry. The scalar sector of the model is composed of by two $SU(2)$ doublet scalars $H_{u,d}$ and one flavon ϕ . Our extended 2HDM with enlarged particle spectrum and symmetries has the interesting feature that the SM Yukawa interactions are forbidden due to the global $U(1)'$ symmetry whereas the Yukawa interactions of SM fermions with vector-like families are allowed. Furthermore, such vector-like families have mass terms which are allowed by the symmetry. Thus, the SM charged fermions masses are generated from a Universal Seesaw mechanism mediated by heavy vector-like fermions. Unlike the $U(1)'$ model proposed in [67], we assume that the $U(1)'$ symmetry is global instead of local. This allows us more flexibility in the allowed range for the scale where the $U(1)'$ symmetry is broken. On top of that, the up-type quarks feature Yukawa interaction with the up-type Higgs whereas the down-type ones interact with down-type Higgs. In this BSM model, the SM particles are neutral under the $U(1)'$ symmetry, while the vector-like particles and all other scalars are charged under the symmetry. The particle content and symmetries of the model are shown in Table I.

The right-handed neutrinos ν_{iR} are absent in this model since we treat the left-handed neutrinos in the lepton doublet as Majorana particles and they are only extended by vector-like neutrinos. The vector-like particles and their partners have exact opposite charge to each other under the extended gauge symmetry to cancel out chiral anomaly. Lastly, the SM Higgses $H_{u,d}$ are negatively charged under the $U(1)'$ symmetry to forbid the renormalizable SM Yukawa interactions.

B. Mass insertion approximation

The renormalizable Yukawa interactions and mass terms for both up and down quark sectors read:

$$\begin{aligned}
\mathcal{L}_q^{\text{Yukawa+Mass}} = & y_{ik}^u \bar{Q}_{iL} \tilde{H}_u u_{kR} + x_{ki}^u \phi \tilde{\bar{u}}_{kL} u_{iR} + x_{ik}^Q \phi \bar{Q}_{iL} \tilde{Q}_{kR} + y_{ki}^u \bar{Q}_{kL} \tilde{H}_u u_{iR} \\
& + y_{ik}^d \bar{Q}_{iL} \tilde{H}_d d_{kR} + x_{ki}^d \phi \tilde{\bar{d}}_{kL} d_{iR} + y_{ki}^d \bar{Q}_{kL} \tilde{H}_d d_{iR} \\
& + M_{kl}^u \tilde{\bar{u}}_{lL} u_{kR} + M_{kl}^d \tilde{\bar{d}}_{lL} d_{kR} + M_{kl}^Q \bar{Q}_{kL} \tilde{Q}_{lR} + \text{h.c.}
\end{aligned} \tag{3}$$

where $i, j = 1, 2, 3$, $k, l = 4, 5$ and $\tilde{H} = i\sigma_2 H^*$. The possible diagrams contributing to the low energy quark Yukawa interaction are given in Figure 2:

The above two diagrams correspond to the up-type quark sector whereas the below two diagrams correspond to the down-type quark sector. The model under consideration is an extended 2HDM where the up-type Higgs H_u is relevant for the up-type quark sector whereas the down-type Higgs H_d is suitable for the down-type quark and charged lepton sectors. Like in the quark sector, the Yukawa interactions and mass terms for charged leptons can be written in a similar way:

$$\mathcal{L}_e^{\text{Yukawa+Mass}} = y_{ik}^e \bar{L}_{iL} \tilde{H}_d e_{kR} + x_{ki}^e \phi \tilde{\bar{e}}_{kL} e_{iR} + x_{ik}^L \phi \bar{L}_{iL} \tilde{L}_{kR} + y_{ki}^e \bar{L}_{kL} \tilde{H}_d e_{iR} + M_{kl}^e \tilde{\bar{e}}_{lL} e_{kR} + M_{kl}^L \bar{L}_{kL} \tilde{L}_{lR} + \text{h.c.} \tag{4}$$

Then, the possible diagrams giving rise to the charged lepton Yukawa interactions are shown in Figure 3:

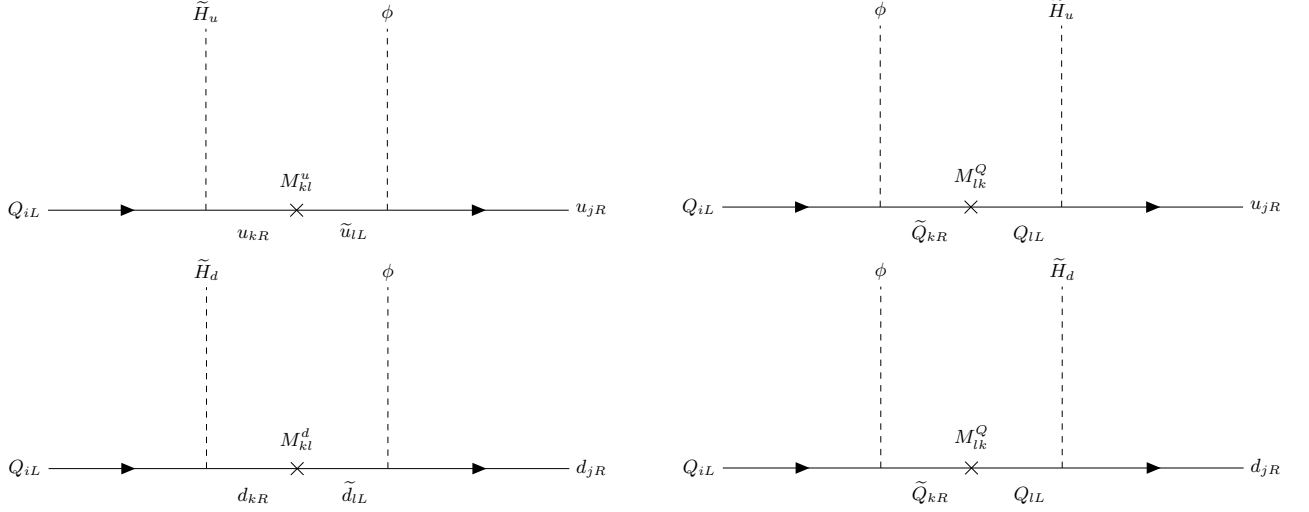


Figure 2: Diagrams in this model which lead to the effective Yukawa interactions for the up quark sector (two above diagrams) and the down quark sector (two below diagrams) in mass insertion approximation, where $i, j = 1, 2, 3$ and $k, l = 4, 5$ and M_{lk} is vector-like mass.

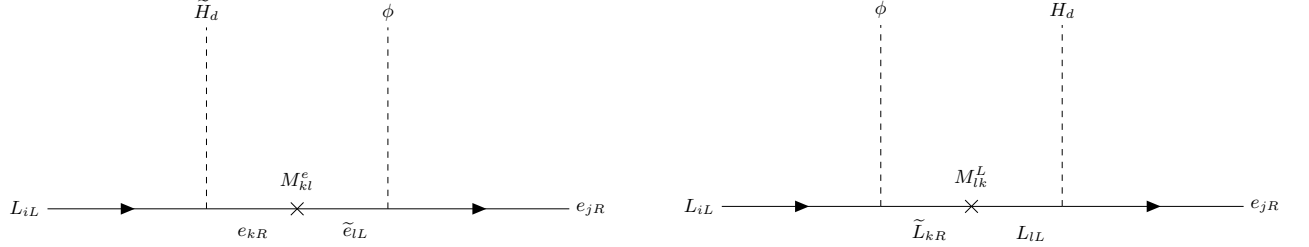


Figure 3: Diagrams in this model which lead to the effective Yukawa interactions for the charged lepton sector in mass insertion approximation, where $i, j = 1, 2, 3$ and $k, l = 4, 5$ and M_{lk} is vector-like mass.

As for the neutrinos, its behaviour is different as compared to the quarks or charged leptons since there exists only Majorana neutrinos in this model so initial and final neutrinos in mass insertion diagrams must be same. The Yukawa interactions and mass terms for the neutrino sector are given by:

$$\mathcal{L}_{\nu}^{\text{Yukawa+Mass}} = y_{ik}^{\nu} \bar{L}_{iL} \tilde{H}_u \nu_{kR} + x_{ik}^L \bar{L}_{iL} H_d \tilde{\nu}_{kR} + M_{kl}^M \tilde{\nu}_{lR} \nu_{kR} + \text{h.c.} \quad (5)$$

Here, one important feature in Equation 5 is the presence of the vector-like mass M . From the two Yukawa interactions in Equation 5, it follows that both ν_R and $\tilde{\nu}_R$ have a lepton number $+1$ and they are different particles. And then taking a look at the vector-like mass term in Equation 5, it can be confirmed that the vector-like mass is not a strict Majorana mass because ν_R and $\tilde{\nu}_R$ are different particles but plays a role of Majorana mass since the mass term violates the lepton number conservation. The corresponding diagram for the neutrino sector in the mass insertion approximation is given in Figure 4:

The operator $\bar{L}_i \bar{L}_j \tilde{H}_u H_d$ resulting from Figure 4 gives rise to the so called type Ib seesaw mechanism [5] which differs from the usual type Ia seesaw mechanism corresponding to the Weinberg operator $\bar{L}_i \bar{L}_j \tilde{H}_u \tilde{H}_u$ and will be discussed later in detail.

III. EFFECTIVE YUKAWA MATRICES USING A MIXING FORMALISM

As seen from Equation 2, we need to mix Higgses with the flavon to generate the effective Yukawa Lagrangian required to produce the SM fermion mass hierarchy. Since there is no an extra symmetry or constraint to keep the mixing

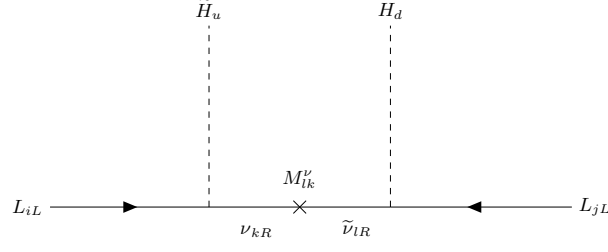


Figure 4: Type Ib seesaw diagram [5] which leads to the effective Yukawa interactions for the Majorana neutrinos in mass insertion approximation, where $i, j = 1, 2, 3$ and $k, l = 4, 5$ and M_{lk} is vector-like mass.

between Higgses and flavon from taking place, it is natural to assume their mixing.

A. The 7×7 matrix

Consider a 7×7 mass matrix for Dirac fermions:

$$M^\psi = \begin{pmatrix} \begin{array}{c|cccccc} & \psi_{1R} & \psi_{2R} & \psi_{3R} & \psi_{4R} & \psi_{5R} & \tilde{\psi}_{4R} & \tilde{\psi}_{5R} \\ \hline \bar{\psi}_{1L} & 0 & 0 & 0 & y_{14}^\psi \langle \tilde{H}^0 \rangle & y_{15}^\psi \langle \tilde{H}^0 \rangle & x_{14}^\psi \langle \phi \rangle & x_{15}^\psi \langle \phi \rangle \\ \bar{\psi}_{2L} & 0 & 0 & 0 & y_{24}^\psi \langle \tilde{H}^0 \rangle & y_{25}^\psi \langle \tilde{H}^0 \rangle & x_{24}^\psi \langle \phi \rangle & x_{25}^\psi \langle \phi \rangle \\ \bar{\psi}_{3L} & 0 & 0 & 0 & y_{34}^\psi \langle \tilde{H}^0 \rangle & y_{35}^\psi \langle \tilde{H}^0 \rangle & x_{34}^\psi \langle \phi \rangle & x_{35}^\psi \langle \phi \rangle \\ \bar{\psi}_{4L} & y_{41}^\psi \langle \tilde{H}^0 \rangle & y_{42}^\psi \langle \tilde{H}^0 \rangle & y_{43}^\psi \langle \tilde{H}^0 \rangle & 0 & 0 & M_{44}^\psi & M_{45}^\psi \\ \bar{\psi}_{5L} & y_{51}^\psi \langle \tilde{H}^0 \rangle & y_{52}^\psi \langle \tilde{H}^0 \rangle & y_{53}^\psi \langle \tilde{H}^0 \rangle & 0 & 0 & M_{54}^\psi & M_{55}^\psi \\ \hline \tilde{\psi}_{4L} & x_{41}^{\psi'} \langle \phi \rangle & x_{42}^{\psi'} \langle \phi \rangle & x_{43}^{\psi'} \langle \phi \rangle & M_{44}^{\psi'} & M_{45}^{\psi'} & 0 & 0 \\ \tilde{\psi}_{5L} & x_{51}^{\psi'} \langle \phi \rangle & x_{52}^{\psi'} \langle \phi \rangle & x_{53}^{\psi'} \langle \phi \rangle & M_{54}^{\psi'} & M_{55}^{\psi'} & 0 & 0 \end{array} \end{pmatrix}, \quad (6)$$

with the coefficients y and x being Yukawa constants where the former is expected to be of order unity whereas the latter is smaller than y . Furthermore, the 125 GeV SM like Higgs boson H will corresponds to the lightest of the CP even neutral scalar states arising from H_u , H_d and ϕ , whereas M is the vector-like mass. The column vector located at the lower left block in Equation 6 consists of left-handed particles while the row vector at the upper right block are made up of right-handed particles. The zeros in the 3×3 upper block in Equation 6 mean that no SM Yukawa interactions take place due to charge conservation as well as zeros in two 2×2 blocks. Since we are interested in explaining the muon and electron anomalous magnetic moments in this model, we first focus on the lepton sector in the next subsection and the method used for obtaining the low energy SM Yukawa matrices in the lepton sector can be applied to the quark sector in the same way with a slight change so that the quark sector will be discussed in appendix.

B. A convenient basis for charged leptons

From Equation 6, we can take a specified basis by rotating some fields as below:

$$M^e = \begin{pmatrix} \begin{array}{c|cccccc} & e_{1R} & e_{2R} & e_{3R} & e_{4R} & e_{5R} & \tilde{L}_{4R} & \tilde{L}_{5R} \\ \hline \bar{L}_{1L} & 0 & 0 & 0 & 0 & y_{15}^e v_d & 0 & x_{15}^L v_\phi \\ \bar{L}_{2L} & 0 & 0 & 0 & y_{24}^e v_d & y_{25}^e v_d & 0 & x_{25}^L v_\phi \\ \bar{L}_{3L} & 0 & 0 & 0 & y_{34}^e v_d & y_{35}^e v_d & x_{34}^L v_\phi & x_{35}^L v_\phi \\ \bar{L}_{4L} & 0 & 0 & y_{43}^e v_d & 0 & 0 & M_{44}^L & M_{45}^L \\ \bar{L}_{5L} & y_{51}^e v_d & y_{52}^e v_d & y_{53}^e v_d & 0 & 0 & 0 & M_{55}^L \\ \hline \tilde{e}_{4L} & 0 & x_{42}^e v_\phi & x_{43}^e v_\phi & M_{44}^e & 0 & 0 & 0 \\ \tilde{e}_{5L} & x_{51}^e v_\phi & x_{52}^e v_\phi & x_{53}^e v_\phi & M_{54}^e & M_{55}^e & 0 & 0 \end{array} \end{pmatrix}, \quad (7)$$

where $v_d = \langle H_d^0 \rangle$ and $v_\phi = \langle \phi \rangle$. We start by pointing out the reason why we take this specific basis for the charged leptons. The reason is that the strong hierarchical structure of the SM fermion Yukawa couplings can be implemented by the rotations with a simple assumption in this model to be specified below. In order to arrive from Equation 6 to Equation 7, we rotate the leptonic fields L_{4L} and L_{5L} to turn off M_{54}^L and rotate e_{4R} and e_{5R} to turn off M_{45}^e . Then, we can rotate L_{1L} and L_{3L} to set $x_{14}^L v_\phi$ to zero and then rotate L_{2L} and L_{3L} to set $x_{24}^L v_\phi$ to zero. The same rotation can be applied to $e_{1R,2R,3R}$ to set $y_{41,42}^e v_d$ to zero. Finally, we can further rotate L_{1L} and L_{2L} to switch off $y_{14}^e v_d$ and this rotation also goes for $e_{1R,2R}$ to switch off $x_{41}^e v_\phi$. The above given mass matrix includes three distinct mass scales which are the vev v_d of the neutral component of the Higgs doublet H_d , the vev v_ϕ of the flavon ϕ and the vector-like mass M , whose orders of magnitude can be in principle be different. Therefore, the mass matrix will be diagonalized by the seesaw mechanism step-by-step instead of diagonalising it at once. This mechanism is also known as Universal Seesaw, and was proposed for the first time, in the context of a left-right symmetric model in [49]. After the flavon ϕ acquires a vev, the diagonalization of the charged lepton mass matrix gives rise to an effective Yukawa matrix for charged leptons, $y_{ij}^e \bar{L}_{iL} \tilde{H}_d e_{jR}$, which is given by:

$$y_{ij}^e = \begin{pmatrix} 0 & -\frac{y_{15}^e x_{42}^e M_{54}^e}{M_{55}^e} & -\frac{y_{15}^e x_{43}^e M_{54}^e}{M_{55}^e} \\ 0 & -\frac{y_{25}^e x_{42}^e M_{54}^e}{M_{55}^e} + y_{24}^e x_{42}^e & -\frac{y_{25}^e x_{43}^e M_{54}^e}{M_{55}^e} + y_{24}^e x_{43}^e \\ 0 & -\frac{y_{35}^e x_{42}^e M_{54}^e}{M_{55}^e} + y_{34}^e x_{42}^e & -\frac{y_{35}^e x_{43}^e M_{54}^e}{M_{55}^e} + y_{34}^e x_{43}^e \end{pmatrix} \frac{\langle \phi \rangle}{M_{44}^e} + \begin{pmatrix} y_{15}^e x_{51}^e & y_{15}^e x_{52}^e & y_{15}^e x_{53}^e \\ y_{25}^e x_{51}^e & y_{25}^e x_{52}^e & y_{25}^e x_{53}^e \\ y_{35}^e x_{51}^e & y_{35}^e x_{52}^e & y_{35}^e x_{53}^e \end{pmatrix} \frac{\langle \phi \rangle}{M_{55}^e} \\ + \begin{pmatrix} y_{51}^e x_{15}^L & y_{52}^e x_{15}^L & y_{53}^e x_{15}^L \\ y_{51}^e x_{25}^L & y_{52}^e x_{25}^L & y_{53}^e x_{25}^L \\ y_{51}^e x_{35}^L & y_{52}^e x_{35}^L & y_{53}^e x_{35}^L \end{pmatrix} \frac{\langle \phi \rangle}{M_{55}^L} + \begin{pmatrix} 0 & 0 & 0 \\ 0 & 0 & 0 \\ -\frac{y_{51}^e x_{34}^L M_{45}^L}{M_{55}^L} & -\frac{y_{52}^e x_{34}^L M_{45}^L}{M_{55}^L} & -\frac{y_{53}^e x_{34}^L M_{45}^L}{M_{55}^L} + x_{34}^L y_{43}^e \end{pmatrix} \frac{\langle \phi \rangle}{M_{44}^L}. \quad (8)$$

With the mass hierarchy assumption $M_{54}^e, M_{45}^L \ll M_{44}^L, M_{44}^e, M_{55}^{L,e}$, the effective Yukawa matrix for charged leptons can be written in a much simpler way as below:

$$y_{ij}^e = \begin{pmatrix} 0 & 0 & 0 \\ 0 & y_{24}^e x_{42}^e & y_{24}^e x_{43}^e \\ 0 & y_{34}^e x_{42}^e & y_{34}^e x_{43}^e \end{pmatrix} \frac{\langle \phi \rangle}{M_{44}^e} + \begin{pmatrix} y_{15}^e x_{51}^e & y_{15}^e x_{52}^e & y_{15}^e x_{53}^e \\ y_{25}^e x_{51}^e & y_{25}^e x_{52}^e & y_{25}^e x_{53}^e \\ y_{35}^e x_{51}^e & y_{35}^e x_{52}^e & y_{35}^e x_{53}^e \end{pmatrix} \frac{\langle \phi \rangle}{M_{55}^e} \\ + \begin{pmatrix} y_{51}^e x_{15}^L & y_{52}^e x_{15}^L & y_{53}^e x_{15}^L \\ y_{51}^e x_{25}^L & y_{52}^e x_{25}^L & y_{53}^e x_{25}^L \\ y_{51}^e x_{35}^L & y_{52}^e x_{35}^L & y_{53}^e x_{35}^L \end{pmatrix} \frac{\langle \phi \rangle}{M_{55}^L} + \begin{pmatrix} 0 & 0 & 0 \\ 0 & 0 & 0 \\ 0 & 0 & x_{34}^L y_{43}^e \end{pmatrix} \frac{\langle \phi \rangle}{M_{44}^L}. \quad (9)$$

There are three notable features in Equation 9, one of which is electron mass is accompanied by one of fifth vector-like masses $M_{55}^{L,e}$ and the other is muon mass is explained by the fourth vector-like mass M_{44}^e and the last is order of $\langle \phi \rangle$ should be similar to that of M_{44}^Q to explain top quark Yukawa constant which is nearly 1 (For better understanding, the last condition is supposed to be explained with quark sector rather than lepton sector).

C. A basis for decoupling heavy fourth and fifth vector-like family

In this approach, the Yukawa matrix in Equation 9 will be expressed in terms of the mixing angles between the SM leptons and the vector-like leptons by decoupling the heavy fourth and fifth vector-like families. The Yukawa matrix

for charged leptons can be intuitively understood how the mixing happens in this model. Let us restart from Equation 7.

$$M^e = \left(\begin{array}{c|cccccc} & e_{1R} & e_{2R} & e_{3R} & e_{4R} & e_{5R} & \tilde{L}_{4R} & \tilde{L}_{5R} \\ \hline \bar{L}_{1L} & 0 & 0 & 0 & 0 & y_{15}^e v_d & 0 & x_{15}^L v_\phi \\ \bar{L}_{2L} & 0 & 0 & 0 & y_{24}^e v_d & y_{25}^e v_d & 0 & x_{25}^L v_\phi \\ \bar{L}_{3L} & 0 & 0 & 0 & y_{34}^e v_d & y_{35}^e v_d & x_{34}^L v_\phi & x_{35}^L v_\phi \\ \bar{L}_{4L} & 0 & 0 & y_{43}^e v_d & 0 & 0 & M_{44}^L & M_{45}^L \\ \bar{L}_{5L} & y_{51}^e v_d & y_{52}^e v_d & y_{53}^e v_d & 0 & 0 & 0 & M_{55}^L \\ \hline \tilde{e}_{4L} & 0 & x_{42}^e v_\phi & x_{43}^e v_\phi & M_{44}^e & 0 & 0 & 0 \\ \tilde{e}_{5L} & x_{51}^e v_\phi & x_{52}^e v_\phi & x_{53}^e v_\phi & M_{54}^e & M_{55}^e & 0 & 0 \end{array} \right) \quad (10)$$

As mentioned in the previous section IIIB, this mass matrix involves three distinct mass scales v_d , v_ϕ and M so it is possible to split this whole mass matrix by partial blocks to group mass terms with vev of H_d as in Equation 11

$$M^e = \left(\begin{array}{c|cccccc} & e_{1R} & e_{2R} & e_{3R} & e_{4R} & e_{5R} & \tilde{L}_{4R} & \tilde{L}_{5R} \\ \hline \bar{L}_{1L} & 0 & 0 & 0 & 0 & y_{15}^e v_d & 0 & x_{15}^L v_\phi \\ \bar{L}_{2L} & 0 & 0 & 0 & y_{24}^e v_d & y_{25}^e v_d & 0 & x_{25}^L v_\phi \\ \bar{L}_{3L} & 0 & 0 & 0 & y_{34}^e v_d & y_{35}^e v_d & x_{34}^L v_\phi & x_{35}^L v_\phi \\ \bar{L}_{4L} & 0 & 0 & y_{43}^e v_d & 0 & 0 & M_{44}^L & M_{45}^L \\ \bar{L}_{5L} & y_{51}^e v_d & y_{52}^e v_d & y_{53}^e v_d & 0 & 0 & 0 & M_{55}^L \\ \hline \tilde{e}_{4L} & 0 & x_{42}^e v_\phi & x_{43}^e v_\phi & M_{44}^e & 0 & 0 & 0 \\ \tilde{e}_{5L} & x_{51}^e v_\phi & x_{52}^e v_\phi & x_{53}^e v_\phi & M_{54}^e & M_{55}^e & 0 & 0 \end{array} \right), \quad (11)$$

and then elements of the blocks involving ϕ can be rotated away to make those zeros by unitary mixing matrices of Equation 13 as per Equation 12:

$$M^e = \left(\begin{array}{c|cccccc} & e_{1R} & e_{2R} & e_{3R} & e_{4R} & e_{5R} & \tilde{L}_{4R} & \tilde{L}_{5R} \\ \hline \bar{L}_{1L} & & & & & & 0 & 0 \\ \bar{L}_{2L} & & & & & & 0 & 0 \\ \bar{L}_{3L} & & & \tilde{y}_{\alpha\beta}^e v_d & & & 0 & 0 \\ \bar{L}_{4L} & & & & & & \widetilde{M}_{44}^L & x_{35}^{L''} v_\phi \\ \bar{L}_{5L} & & & & & & 0 & \widetilde{M}_{55}^L \\ \hline \tilde{e}_{4L} & 0 & 0 & 0 & \widetilde{M}_{44}^e & 0 & 0 & 0 \\ \tilde{e}_{5L} & 0 & 0 & 0 & x_{53}^{e'''} v_\phi & \widetilde{M}_{55}^e & 0 & 0 \end{array} \right), \quad (12)$$

where the indices α, β run from 1 to 5, and tilde, primes repeated in the mass matrix mean that the parameters are rotated. The unitary 5×5 matrices are defined to be

$$V_L = V_{45}^L V_{35}^L V_{25}^L V_{15}^L V_{34}^L V_{24}^L V_{14}^L, \quad V_e = V_{45}^e V_{35}^e V_{25}^e V_{15}^e V_{34}^e V_{24}^e V_{14}^e, \quad (13)$$

where each of the unitary matrices $V_{i4,5}$ are parameterized by a single angle $\theta_{i4,5}$ describing the mixing between the i th chiral family and the 4,5th vector-like family. The 5×5 Yukawa constant matrix in a mass basis (primed) can be diagonalized by the unitary rotation matrices as below:

$$\tilde{y}_{\alpha\beta}^e = V_L \tilde{y}_{\alpha\beta}^e V_e^\dagger \quad (14)$$

From Equation 7, we can read off the 5×5 upper block and confirm that the $(3, 4), (1, 5), (2, 5), (3, 5)$ mixings in the L sector and $(2, 4), (3, 4), (1, 5), (2, 5), (3, 5)$ mixings in the e sector are required to go to the decoupling basis. The unitary matrices of Equation 13 and mixing angles appearing in the unitary matrices are parameterized by

$$\begin{aligned}
V_L &= V_{35}^L V_{25}^L V_{15}^L V_{34}^L \\
&= \begin{pmatrix} 1 & 0 & 0 & 0 & 0 \\ 0 & 1 & 0 & 0 & 0 \\ 0 & 0 & c_{35}^L & 0 & s_{35}^L \\ 0 & 0 & 0 & 1 & 0 \\ 0 & 0 & -s_{35}^L & 0 & c_{35}^L \end{pmatrix} \begin{pmatrix} 1 & 0 & 0 & 0 & 0 \\ 0 & c_{25}^L & 0 & 0 & s_{25}^L \\ 0 & 0 & 1 & 0 & 0 \\ 0 & 0 & 0 & 1 & 0 \\ 0 & -s_{25}^L & 0 & 0 & c_{25}^L \end{pmatrix} \begin{pmatrix} c_{15}^L & 0 & 0 & 0 & s_{15}^L \\ 0 & 1 & 0 & 0 & 0 \\ 0 & 0 & 1 & 0 & 0 \\ 0 & 0 & 0 & 1 & 0 \\ -s_{15}^L & 0 & 0 & 0 & c_{15}^L \end{pmatrix} \begin{pmatrix} 1 & 0 & 0 & 0 & 0 \\ 0 & 1 & 0 & 0 & 0 \\ 0 & 0 & c_{34}^L & s_{34}^L & 0 \\ 0 & 0 & -s_{34}^L & c_{34}^L & 0 \\ 0 & 0 & 0 & 0 & 1 \end{pmatrix} \\
&\approx \begin{pmatrix} 1 & 0 & 0 & 0 & s_{15}^L \\ 0 & 1 & 0 & 0 & s_{25}^L \\ 0 & 0 & 1 & s_{34}^L & s_{35}^L \\ 0 & 0 & -s_{34}^L & 1 & 0 \\ -s_{15}^L & -s_{25}^L & -s_{35}^L & 0 & 1 \end{pmatrix}, \\
s_{34}^L &= \frac{x_{34}^L \langle \phi \rangle}{\sqrt{(x_{34}^L \langle \phi \rangle)^2 + (M_{44}^L)^2}}, \quad s_{15}^L = \frac{x_{15}^L \langle \phi \rangle}{\sqrt{(x_{15}^L \langle \phi \rangle)^2 + (M_{55}^L)^2}}, \\
s_{25}^L &= \frac{x_{25}^L \langle \phi \rangle}{\sqrt{(x_{25}^L \langle \phi \rangle)^2 + (M_{55}^L)^2}}, \quad s_{35}^L = \frac{x_{35}^L \langle \phi \rangle}{\sqrt{(x_{35}^L \langle \phi \rangle)^2 + (M_{55}^L)^2}}, \\
x_{35}^L \langle \phi \rangle &= c_{34}^L x_{35}^L \langle \phi \rangle + s_{34}^L M_{45}^L, \quad M_{45}^L = -s_{34}^L x_{35}^L \langle \phi \rangle + c_{34}^L M_{45}^L \\
\widetilde{M}_{44}^L &= \sqrt{(x_{34}^L \langle \phi \rangle)^2 + (M_{44}^L)^2}, \\
M_{55}^L &= \sqrt{(x_{15}^L \langle \phi \rangle)^2 + (M_{55}^L)^2}, \quad M_{55}^L = \sqrt{(x_{25}^L \langle \phi \rangle)^2 + (M_{55}^L)^2}, \quad \widetilde{M}_{55}^L = \sqrt{(x_{35}^L \langle \phi \rangle)^2 + (M_{55}^L)^2}
\end{aligned} \tag{15}$$

$$\begin{aligned}
V_e &= V_{35}^e V_{25}^e V_{15}^e V_{34}^e V_{24}^e \\
&= \begin{pmatrix} 1 & 0 & 0 & 0 & 0 \\ 0 & 1 & 0 & 0 & 0 \\ 0 & 0 & c_{35}^e & 0 & s_{35}^e \\ 0 & 0 & 0 & 1 & 0 \\ 0 & 0 & -s_{35}^e & 0 & c_{35}^e \end{pmatrix} \begin{pmatrix} 1 & 0 & 0 & 0 & 0 \\ 0 & c_{25}^e & 0 & 0 & s_{25}^e \\ 0 & 0 & 1 & 0 & 0 \\ 0 & 0 & 0 & 1 & 0 \\ 0 & -s_{25}^e & 0 & 0 & c_{25}^e \end{pmatrix} \begin{pmatrix} c_{15}^e & 0 & 0 & 0 & s_{15}^e \\ 0 & 1 & 0 & 0 & 0 \\ 0 & 0 & 1 & 0 & 0 \\ 0 & 0 & 0 & 1 & 0 \\ -s_{15}^e & 0 & 0 & 0 & c_{15}^e \end{pmatrix} \\
&\times \begin{pmatrix} 1 & 0 & 0 & 0 & 0 \\ 0 & 1 & 0 & 0 & 0 \\ 0 & 0 & c_{34}^e & s_{34}^e & 0 \\ 0 & 0 & -s_{34}^e & c_{34}^e & 0 \\ 0 & 0 & 0 & 0 & 1 \end{pmatrix} \begin{pmatrix} 1 & 0 & 0 & 0 & 0 \\ 0 & c_{24}^e & 0 & s_{24}^e & 0 \\ 0 & 0 & 1 & 0 & 0 \\ 0 & -s_{24}^e & 0 & c_{24}^e & 0 \\ 0 & 0 & 0 & 0 & 1 \end{pmatrix} \approx \begin{pmatrix} 1 & 0 & 0 & 0 & \theta_{15}^e \\ 0 & 1 & 0 & \theta_{24}^e & \theta_{25}^e \\ 0 & 0 & 1 & \theta_{34}^e & \theta_{35}^e \\ 0 & -\theta_{24}^e & -\theta_{34}^e & 1 & 0 \\ -\theta_{15}^e & -\theta_{25}^e & -\theta_{35}^e & 0 & 1 \end{pmatrix}, \\
s_{24}^e &\approx \frac{x_{42}^e \langle \phi \rangle}{M_{44}^e}, \quad s_{34}^e \approx \frac{x_{43}^e \langle \phi \rangle}{M_{44}^e}, \quad s_{15}^e \approx \frac{x_{51}^e \langle \phi \rangle}{M_{55}^e}, \quad s_{25}^e \approx \frac{x_{52}^e \langle \phi \rangle}{M_{55}^e}, \quad s_{35}^e \approx \frac{x_{53}^e \langle \phi \rangle}{M_{55}^e}, \\
x_{52}^e \langle \phi \rangle &= c_{24}^e x_{52}^e \langle \phi \rangle + s_{24}^e M_{54}^e, \quad M_{54}^e = -s_{24}^e x_{52}^e \langle \phi \rangle + c_{24}^e M_{54}^e, \\
x_{53}^e \langle \phi \rangle &= c_{34}^e x_{53}^e \langle \phi \rangle + s_{34}^e M_{54}^e, \quad M_{54}^e = -s_{34}^e x_{53}^e \langle \phi \rangle + c_{34}^e M_{54}^e, \\
M_{44}^e &= \sqrt{(x_{42}^e \langle \phi \rangle)^2 + (M_{44}^e)^2}, \quad \widetilde{M}_{44}^e = \sqrt{(x_{43}^e \langle \phi \rangle)^2 + (M_{44}^e)^2}, \\
M_{55}^e &= \sqrt{(x_{51}^e \langle \phi \rangle)^2 + (M_{55}^e)^2}, \quad M_{55}^e = \sqrt{(x_{52}^e \langle \phi \rangle)^2 + (M_{55}^e)^2}, \quad \widetilde{M}_{55}^e = \sqrt{(x_{53}^e \langle \phi \rangle)^2 + (M_{55}^e)^2}.
\end{aligned} \tag{16}$$

Given the above unitary rotations, the 5×5 Yukawa matrices are computed in terms of the mixing angles and the upper 3×3 block would be the effective SM Yukawa matrix. Assuming all $\cos \theta$ to be 1 and neglecting order of θ square or more than that, we have a simple 3×3 Yukawa matrix of Equation 17.

$$y_{ij}^e = \begin{pmatrix} s_{15}^L y_{51}^e + y_{15}^e \theta_{15}^e & s_{15}^L y_{52}^e + y_{15}^e \theta_{25}^e & s_{15}^L y_{53}^e + y_{15}^e \theta_{35}^e \\ s_{25}^L y_{51}^e + y_{25}^e \theta_{25}^e & s_{25}^L y_{52}^e + y_{25}^e \theta_{24}^e + y_{25}^e \theta_{25}^e & s_{25}^L y_{53}^e + y_{25}^e \theta_{34}^e + y_{25}^e \theta_{35}^e \\ s_{35}^L y_{51}^e + y_{35}^e \theta_{35}^e & s_{35}^L y_{52}^e + y_{35}^e \theta_{24}^e + y_{35}^e \theta_{25}^e & s_{35}^L y_{53}^e + y_{35}^e \theta_{34}^e + y_{35}^e \theta_{35}^e \end{pmatrix} \tag{17}$$

Note that Equation 9 and Equation 17 are the same however they are obtained by considering different viewpoints.

D. A convenient basis for neutrinos

The relevant Yukawa and mass terms of the neutrino sector give rise to the following neutrino mass matrix:

$$M^\nu = \left(\begin{array}{c|ccc|ccc} & L_{1L} & L_{2L} & L_{3L} & \bar{\nu}_{4R} & \bar{\nu}_{5R} & \tilde{\nu}_{4R} & \tilde{\nu}_{5R} \\ \hline L_{1L} & 0 & 0 & 0 & y_{14}^\nu v_u & y_{15}^\nu v_u & x_{14}^L v_d & x_{15}^L v_d \\ L_{2L} & 0 & 0 & 0 & y_{24}^\nu v_u & y_{25}^\nu v_u & x_{24}^L v_d & x_{25}^L v_d \\ L_{3L} & 0 & 0 & 0 & y_{34}^\nu v_u & y_{35}^\nu v_u & x_{34}^L v_d & x_{35}^L v_d \\ \hline \bar{\nu}_{4R} & y_{14}^\nu v_u & y_{24}^\nu v_u & y_{34}^\nu v_u & 0 & 0 & M_{44}^\nu & M_{54}^\nu \\ \bar{\nu}_{5R} & y_{15}^\nu v_u & y_{25}^\nu v_u & y_{35}^\nu v_u & 0 & 0 & M_{45}^\nu & M_{55}^\nu \\ \tilde{\nu}_{4R} & x_{14}^L v_d & x_{24}^L v_d & x_{34}^L v_d & M_{44}^\nu & M_{45}^\nu & 0 & 0 \\ \tilde{\nu}_{5R} & x_{15}^L v_d & x_{25}^L v_d & x_{35}^L v_d & M_{54}^\nu & M_{55}^\nu & 0 & 0 \end{array} \right) \quad (18)$$

Here, the zeros in the upper 3×3 block of Equation 18 mean that neutrinos remain massless in the SM. Therefore, the SM neutrinos can be massive via the inclusion of two vector-like families. In order to make this mass matrix as simple as possible, the only choice left is to rotate ν_{4R} and ν_{5R} to turn off M_{45}^ν since rotations between $L_{1L,2L,3L}$ are already used in the charged lepton sector. With this simplification, and using the Weinberg-like operator, $y_{ij}^\nu L_i L_j \tilde{H}_u^\dagger H_d^\dagger$, we obtain the following effective 3×3 Yukawa matrix for light active neutrinos:

$$y_{ij}^\nu = \left(\begin{array}{ccc} 2x_{14}^L y_{14}^\nu & x_{24}^L y_{14}^\nu + x_{14}^L y_{24}^\nu & x_{34}^L y_{14}^\nu + x_{14}^L y_{34}^\nu \\ x_{24}^L y_{14}^\nu + x_{14}^L y_{24}^\nu & 2x_{24}^L y_{24}^\nu & x_{34}^L y_{24}^\nu + x_{24}^L y_{34}^\nu \\ x_{34}^L y_{14}^\nu + x_{14}^L y_{34}^\nu & x_{34}^L y_{24}^\nu + x_{24}^L y_{34}^\nu & 2x_{34}^L y_{34}^\nu \end{array} \right) \frac{1}{M_{44}^\nu} \\ + \left(\begin{array}{ccc} 2x_{15}^L y_{15}^\nu & x_{25}^L y_{15}^\nu + x_{15}^L y_{25}^\nu & x_{35}^L y_{15}^\nu + x_{15}^L y_{35}^\nu \\ x_{25}^L y_{15}^\nu + x_{15}^L y_{25}^\nu & 2x_{25}^L y_{25}^\nu & x_{35}^L y_{25}^\nu + x_{25}^L y_{35}^\nu \\ x_{35}^L y_{15}^\nu + x_{15}^L y_{35}^\nu & x_{35}^L y_{25}^\nu + x_{25}^L y_{35}^\nu & 2x_{35}^L y_{35}^\nu \end{array} \right) \frac{1}{M_{55}^\nu} \\ + \left(\begin{array}{ccc} -2x_{14}^L y_{15}^\nu & -x_{24}^L y_{15}^\nu - x_{14}^L y_{25}^\nu & -x_{34}^L y_{15}^\nu - x_{14}^L y_{35}^\nu \\ -x_{24}^L y_{15}^\nu - x_{14}^L y_{25}^\nu & -2x_{24}^L y_{25}^\nu & -x_{34}^L y_{25}^\nu - x_{24}^L y_{35}^\nu \\ -x_{34}^L y_{15}^\nu - x_{14}^L y_{35}^\nu & -x_{34}^L y_{25}^\nu - x_{24}^L y_{35}^\nu & -2x_{34}^L y_{35}^\nu \end{array} \right) \frac{M_{54}^\nu}{M_{44}^\nu M_{55}^\nu} \quad (19)$$

IV. W BOSON EXCHANGE CONTRIBUTIONS TO $(g-2)_\mu, (g-2)_e$ AND $\text{BR}(\mu \rightarrow e\gamma)$

Within the framework of our proposed model, we start by investigating the muon and electron anomalous magnetic moments with W boson exchange first. Given that such W boson exchange contribution also involves virtual neutrinos in the internal lines of the loop, we revisit the mass matrix for neutrinos. In this mass matrix, we remove fifth vector-like neutrinos ν_{5R} and $\tilde{\nu}_{5R}$ since they are too heavy to contribute to the phenomenology under study. As mentioned in the previous section, we stick to a condition where the coefficient y is expected to be of order unity, whereas the coupling x is expected to be smaller than y . Such condition can be easily seen by substituting the coefficients y_{i4}^ν by y_i^ν and the coefficients x_{i4}^L by $\epsilon y_i^{\nu'}$ where ϵ is a suppression factor. Putting all these considerations together, the mass matrix for neutrinos in Equation 18 after electroweak symmetry breaking takes the form:

$$M^\nu \approx \left(\begin{array}{c|ccc|cc} & \nu_{1L} & \nu_{2L} & \nu_{3L} & \bar{\nu}_{4R} & \tilde{\nu}_{4R} \\ \hline \nu_{1L} & 0 & 0 & 0 & y_1^\nu v_u & \epsilon y_1^{\nu'} v_d \\ \nu_{2L} & 0 & 0 & 0 & y_2^\nu v_u & \epsilon y_2^{\nu'} v_d \\ \nu_{3L} & 0 & 0 & 0 & y_3^\nu v_u & \epsilon y_3^{\nu'} v_d \\ \hline \bar{\nu}_{4R} & y_1^\nu v_u & y_2^\nu v_u & y_3^\nu v_u & 0 & M_{44}^\nu \\ \tilde{\nu}_{4R} & \epsilon y_1^{\nu'} v_d & \epsilon y_2^{\nu'} v_d & \epsilon y_3^{\nu'} v_d & M_{44}^\nu & 0 \end{array} \right) \equiv \left(\begin{array}{cc} 0 & m_D \\ m_D^T & M_N \end{array} \right), \quad (20)$$

where $v_u(v_d)$ is the vev of $\tilde{H}_u(H_d)$, v_u runs from $246/\sqrt{2} \text{ GeV} \simeq 174 \text{ GeV}$ to 246 GeV and $v_u^2 + v_d^2 = (246 \text{ GeV})^2$.

A. Type 1b seesaw mechanism

Now that we constructed the neutrino mass matrix for this task, the next step is to read off the operator which gives rise to the neutrino mass from the mass matrix. Generally, the well-known operator for neutrino mass is the

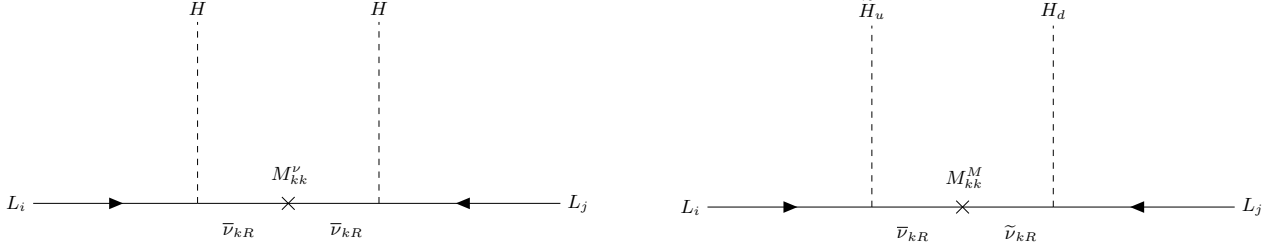


Figure 5: Diagrams which lead to effective Weinberg operators for the Majorana and vector-like mass in the mass insertion approximation, where $i, j = 1, 2, 3$ and $k = 4$, respectively. The left is the Weinberg operator(or type 1a seesaw mechanism) in which mass M is Majorana mass and the right is Weinberg-like operator(or type 1b seesaw mechanism) in which mass M is vector-like mass.

Weinberg operator(type 1a seesaw mechanism) $\frac{1}{\Lambda} L_i L_j H H$. A main feature of the Weinberg operator is the same SM Higgs should be repeated in the operator, however that property is not present in our model since the Higgs doublets $H_{u,d}$ are negatively charged under the $U(1)'$ symmetry, which implies the corresponding Weinberg operator having such fields will not be invariant under the $U(1)'$ unless an insertion of a quadratic power of the gauge singlet scalar ϕ is considered. However we do not consider the operators $\frac{1}{\Lambda^3} (\bar{L}_i \tilde{H}_u) (\tilde{H}_u L_j^C) (\phi^*)^2$ and $\frac{1}{\Lambda^3} (\bar{L}_i H_d) (H_d L_j^C) \phi^2$ in the neutrino sector, since they are very subleading and thus will give a tiny contribution to the light active neutrino masses. Instead of relying on a seven dimensional Weinberg to generate the tiny masses for the light active neutrinos, we take another approach named type 1b seesaw mechanism (we call the Weinberg operator “type 1a seesaw mechanism” to differentiate with) where the mixing of different $SU(2)$ Higgs doublets can appear satisfying charge conservation. Diagrams for the operators are given in Figure 5 for comparison:

The diagrams in Figure 5 clearly tell the difference between Majorana mass and vector-like mass. They share a common property that they violate the lepton number conservation, whereas the particles appearing in a Majorana mass term are same but those ones involved in vector-like mass terms are different. As the type 1b seesaw mechanism only works in this model, we make use of this seesaw mechanism for the analysis of neutrinos. With the operator, the renormalizable Lagrangian for neutrinos can be written as:

$$\mathcal{L}_\nu^{\text{Yukawa+Mass}} = y_i^\nu \bar{L}_{iL} \tilde{H}_u \nu_{kR} + \epsilon y_i^{\nu'} \bar{L}_{iL} H_d \tilde{\nu}_{kR} + M_{kk}^M \tilde{\nu}_{kR} \nu_{kR} + \text{h.c.}, \quad (21)$$

where $i = 1, 2, 3$ and $k = 4$. The renormalizable Lagrangian of Equation 21 above the electroweak scale generates an effective Lagrangian after decoupling the heavy vector-like neutrinos, which is suitable for study of low energy neutrino phenomenology. The effective Lagrangian for neutrino at electroweak scale is given by[5]

$$\mathcal{L}^{d=5} = c_{ij}^{d=5} \left((L_i^T \tilde{H}_u) (H_d^T L_j) + (L_i^T H_d) (\tilde{H}_u^T L_j) \right), \quad (22)$$

where the coefficient $c_{ij}^{d=5}$ is suppressed by a factor of the vector-like mass M . The neutrino mass matrix of Equation 20 can be diagonalized by the unitary matrix U as below:

$$U^T \begin{pmatrix} 0 & m_D^T \\ m_D & M_N \end{pmatrix} U = \begin{pmatrix} m_\nu^{\text{diag}} & 0 \\ 0 & M_N^{\text{diag}} \end{pmatrix}, \quad (23)$$

where m_ν^{diag} is a diagonal matrix for the light left-handed neutrinos ν_{iL} and M_N^{diag} is that for the heavy vector-like neutrinos $\nu_{4R}, \tilde{\nu}_{4R}$. Here, the unitary mixing matrix U is defined by multiplication of two unitary matrices which we call U_A and U_B , respectively[68]:

$$\begin{aligned} U &= U_A \cdot U_B \\ U_A &= \exp \begin{pmatrix} 0 & \Theta \\ -\Theta^\dagger & 0 \end{pmatrix} \simeq \begin{pmatrix} I - \frac{\Theta\Theta^\dagger}{2} & \Theta \\ -\Theta^\dagger & I - \frac{\Theta\Theta^\dagger}{2} \end{pmatrix} \quad \text{at leading order in } \Theta \\ U_B &= \begin{pmatrix} U_{\text{PMNS}} & 0 \\ 0 & I \end{pmatrix} \end{aligned} \quad (24)$$

The unitary matrix U_{PMNS} in U_B is the well-known Pontecorvo-Maki-Nakagawa-Sakata matrix and is parameterized by [5, 69]

$$U_{\text{PMNS}} = \begin{pmatrix} 1 & 0 & 0 \\ 0 & \cos \theta_{23} & \sin \theta_{23} \\ 0 & -\sin \theta_{23} & \cos \theta_{23} \end{pmatrix} \begin{pmatrix} \cos \theta_{13} & 0 & \sin \theta_{13} e^{-i\delta_{\text{CP}}} \\ 0 & 1 & 0 \\ -\sin \theta_{13} e^{i\delta_{\text{CP}}} & 0 & \cos \theta_{13} \end{pmatrix} \begin{pmatrix} \cos \theta_{12} & \sin \theta_{12} & 0 \\ -\sin \theta_{12} & \cos \theta_{12} & 0 \\ 0 & 0 & 1 \end{pmatrix} \begin{pmatrix} e^{-i\alpha'/2} & 0 & 0 \\ 0 & e^{-i\alpha/2} & 0 \\ 0 & 0 & 1 \end{pmatrix}, \quad (25)$$

where the Majorana phase α' is set to zero in this model. The mixing matrices $U_{A,B}$ are unitary, however the 3×3 upper block of the unitary matrix U is not unitary due to the factor $(I - \Theta\Theta^\dagger/2)$ for the light neutrinos. An interesting feature of the unitary matrix U is it is unitary globally, but non-unitary locally and this non-unitarity contributes to explain muon and electron anomalous magnetic moments. Replacing the unitary matrices in Equation 24 back to Equation 23, the result is simplified with the assumption $M_N \gg m_D$ to the conventional seesaw mechanism:

$$\begin{aligned} \Theta &\simeq m_D^\dagger M_N^{-1} \\ U_{\text{PMNS}}^* m_\nu^{\text{diag}} U_{\text{PMNS}}^\dagger &\simeq -m_D^T M_N^{-1} m_D \equiv -m \\ M_N^{\text{diag}} &\simeq M_N, \end{aligned} \quad (26)$$

where m is the effective mass matrix resulted from Equation 20.

$$m_{ij} = \frac{\epsilon v_u v_d}{M_{44}^\nu} (y_i^\nu y_j^{\nu'} + y_i^{\nu'} y_j^\nu) \quad (27)$$

Therefore, smallness of the light neutrino masses can be understood not only from mass of vector-like mass M_{44}^ν but also from the suppression factor ϵ and the presence of ϵ allows more flexibility in the allowed mass values of the vector-like neutrinos. Revisiting non-unitarity part for the light neutrinos from the unitary matrix U [68, 70], it reads:

$$\left(I - \frac{\Theta_i \Theta_j^\dagger}{2} \right) U_{\text{PMNS}} = (I - \eta_{ij}) U_{\text{PMNS}} \quad (28)$$

The non-unitarity η is associated with the presence of the heavy vector-like neutrinos and can be derived from a coefficient of the effective Lagrangian at dimension 6 [71]:

$$\mathcal{L}^{d=6} = c_{ij}^{d=6} \left((L_i^\dagger \tilde{H}_u) i\cancel{\phi} (\tilde{H}_u^\dagger L_j) + (L_i^\dagger H_d) i\cancel{\phi} (H_d^\dagger L_j) \right) \quad (29)$$

Once the SM Higgs doublets in Equation 29 develop its vev, the Lagrangian at dimension 6 causes non-diagonal kinetic terms for the light neutrinos and it gives rise to deviations of unitarity when it is diagonalized. The deviations of unitarity can be expressed in terms of the coefficient at dimension 6 $\eta_{ij} \equiv v^2 c_{ij}^{d=6}/2$.

$$\eta_{ij} = \frac{\Theta_i \Theta_j^\dagger}{2} = \frac{1}{2} \frac{m_D^\dagger m_D}{M_N^2} = \frac{1}{2M_{44}^{\nu 2}} (v_u^2 y_i^{\nu*} y_j^\nu + \epsilon^2 v_d^2 y_i^{\nu'*} y_j^{\nu'}) \simeq \frac{v_u^2}{2M_{44}^{\nu 2}} y_i^{\nu*} y_j^\nu \quad (30)$$

From the fourth term in Equation 30, the term with ϵ^2 can be safely ignored due to both relative smallness of v_d and the suppression factor ϵ . Thus, the deviation of unitarity η consists of the vector-like mass M_{44}^ν and the Yukawa couplings $y_{i,j}^\nu$. As an interesting example, it is possible that the Yukawa couplings $y_{i,j}^\nu$ can be obtained from the observables such as the PMNS mixing matrix and two mass squared splitting, Δm_{sol}^2 and Δm_{atm}^2 , in the neutrino oscillation experiments. Since the hierarchy between the light neutrinos is not yet determined, there are two possible scenarios, normal hierarchy(NH) and inverted hierarchy(IH), and the lightest neutrino remains massless, whereas two other neutrinos get massive. The Yukawa couplings $y_i^{\nu,\nu'}$ for the NH($m_1 = 0$) are determined by

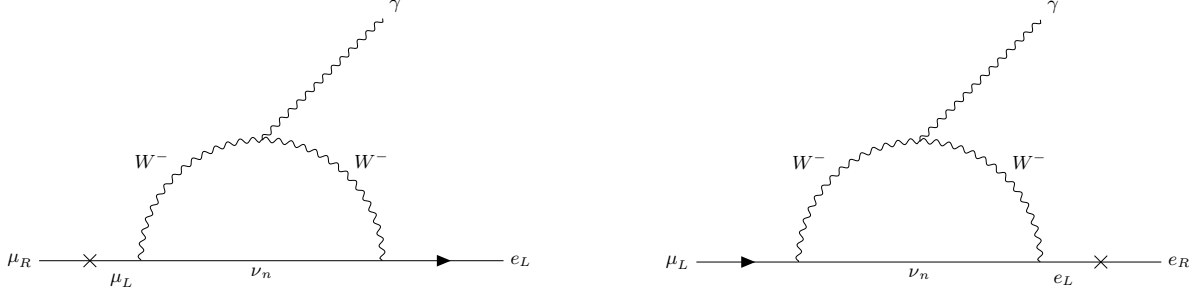


Figure 6: Diagrams for CLFV $\mu \rightarrow e\gamma$ decay with all neutrinos ($n = 1, 2, 3, 4, 5$)

$$\begin{aligned} y_i^\nu &= \frac{y}{\sqrt{2}} \left(\sqrt{1+\rho} (U_{\text{PMNS}}^*)_{i3} + \sqrt{1-\rho} (U_{\text{PMNS}}^*)_{i2} \right) \\ y_i^{\nu'} &= \frac{y'}{\sqrt{2}} \left(\sqrt{1+\rho} (U_{\text{PMNS}}^*)_{i3} - \sqrt{1-\rho} (U_{\text{PMNS}}^*)_{i2} \right), \end{aligned} \quad (31)$$

where y and y' are real numbers and $\rho = (1 - \sqrt{r})/(1 + \sqrt{r})$ with $r \equiv |\Delta m_{\text{sol}}^2|/|\Delta m_{\text{atm}}^2| = \Delta m_{21}^2/\Delta m_{31}^2$, whereas the Yukawa couplings $y_i^{\nu, \nu'}$ for the IN ($m_3 = 0$) are

$$\begin{aligned} y_i^\nu &= \frac{y}{\sqrt{2}} \left(\sqrt{1+\rho} (U_{\text{PMNS}}^*)_{i2} + \sqrt{1-\rho} (U_{\text{PMNS}}^*)_{i1} \right) \\ y_i^{\nu'} &= \frac{y'}{\sqrt{2}} \left(\sqrt{1+\rho} (U_{\text{PMNS}}^*)_{i2} - \sqrt{1-\rho} (U_{\text{PMNS}}^*)_{i1} \right), \end{aligned} \quad (32)$$

where $\rho = (1 - \sqrt{1+r})/(1 + \sqrt{1+r})$ with $r \equiv |\Delta m_{\text{sol}}^2|/|\Delta m_{\text{atm}}^2| = \Delta m_{21}^2/\Delta m_{32}^2$.

B. The charged lepton flavour violation (CLFV) $\mu \rightarrow e\gamma$ decay

Consider the three light neutrinos in the SM for the CLFV $\mu \rightarrow e\gamma$ decay first. In this case, the unitary mixing matrix becomes just the PMNS mixing matrix and the GIM mechanism which suppresses flavour-changing process works, therefore it leads quite suppressed sensitivity for BR ($\mu \rightarrow e\gamma$) about 10^{-55} [72], which is impossible to observe with the current sensitivity of $\mu \rightarrow e\gamma$ decay. This impractical sensitivity can be enhanced to the observable level by introducing the heavy vector-like neutrinos which give rise to deviation of unitarity. With the presence of heavy vector-like neutrinos, the GIM mechanism is gone and the factor suppressed by GIM mechanism can survive with a factor of deviation of unitarity, which plays a crucial role to increase significantly order of theoretical prediction for $\mu \rightarrow e\gamma$ decay [73]. Therefore, the strongest constraint for deviation of unitarity in the modified PMNS mixing matrix comes from CLFV $\mu \rightarrow e\gamma$ decay. The possible one-loop diagrams for the CLFV $\mu \rightarrow e\gamma$ with all neutrinos in this model are given in Figure 6.

The amplitude from above diagrams in Figure 6 reads [72]:

$$\begin{aligned} \mathcal{M}(\mu \rightarrow e\gamma) &= \bar{u}_e i\sigma_{\mu\nu} q^\nu (F_1 + F_2 \gamma^5) u_\mu \epsilon^{*\mu} \\ &= \bar{u}_e i\sigma_{\mu\nu} q^\nu (A_R P_R + A_L P_L) u_\mu \epsilon^{*\mu}, \end{aligned} \quad (33)$$

where u is Dirac spinor for the muon and electron, q is four momentum of an outgoing photon, $F_{1,2}$ are form factors, $A_{L,R}$ are left- and right-handed amplitude defined to be $A_{L,R} = F_1 \pm F_2$ and lastly $P_{L,R}$ are projection operators. From the amplitude, the helicity flip between initial particle and final particle should arise and this makes the helicity flip process takes place on one of external legs since the W gauge boson couples only to left-handed fields. Comparing the left diagram with the right, the left is proportional to the muon mass, while the right is proportional to the electron mass, which means that impact of the right is ignorable. The unpolarized squared amplitude $|\mathcal{M}|^2$ takes the form:

$$|\mathcal{M}|^2 = m_\mu^4 (A_R + A_L)^2 \simeq m_\mu^4 (A_R)^2 \quad (34)$$

Then, the decay rate is given by

$$\Gamma(\mu \rightarrow e\gamma) = \frac{|\mathcal{M}|^2}{16\pi m_\mu} = \frac{m_\mu^3}{16\pi} |A_R|^2 \quad (35)$$

where A_R is expressed by [72, 74]²

$$A_R = \frac{g^2 e}{128\pi^2} \frac{m_\mu}{M_W^2} \sum_{n=1,2,3,4,5} U_{2n} U_{1n}^* F(x_n) \left[1 - \frac{1}{3} \frac{\ln \xi}{\xi - 1} + \frac{1}{\xi - 1} \left(\frac{\xi \ln \xi}{\xi - 1} - 1 \right) \right] \quad (36)$$

Taking the unitary gauge into account, $\xi \rightarrow \infty$, the additional ξ -dependent terms in A_R all are cancelled by contribution of Goldstone bosons so A_R is gauge invariant. Substituting the gauge invariant A_R back into the decay rate of Equation 35 and dividing the expanded decay rate by the total muon decay rate $\Gamma(\mu \rightarrow e\nu\bar{\nu}) = G_F^2 m_\mu^5 / 192\pi^3$, we have the prediction for $\mu \rightarrow e\gamma$ decay [5, 72]:

$$\text{BR}(\mu \rightarrow e\gamma) = \frac{\Gamma(\mu \rightarrow e\gamma)}{\Gamma(\mu \rightarrow e\nu_\mu \bar{\nu}_e)} = \frac{3\alpha}{32\pi} \frac{|\sum_{n=1}^5 U_{2n} U_{n1}^\dagger F(x_n)|^2}{(UU^\dagger)_{11} (UU^\dagger)_{22}}, \quad (37)$$

where $x_n = M_n^2/M_W^2$ and the loop function $F(x_n)$ is

$$F(x_n) = \frac{10 - 43x_n + 78x_n^2 - (49 - 18 \log x_n)x_n^3 + 4x_n^4}{3(x_n - 1)^4}. \quad (38)$$

Numerator in Equation 37 can be simplified by separating the light neutrinos and heavy vector-like neutrinos as below (Contribution of the fifth neutrino $\tilde{\nu}_{4R}$ is safely ignored both by the suppression factor ϵ and by relative smallness of v_d compared to v_u):

$$\begin{aligned} \left| \sum_{n=1}^5 U_{2n} U_{n1}^\dagger F(x_n) \right|^2 &\simeq |U_{2i} U_{i1}^\dagger F(0) + U_{24} U_{41}^\dagger F(x_4)|^2 \\ U_{2i} U_{i1}^\dagger &= -\eta_{12}^* - \eta_{21} = -2\eta_{21} \\ U_{24} U_{41}^\dagger &= \Theta_{24} \Theta_{14}^* = 2\eta_{21} \\ \left| \sum_{n=1}^5 U_{2n} U_{n1}^\dagger F(x_n) \right|^2 &\simeq |4\eta_{21}|^2 (F(x_4) - F(0))^2 \end{aligned} \quad (39)$$

The final form for the CLFV $\mu \rightarrow e\gamma$ decay in this model reads:

$$\text{BR}(\mu \rightarrow e\gamma) = \frac{3\alpha_{\text{em}}}{8\pi} |\eta_{21}|^2 (F(x_4) - F(0))^2, \quad (40)$$

where α_{em} is the fine structure constant. We find that our theoretical prediction for the $\mu \rightarrow e\gamma$ decay can be expressed in terms of the deviation of unitarity η_{21} .

² Since the PMNS mixing matrix is multiplied by a factor of deviation of unitarity, it is not unitary any more. Therefore, the first term of sum over neutrino eigenstates in Equation (28) of [72] does not vanish and come in our prediction with a loop function $F(x_n)$.

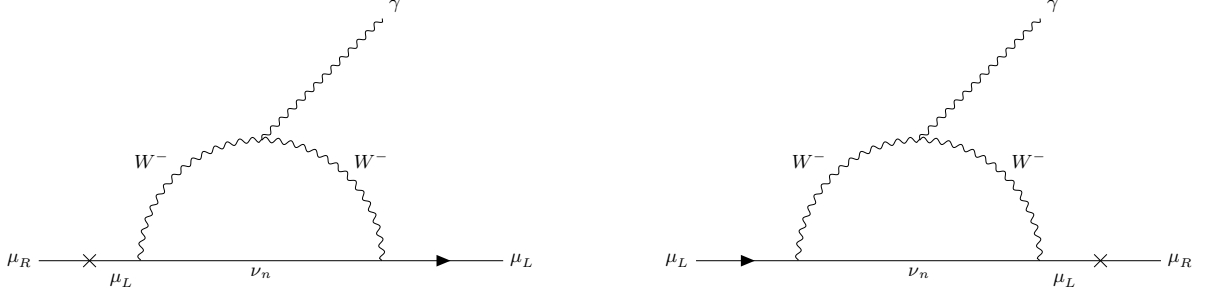


Figure 7: Diagrams for muon anomalous magnetic moment with all neutrinos($n = 1, 2, 3, 4, 5$)

C. The anomalous muon magnetic moment $g - 2$

We derive our prediction for the muon anomalous magnetic moment in this section and confirm the derived expression can be consistent with an expression of the theoretical prediction for $\mu \rightarrow e\gamma$ in references[72, 75]. Consider two possible diagrams for muon anomalous magnetic moment at one-loop level in Figure 7.

The amplitude for the muon anomalous magnetic moment at one-loop level is:

$$\begin{aligned}\mathcal{M}(\Delta a_\mu) &= \bar{u}_\mu i\sigma_{\mu\nu} q^\nu (F_1 + F_2 \gamma^5) u_\mu \epsilon^{*\mu} \\ &= \bar{u}_\mu i\sigma_{\mu\nu} q^\nu (A_R P_R + A_L P_L) u_\mu \epsilon^{*\mu}\end{aligned}\quad (41)$$

Unlike the CLFV $\mu \rightarrow e\gamma$ decay, muon anomaly diagrams have the same structure for helicity flip process. So we conclude A_R is equal to A_L and can make use of other expression of this amplitude to derive our own expression for Δa_μ [75].

$$\begin{aligned}V &= \bar{u}_\mu i\sigma_{\alpha\beta} q^\beta em_\mu (A_{\mu\mu}^M + \gamma_5 A_{\mu\mu}^E) u_\mu \epsilon^{*\alpha} \\ &= \bar{u}_\mu i\sigma_{\alpha\beta} q^\beta em_\mu ((A_{\mu\mu}^M + A_{\mu\mu}^E) P_R + (A_{\mu\mu}^M - A_{\mu\mu}^E) P_L) u_\mu \epsilon^{*\alpha}\end{aligned}\quad (42)$$

Comparing Equation 41 with Equation 42, we confirm that

$$\begin{aligned}A_R &= em_\mu (A_{\mu\mu}^M + A_{\mu\mu}^E) \\ A_L &= em_\mu (A_{\mu\mu}^M - A_{\mu\mu}^E)\end{aligned}\quad (43)$$

Here, we can use the condition that $A_R = A_L$ identified in Figure 7 and can rearrange $A_{L,R}$ in terms of $A_{\mu\mu}^{M,E}$, which are essential to derive our theoretical muon anomaly prediction. Then, we find our desirable form $A_{\mu\mu}^{M,E}$ for the muon anomalous magnetic moment.

$$\begin{aligned}A_{\mu\mu}^M &= \frac{1}{em_\mu} A_R = \frac{g^2}{128\pi^2} \frac{1}{M_W^2} \sum_{n=1,2,3,4,5} U_{2n} U_{2n}^* F(x_n) \\ A_{\mu\mu}^E &= 0\end{aligned}\quad (44)$$

Using the definition for both the muon anomalous magnetic moment and branching ratio of $\mu \rightarrow e\gamma$ decay in [75], we can check our analytic argument for the observable and constraint are correct.

$$\begin{aligned}\Delta a_\mu &= A_{\mu\mu}^M m_\mu^2 \\ \text{BR}(\mu \rightarrow e\gamma) &= \frac{3(4\pi)^3 \alpha_{\text{em}}}{4G_F^2} (|A_{\mu e}^M|^2 + |A_{\mu e}^E|^2)\end{aligned}\quad (45)$$

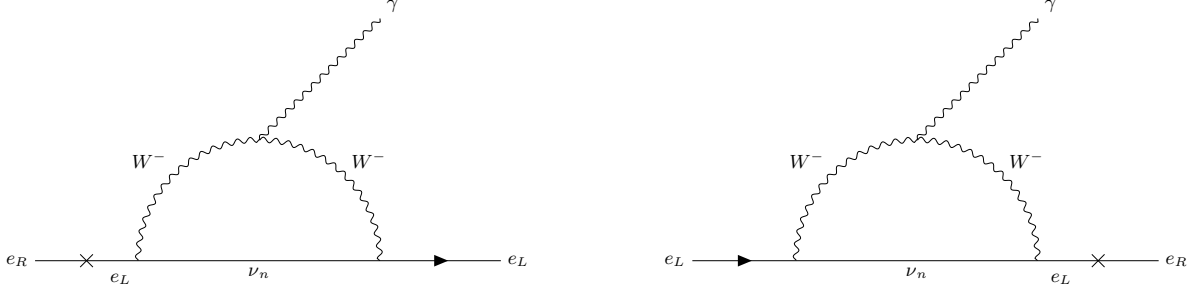


Figure 8: Diagrams for electron anomalous magnetic moment with all neutrinos($n = 1, 2, 3, 4, 5$)

One difference between $A_{\mu\mu}^{M,E}$ and $A_{L,R}$ is that $A_{\mu\mu}^{M,E}$ is only determined by the internal structure of the loop in Figure 7, whereas $A_{L,R}$ is the extended factor by multiplying $A_{\mu\mu}^{M,E}$ by the helicity flip mass in one of the external legs. Therefore, it is natural to think $A_{\mu\mu}^{M,E}$ is the same as $A_{\mu e}^{M,E}$ since their internal structure of loop are exactly same³. The muon anomalous magnetic moment and the branching ratio of $\mu \rightarrow e\gamma$ take the form:

$$\Delta a_\mu = \frac{\alpha_W}{32\pi} \frac{m_\mu^2}{M_W^2} \sum_{n=1,2,3,4,5} U_{2n} U_{2n}^* F(x_n)$$

$$\text{BR}(\mu \rightarrow e\gamma) = \frac{3\alpha_{\text{em}}}{32\pi} \left| \sum_{n=1,2,3,4,5} U_{2n} U_{1n}^* F(x_n) \right|^2 \quad (46)$$

where the α_W is the weak coupling constant. As for the branching ratio of $\mu \rightarrow e\gamma$ in Equation 46, we showed that substituting $A_{\mu e}$ back into the branching ratio in Equation 45 is exactly consistent with the one in Equation 37. Expanding the unitary mixing matrices in the muon anomaly prediction in Equation 46, yields the following relation:

$$\Delta a_\mu = \frac{\alpha_W}{32\pi} \frac{m_\mu^2}{M_W^2} ((1 - 2\eta_{22})F(0) + 2\eta_{22}F(x_4)). \quad (47)$$

Looking at Equation 47, it is clear that the SM part which is without η and the BSM having η are entangled together. We arrive at the right prediction for the muon anomaly at one-loop by removing the SM part from Equation 47

$$\Delta a_\mu = \frac{\alpha_W}{16\pi} \frac{m_\mu^2}{M_W^2} \eta_{22} (F(x_4) - F(0)). \quad (48)$$

Similarly to the branching ratio of $\mu \rightarrow e\gamma$ decay, it can be confirmed that the prediction for the muon anomaly also consists of the factor of deviation of unitarity η .

D. The anomalous electron magnetic moment $g - 2$

As in the muon anomalous magnetic moment, the same diagrams with external particles replaced by electrons can be generated in Figure 8.

Using the complete form of the muon anomaly prediction in Equation 48, we can derive the right prediction for the electron anomalous magnetic moment with slight modifications $m_\mu \rightarrow m_e, \eta_{22} \rightarrow \eta_{11}$.

³ One can concern the coefficient at the vertex with electron. However, this change is already reflected on the loop integration A_R of Equation 36 by U_{1n} . For the muon anomaly, the coefficient is simply replaced by U_{2n} , therefore, modification of the coefficient at the vertex does not harm our argument.

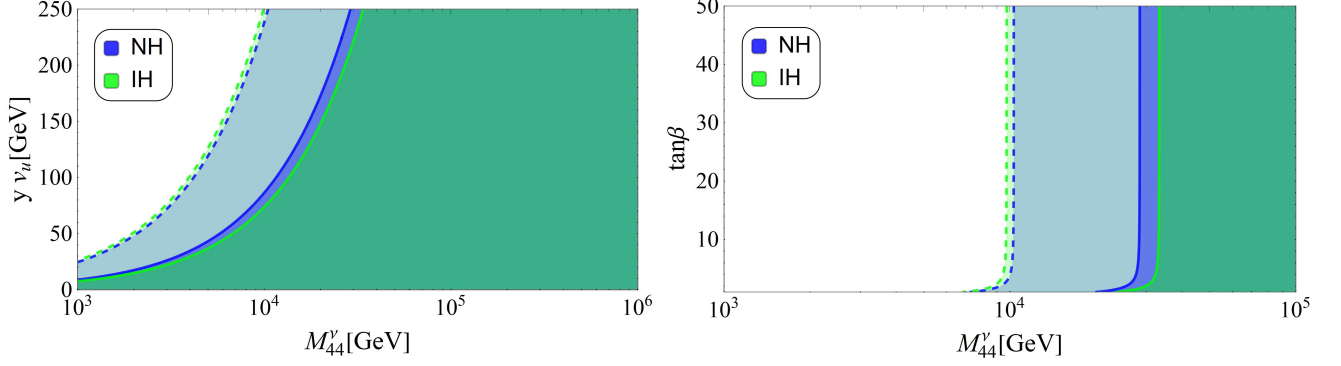


Figure 9: The left plot is an available parameter space for two free parameters: mass of vector-like neutrino M_{44}^ν and SM up-type Higgs vev v_u . Here, the free parameter y is set to 1. The right plot is the case where vev of the up-type Higgs is constrained from $246/\sqrt{2} \simeq 174$ to 246 GeV or from $\tan \beta = 1$ to 50 in a same way

$$\Delta a_e = \frac{\alpha_W}{16\pi} \frac{m_e^2}{M_W^2} \eta_{11} (F(x_4) - F(0)). \quad (49)$$

E. NUMERICAL ANALYSIS OF W EXCHANGE CONTRIBUTIONS

The presence of heavy vector-like neutrinos leads to the deviation of unitarity and the observables $\Delta a_{\mu,e}$ and constraint $\text{BR}(\mu \rightarrow e\gamma)$ can be written in terms of the factor of non-unitarity η .

$$\begin{aligned} \text{BR}(\mu \rightarrow e\gamma) &= \frac{3\alpha_{\text{em}}}{8\pi} |\eta_{21}|^2 (F(x_4) - F(0))^2 \\ \Delta a_\mu &= \frac{\alpha_W}{16\pi} \frac{m_\mu^2}{M_W^2} \eta_{22} (F(x_4) - F(0)) \\ \Delta a_e &= \frac{\alpha_W}{16\pi} \frac{m_e^2}{M_W^2} \eta_{11} (F(x_4) - F(0)). \end{aligned} \quad (50)$$

1. The branching ratio of $\mu \rightarrow e\gamma$ decay

We consider the branching ratio of $\mu \rightarrow e\gamma$ decay first. Since we assume that mass of heavy vector-like neutrinos are heavier than 1 TeV, the value of $F(0)$ for the light neutrinos converges to approximately 3.3, while that of $F(x_4)$ for the heavy vector-like neutrino converges to 1.3. Therefore, the branching ratio of $\mu \rightarrow e\gamma$ decay can be reduced to [5]

$$\text{BR}(\mu \rightarrow e\gamma) = \frac{3\alpha_{\text{em}}}{8\pi} |\eta_{21}|^2 (F(x_4) - F(0))^2 \leq \frac{3\alpha_{\text{em}}}{2\pi} |\eta_{21}|^2. \quad (51)$$

The non-unitarity η of Equation 30 consists of four free parameters: mass of heavy vector-like neutrinos M_{44}^ν , a real number y , a CP violation phase δ , and a Majorana phase α . The experimental branching ratio of $\mu \rightarrow e\gamma$ decay constrains the minimal parameter space in terms of M_{44}^ν and y , while setting up two phases δ, α which maximize or minimize the branching ratio of $\mu \rightarrow e\gamma$ [5], and the minimal parameter space is shown in Figure 9.

The left plot in Figure 9 is an available parameter space for mass of the vector-like neutrino versus the free parameter y times SM up-type Higgs vev v_u . The blue bold line corresponds to bound of the branching ratio of $\mu \rightarrow e\gamma$ decay at the normal hierarchy with CP violation phase $\delta = 0$ and Majorana phase $\alpha = 0$ and this line can be relaxed up to the blue dotted line where $\delta = 0$, $\alpha = 2\pi$. The green bold(dotted) line corresponds to the inverted hierarchy with $\delta = \pi/2(0)$ and $\alpha = \frac{9\pi}{10}(0)$. Since we are especially interested in the range of SM up-type Higgs vev v_u from

174 to 246 GeV, the right plot consistent with the interested range is extracted from the left after replacing v_u by $\tan \beta = v_u/v_d$ using the relation $v_u^2 + v_d^2 = (246 \text{ GeV})^2$.

As for the constraint of deviation of unitarity η with the CLFV $\mu \rightarrow e\gamma$ decay at 1σ , it is given by[76, 77]

$$|\eta_{21}| \leq 8.4 \times 10^{-6}. \quad (52)$$

2. The muon and electron anomalous magnetic moments $\Delta a_{\mu,e}$

As in the constraint for η_{21} in Equation 52, the other non-unitarities $\eta_{11,22}$ for the electron and muon anomalous magnetic moment are given by[5, 76]

$$\begin{aligned} \eta_{11} &< 4.2 \times 10^{-4} \text{ (for NH) , } < 4.8 \times 10^{-4} \text{ (for IH)} \\ \eta_{22} &< 2.9 \times 10^{-7} \text{ (for NH) , } < 2.4 \times 10^{-7} \text{ (for IH)} \end{aligned} \quad (53)$$

With the constraints $\eta_{11,22}$ in Equation 53, we can calculate impact of the muon and electron anomalous magnetic moments at NH(IH) using Equation 50.

$$\begin{aligned} \Delta a_\mu &= \frac{\alpha_W}{16\pi} \frac{m_\mu^2}{M_W^2} \eta_{22} (F(x_4) - F(0)) \simeq -6.6(-5.5) \times 10^{-16} \\ \Delta a_e &= \frac{\alpha_W}{16\pi} \frac{m_e^2}{M_W^2} \eta_{11} (F(x_4) - F(0)) \simeq -2.2(-2.6) \times 10^{-17} \end{aligned} \quad (54)$$

There are two interesting features in the above prediction for the muon and electron anomalous magnetic moments. One feature is sign of each prediction. As mentioned in the introduction, this prediction with the W exchange can not flip the sign of each anomaly. In order to explain both anomalies at 1σ , the prediction for both anomalies with W exchange requires additional contributions such as Z' or scalar exchange. Another feature is magnitude of each prediction. For the muon anomaly, the experimental order of magnitude at 1σ is about 10^{-9} , however our prediction is much smaller than that of the experimental bound as well as the electron anomaly, which means the non-unitarity derived from the presence of heavy vector-like neutrino can not bring the anomalies to the observable level. This inadequate prediction with W exchange has been a good motivation to search for another possibility such as scalar exchange.

V. HIGGS EXCHANGE CONTRIBUTIONS TO $(g-2)_\mu, (g-2)_e$ AND $\text{BR}(\mu \rightarrow e\gamma)$

The relevant sector for the muon and electron anomalous magnetic moments with scalar exchange is charged lepton, so revisit the effective Yukawa matrix for the charged leptons of Equation 9.

$$\begin{aligned} y_{ij}^e &= \begin{pmatrix} 0 & 0 & 0 \\ 0 & y_{24}^e x_{42}^e & y_{24}^e x_{43}^e \\ 0 & y_{34}^e x_{42}^e & y_{34}^e x_{43}^e \end{pmatrix} \frac{\langle \phi \rangle}{M_{44}^e} + \begin{pmatrix} y_{15}^e x_{51}^e & y_{15}^e x_{52}^e & y_{15}^e x_{53}^e \\ y_{25}^e x_{51}^e & y_{25}^e x_{52}^e & y_{25}^e x_{53}^e \\ y_{35}^e x_{51}^e & y_{35}^e x_{52}^e & y_{35}^e x_{53}^e \end{pmatrix} \frac{\langle \phi \rangle}{M_{55}^e} \\ &+ \begin{pmatrix} y_{51}^e x_{15}^L & y_{52}^e x_{15}^L & y_{53}^e x_{15}^L \\ y_{51}^e x_{25}^L & y_{52}^e x_{25}^L & y_{53}^e x_{25}^L \\ y_{51}^e x_{35}^L & y_{52}^e x_{35}^L & y_{53}^e x_{35}^L \end{pmatrix} \frac{\langle \phi \rangle}{M_{55}^L} + \begin{pmatrix} 0 & 0 & 0 \\ 0 & 0 & 0 \\ 0 & 0 & x_{34}^L y_{43}^e \end{pmatrix} \frac{\langle \phi \rangle}{M_{44}^L} \end{aligned} \quad (55)$$

The effective Yukawa matrix of Equation 55 in the mass basis is diagonalized by the universal seesaw mechanism due to involving a few of different mass scales. Therefore, the only diagonal components should alive in the mass matrix. In order to make the mass matrix diagonal, we assume that $y_{34}^e = x_{43}^e = y_{15,25,35}^e = x_{51,52,53}^e = x_{25,35}^L = y_{52,53}^e = 0$. Then, the mass matrix is reduced to

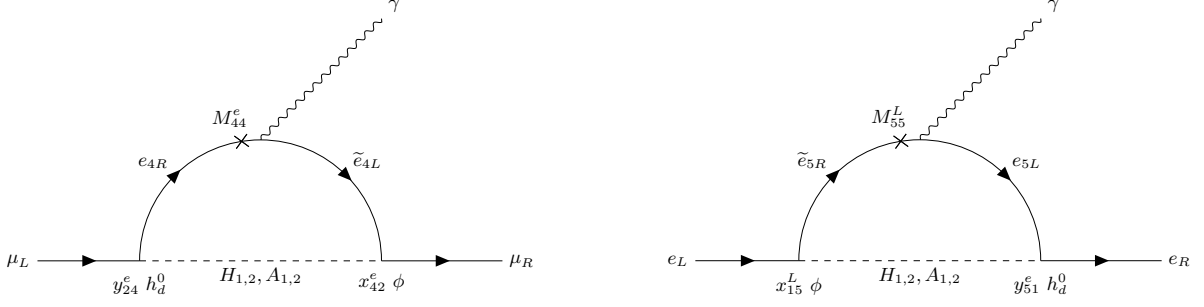


Figure 10: Diagrams contributing to the muon anomaly (left) and the electron anomaly (right) where $H_{1,2}$ are CP-even non-SM scalars and $A_{1,2}$ are CP-odd scalars in the physical basis

$$\begin{aligned}
 y_{ij}^e &= \begin{pmatrix} 0 & 0 & 0 \\ 0 & y_{24}^e x_{42}^e & 0 \\ 0 & 0 & 0 \end{pmatrix} \frac{\langle \phi \rangle}{M_{44}^e} + \begin{pmatrix} 0 & 0 & 0 \\ 0 & 0 & 0 \\ 0 & 0 & 0 \end{pmatrix} \frac{\langle \phi \rangle}{M_{55}^e} + \begin{pmatrix} y_{51}^e x_{15}^L & 0 & 0 \\ 0 & 0 & 0 \\ 0 & 0 & 0 \end{pmatrix} \frac{\langle \phi \rangle}{M_{55}^L} + \begin{pmatrix} 0 & 0 & 0 \\ 0 & 0 & 0 \\ 0 & 0 & x_{34}^L y_{43}^e \end{pmatrix} \frac{\langle \phi \rangle}{M_{44}^L} \\
 y_{ij}^e &= \begin{pmatrix} y_{51}^e s_{15}^L & 0 & 0 \\ 0 & y_{24}^e s_{24}^e & 0 \\ 0 & 0 & y_{43}^e s_{34}^L \end{pmatrix},
 \end{aligned} \tag{56}$$

where $s_{15}^L \simeq x_{15}^L \langle \phi \rangle / M_{55}^L$, $s_{24}^e \simeq x_{42}^e \langle \phi \rangle / M_{44}^e$, $s_{34}^L \simeq x_{34}^L \langle \phi \rangle / M_{44}^L$ and the diagonal elements from top-left to bottom-right should be responsible for electron, muon and tau Yukawa constants, respectively. After removing all irrelevant terms to both anomalies and applying the assumption, the 7×7 mass matrix in the interaction basis is also reduced to as below:

$$M^e = \left(\begin{array}{c|cccc} & e_{1R} & e_{2R} & e_{4R} & \tilde{L}_{5R} \\ \hline \bar{L}_{1L} & 0 & 0 & 0 & x_{15}^L v_\phi \\ \bar{L}_{2L} & 0 & 0 & y_{24}^e v_d & 0 \\ \bar{L}_{5L} & y_{51}^e v_d & 0 & 0 & M_{55}^L \\ \hline \tilde{e}_{4L} & 0 & x_{42}^e v_\phi & M_{44}^e & 0 \end{array} \right) \tag{57}$$

The reduced charged lepton mass matrix of Equation 57 clearly tells that no mixing between charged leptons arise so the branching ratio of $\mu \rightarrow e \gamma$ is naturally satisfied under this scenario. The scalar exchange for both anomalies can be realized by closing the Higgs sectors in Figure 3 as per Figure 10.

In Figure 10, the CP-even non-SM scalars $H_{1,2}$ and CP-odd scalars $A_{1,2}$ appear as a result of mixing between Higgses H_u, H_d and ϕ in the interaction basis. The Higgs sector in the interaction basis is defined by

$$H_u = \left(v_u + \frac{1}{\sqrt{2}} \begin{pmatrix} H_u^+ \\ \text{Re } H_u^0 + i \text{Im } H_u^0 \end{pmatrix} \right), \quad H_d = \left(v_d + \frac{1}{\sqrt{2}} \begin{pmatrix} \text{Re } H_d^0 + i \text{Im } H_d^0 \\ H_d^- \end{pmatrix} \right), \quad \phi = \frac{1}{\sqrt{2}} (v_\phi + \text{Re } \phi + i \text{Im } \phi). \tag{58}$$

For consistency, we equate v_u, v_d and v_ϕ to v_1, v_2 and v_3 , respectively.

A. The 2HDM scalar potential

The scalar potential of the model under consideration takes the form:

$$\begin{aligned}
 V &= \mu_1^2 (H_u H_u^\dagger) + \mu_2^2 (H_d H_d^\dagger) + \mu_3^2 (\phi \phi^*) - \mu_{\text{sb}}^2 [\phi^2 + (\phi^*)^2] + \lambda_1 (H_u H_u^\dagger)^2 + \lambda_2 (H_d H_d^\dagger)^2 \\
 &+ \lambda_3 (H_u H_u^\dagger) (H_d H_d^\dagger) + \lambda_4 (H_u H_u^\dagger) (H_d H_u^\dagger) + \lambda_5 (\epsilon_{ij} H_u^i H_d^j \phi^2 + \text{h.c.}) \\
 &+ \lambda_6 (\phi \phi^*)^2 + \lambda_7 (\phi \phi^*) (H_u H_u^\dagger) + \lambda_8 (\phi \phi^*) (H_d H_d^\dagger),
 \end{aligned} \tag{59}$$

where the λ_i ($i = 1, 2, \dots, 8$) are dimensionless parameters whereas the μ_j ($j = 1, 2, 3$) are dimensionful parameters and μ_{sb} is a dimensionfull soft-breaking parameter. We consider the $U(1)'$ symmetry as global in this model so our model does not feature Z' boson and the scalar potential requires the inclusion of the soft-breaking mass term $-\mu_{\text{sb}}^2 [\phi^2 + (\phi^*)^2]$ in order to prevent the appearance of a massless scalar state arising from the imaginary part of ϕ .

The minimization conditions of the scalar potential yield the following relations:

$$\begin{aligned}\mu_1^2 &= -2\lambda_1 v_1^2 - \lambda_3 v_2^2 - \frac{1}{2}\lambda_7 v_3^2 - \frac{\lambda_5 v_2 v_3^2}{2v_1}, \\ \mu_2^2 &= -\lambda_3 v_1^2 - \frac{\lambda_5 v_3^2 v_1}{2v_2} - 2\lambda_2 v_2^2 - \frac{1}{2}\lambda_8 v_3^2, \\ \mu_3^2 &= -\lambda_8 v_2^2 - \lambda_6 v_3^2 - v_1 (2\lambda_5 v_2 + \lambda_7 v_1) - 2\mu_{\text{sb}}^2.\end{aligned}\tag{60}$$

B. Mass matrix for CP-even, CP-odd neutral and charged scalars

The squared mass matrix for the CP-even scalars in the basis $(\text{Re } H_u^0, \text{Re } H_d^0, \text{Re } \phi)$ takes the form:

$$\mathbf{M}_{\text{CP-even}}^2 = \begin{pmatrix} 4\lambda_1 v_1^2 - \frac{\lambda_5 v_2 v_3^2}{2v_1} & \frac{1}{2}\lambda_5 v_3^2 + 2\lambda_3 v_1 v_2 & \sqrt{2}v_3 (\lambda_5 v_2 + \lambda_7 v_1) \\ \frac{1}{2}\lambda_5 v_3^2 + 2\lambda_3 v_1 v_2 & 4\lambda_2 v_2^2 - \frac{\lambda_5 v_1 v_3^2}{2v_2} & \sqrt{2}v_3 (\lambda_5 v_1 + \lambda_8 v_2) \\ \sqrt{2}v_3 (\lambda_5 v_2 + \lambda_7 v_1) & \sqrt{2}v_3 (\lambda_5 v_1 + \lambda_8 v_2) & 2\lambda_6 v_3^2 \end{pmatrix}.\tag{61}$$

From the mass matrix given above, we find that the CP-even scalar spectrum is composed of the 125 GeV SM-like Higgs h and two non-SM CP-even Higgses $H_{1,2}$. Furthermore, we assume that no mixing between the SM physical Higgs h and the two non-SM CP-even Higgses $H_{1,2}$ arise and this assumption constrains the $(1, 2)$, $(1, 3)$, $(2, 1)$ and $(3, 1)$ elements of CP-even mass matrix of Equation 61. The constraints are given by the following decoupling limit scenario

$$\begin{aligned}\lambda_5 &= \frac{-4v_1 v_2}{v_3^2} \lambda_3 \\ \lambda_7 &= -\frac{v_2}{v_1} \lambda_5 = \frac{4v_2^2}{v_3^2} \lambda_3,\end{aligned}\tag{62}$$

and then the CP-even mass matrix of Equation 61 with the constraints is simplified to

$$\mathbf{M}_{\text{CP-even}}^2 = \begin{pmatrix} 4\lambda_1 v_1^2 + 2v_2^2 \lambda_3 & 0 & 0 \\ 0 & 4\lambda_2 v_2^2 + 2v_1^2 \lambda_3 & \sqrt{2}v_3 \left(-\frac{4v_1^2 v_2}{v_3^2} \lambda_3 + \lambda_8 v_2\right) \\ 0 & \sqrt{2}v_3 \left(-\frac{4v_1^2 v_2}{v_3^2} \lambda_3 + \lambda_8 v_2\right) & 2\lambda_6 v_3^2 \end{pmatrix}.\tag{63}$$

In the above given decoupling limit scenario, chosen in order to simplify our analysis, the CP-even neutral scalar states contained in the $SU(2)$ doublet H_u will not mix with the CP-even neutral ones contained in H_d . In such limit, the neutral CP-even states of H_u will not feature mixing with the gauge singlet scalar ϕ . Thus, the lightest 125 GeV CP-even scalar of our model will have couplings to the SM particles close to the SM expectation, which is consistent with the current experimental data.

Diagonalizing the simplified CP-even mass matrix, it reveals masses of the physical SM Higgs h and non-SM CP-even scalars $H_{1,2}$ in the physical basis (h, H_1, H_2)

$$R_{\text{CP-even}}^\dagger \mathbf{M}_{\text{CP-even}}^2 R_{\text{CP-even}} = \text{diag} (m_h^2, m_{H_1}^2, m_{H_2}^2).\tag{64}$$

The SM Higgs h is appeared as $\text{Re } H_u^0$ itself and the non-SM CP-even scalars $H_{1,2}$ are the states which $\text{Re } H_d^0$ is mixed with $\text{Re } \phi$. Regarding the CP-odd scalar sector, we find that the squared mass matrix for the CP-odd scalars in the

basis $(\text{Im } H_u^0, \text{Im } H_d^0, \text{Im } \phi)$ is given by:

$$\mathbf{M}_{\text{CP-odd}}^2 = \begin{pmatrix} -\frac{\lambda_5 v_2 v_3^2}{2v_1} & -\frac{1}{2}\lambda_5 v_3^2 & -\sqrt{2}\lambda_5 v_2 v_3 \\ -\frac{1}{2}\lambda_5 v_3^2 & -\frac{\lambda_5 v_1 v_3^2}{2v_2} & -\sqrt{2}\lambda_5 v_1 v_3 \\ -\sqrt{2}\lambda_5 v_2 v_3 & -\sqrt{2}\lambda_5 v_1 v_3 & -4\lambda_5 v_1 v_2 - 4\mu_{\text{sb}}^2 \end{pmatrix}. \quad (65)$$

The squared CP-odd mass matrix is diagonalized in the same way as in the CP-even mass matrix and the CP-odd physical basis is given by (G_Z, A_1, A_2) where G_Z is the massless Goldstone bosons associated with the longitudinal components of the Z gauge boson, whereas A_1 and A_2 are massive non-SM CP-odd scalars

$$R_{\text{CP-odd}}^\dagger \mathbf{M}_{\text{CP-odd}}^2 R_{\text{CP-odd}} = \text{diag}(0, m_{A_1}^2, m_{A_2}^2). \quad (66)$$

Furthermore, the squared mass matrix for the electrically charged scalars is given by:

$$\mathbf{M}_{\text{charged}}^2 = \begin{pmatrix} \lambda_4 v_2^2 - \frac{\lambda_5 v_2 v_3^2}{2v_1} & \lambda_4 v_1 v_2 - \frac{1}{2}\lambda_5 v_3^2 \\ \lambda_4 v_1 v_2 - \frac{1}{2}\lambda_5 v_3^2 & \lambda_4 v_1^2 - \frac{\lambda_5 v_1 v_3^2}{2v_2} \end{pmatrix}. \quad (67)$$

The charged scalar mass matrix can be diagonalized in the basis (H_1^\pm, H_2^\pm) as in CP-even or -odd mass matrix:

$$R_{\text{charged}}^\dagger \mathbf{M}_{\text{charged}}^2 R_{\text{charged}} = \text{diag}(0, m_{H^\pm}^2). \quad (68)$$

Then, the electrically charged scalar sector contains the massive scalars H^\pm and the massless electrically charged scalars G_W^\pm which correspond to the Goldstone bosons associated with the longitudinal components of the W^\pm gauge bosons. In the following sections we will analyze the phenomenological implications of our model in the Higgs diphoton decay as well as in the muon and electron anomalous magnetic moments.

C. The Higgs diphoton signal strength

The rate for the $h \rightarrow \gamma\gamma$ decay is given by:

$$\Gamma(h \rightarrow \gamma\gamma) = \frac{\alpha_{\text{em}}^2 m_h^3}{256\pi^3 v^2} \left| \sum_f a_{hff} N_C Q_f^2 F_{1/2}(\rho_f) + a_{hWW} F_1(\rho_W) + \frac{C_{hH^\pm H^\mp} v}{2m_{H^\pm}^2} F_0(\rho_{H_k^\pm}) \right|^2, \quad (69)$$

where ρ_i are the mass ratios $\rho_i = \frac{m_h^2}{4M_i^2}$ with $M_i = m_f, M_W$; α_{em} is the fine structure constant; N_C is the color factor ($N_C = 1$ for leptons and $N_C = 3$ for quarks) and Q_f is the electric charge of the fermion in the loop. From the fermion-loop contributions we only consider the dominant top quark term. Furthermore, $C_{hH^\pm H^\mp}$ is the trilinear coupling between the SM-like Higgs and a pair of charged Higgses, whereas a_{htt} and a_{hWW} are the deviation factors from the SM Higgs-top quark coupling and the SM Higgs-W gauge boson coupling, respectively (in the SM these factors are unity). Such deviation factors are close to unity in our model and they are defined as below:

$$a_{htt} \simeq 1, \quad a_{hWW} = \frac{1}{\sqrt{v_1^2 + v_2^2}} \frac{\partial}{\partial h} \left(\sum_{i,j=1,2,3} v_i (R_{\text{CP-even}}^T)_{ij} (h, H_1, H_2)_j \right) = \frac{v_1}{\sqrt{v_1^2 + v_2^2}} \quad (70)$$

Furthermore, $F_{1/2}(z)$ and $F_1(z)$ are the dimensionless loop factors for spin-1/2 and spin-1 particles running in the internal lines of the loops. These loop factors take the form:

$$\begin{aligned} F_{1/2}(z) &= 2(z + (z-1)f(z))z^{-2}, \\ F_1(z) &= -2(2z^2 + 3z + 3(2z-1)f(z))z^{-2}, \\ F_0(z) &= -(z - f(z))z^{-2}, \end{aligned} \quad (71)$$

with

$$f(z) = \begin{cases} \arcsin^2 \sqrt{z} & \text{for } z \leq 1 \\ -\frac{1}{4} \left(\ln \left(\frac{1+\sqrt{1-z^{-1}}}{1-\sqrt{1-z^{-1}}-i\pi} \right) \right)^2 & \text{for } z > 1 \end{cases} \quad (72)$$

In order to study the implications of our model in the decay of the 125 GeV Higgs into a photon pair, one introduces the Higgs diphoton signal strength $R_{\gamma\gamma}$, which is defined as:

$$R_{\gamma\gamma} = \frac{\sigma(pp \rightarrow h)\Gamma(h \rightarrow \gamma\gamma)}{\sigma(pp \rightarrow h)_{\text{SM}}\Gamma(h \rightarrow \gamma\gamma)_{\text{SM}}} \simeq a_{htt}^2 \frac{\Gamma(h \rightarrow \gamma\gamma)}{\Gamma(h \rightarrow \gamma\gamma)_{\text{SM}}}. \quad (73)$$

That Higgs diphoton signal strength, normalizes the $\gamma\gamma$ signal predicted by our model in relation to the one given by the SM. Here we have used the fact that in our model, single Higgs production is also dominated by gluon fusion as in the Standard Model.

The ratio $R_{\gamma\gamma}$ has been measured by CMS and ATLAS collaborations with the best fit signals [78, 79]:

$$R_{\gamma\gamma}^{\text{CMS}} = 1.18^{+0.17}_{-0.14} \quad \text{and} \quad R_{\gamma\gamma}^{\text{ATLAS}} = 0.96 \pm 0.14. \quad (74)$$

As it will be shown in the next subsection, the constraints arising from the Higgs diphoton decay rate will be considered in our numerical analysis.

D. The muon and electron anomalous magnetic moments

The Yukawa interactions relevant for the computation of the muon anomalous magnetic moment are:

$$\mathcal{L}_{\Delta a_\mu} = y_{24}^e \mu (\text{Re } H_d^0 - i\gamma^5 \text{Im } H_d^0) \bar{e}_4 + x_{42}^e \tilde{e}_4 (\text{Re } \phi - i\gamma^5 \text{Im } \phi) \bar{e}_2 + M_{44}^e \tilde{e}_4 \bar{e}_4 + \text{h.c.} \quad (75)$$

where the Yukawa coupling constants y_{24}^e, x_{42}^e are assumed to be real, the scalar fields have been expanded by their real and imaginary parts and the properties of the projection operators $P_{L,R}$ acting on the charged leptonic fields have been used.

By expressing the scalar fields in the interaction basis in terms of the scalar fields in the physical basis, the charged lepton Yukawa interactions relevant for the computation of the $g-2$ anomalies take the form:

$$\begin{aligned} \mathcal{L}_{\Delta a_\mu} = & y_{24}^e \mu ((R_e^T)_{22} H_1 + (R_e^T)_{23} H_2 - i\gamma^5 (R_o^T)_{22} A_1 - i\gamma^5 (R_o^T)_{23} A_2) \bar{e}_4 \\ & + x_{42}^e \tilde{e}_4 ((R_e^T)_{32} H_1 + (R_e^T)_{33} H_2 - i\gamma^5 (R_o^T)_{32} A_1 - i\gamma^5 (R_o^T)_{33} A_2) \bar{e}_2 + M_{44}^e \tilde{e}_4 \bar{e}_4 + \text{h.c.} \end{aligned} \quad (76)$$

where we are using the unitary gauge where the contributions arising from unphysical Goldstone bosons to the muon anomaly are excluded and we shorten the notations R_{CP} by $R_{e(o)}$. Here R_e and R_o are the rotation matrices that diagonalize the squared mass matrices for the CP even and CP odd scalars, respectively. Then, it follows that the muon and electron anomalous magnetic moments in the scenario of diagonal SM charged lepton mass matrix take the form:

$$\begin{aligned} \Delta a_\mu = & y_{24}^e x_{42}^e \frac{m_\mu^2}{8\pi^2} \left[(R_e^T)_{22} (R_e^T)_{32} I_S^{(\mu)}(m_{e_4}, m_{H_1}) + (R_e^T)_{23} (R_e^T)_{33} I_S^{(\mu)}(m_{e_4}, m_{H_2}) \right. \\ & \left. - (R_o^T)_{22} (R_o^T)_{32} I_P^{(\mu)}(m_{e_4}, m_{A_1}) - (R_o^T)_{23} (R_o^T)_{33} I_P^{(\mu)}(m_{e_4}, m_{A_2}) \right] \\ \Delta a_e = & y_{51}^e x_{15}^L \frac{m_e^2}{8\pi^2} \left[(R_e^T)_{22} (R_e^T)_{32} I_S^{(e)}(m_{e_5}, m_{H_1}) + (R_e^T)_{23} (R_e^T)_{33} I_S^{(e)}(m_{e_5}, m_{H_2}) \right. \\ & \left. - (R_o^T)_{22} (R_o^T)_{32} I_P^{(e)}(m_{e_5}, m_{A_1}) - (R_o^T)_{23} (R_o^T)_{33} I_P^{(E)}(m_{e_5}, m_{A_2}) \right], \end{aligned} \quad (77)$$

where the loop integrals are given by [75, 80–83]:

$$I_{S(P)}^{(e,\mu)}(m_{E_{4,5}}, m_S) = \int_0^1 \frac{x^2 \left(1 - x \pm \frac{m_{E_{4,5}}}{m_{e,\mu}}\right)}{m_{e,\mu}^2 x^2 + \left(m_{E_{4,5}}^2 - m_{e,\mu}^2\right)x + m_{S,P}^2(1-x)} dx \quad (78)$$

and $S(P)$ means scalar (pseudoscalar) and $E_{4,5}$ stands for the vector-like family. It is worth mentioning that E_4 and E_5 only contribute to the muon and electron anomalous magnetic moments, respectively.

VI. NUMERICAL ANALYSIS OF THE HIGGS EXCHANGE CONTRIBUTIONS

For the sake of simplicity, we consider the scenario of absence of mixing between SM charged leptons, which automatically prevents charged lepton flavour violating decays. In our numerical analysis we have found that the non-SM CP-even scalar mass can reach values around 200 GeV. Despite the fact that the non SM CP-even scalar is quite light and can have a sizeable decay mode into a bottom-anti bottom quark pair, its single LHC production via gluon fusion mechanism is strongly suppressed since it is dominated by the triangular bottom quark loop. Such non SM CP-even scalar H can also be produced by vector boson fusion but such production is expected to have a low total cross section due to small HWW and HZZ couplings, which are proportional to v_d . In this section we will discuss the implications of our model in the muon and electron anomalous magnetic moments.

A. The fitting function χ^2 and free parameter setup

For the first approach to both anomalies, we construct the fitting function χ^2

$$\begin{aligned} \chi^2 = & \frac{\left(m_h^{\text{Thy}} - m_h^{\text{Cen}}\right)^2}{\left(\delta m_h^{\text{Dev}}\right)^2} + \frac{\left(a_{hWW}^{\text{Thy}} - a_{hWW}^{\text{Cen}}\right)^2}{\left(\delta a_{hWW}^{\text{Dev}}\right)^2} + \frac{\left(R_{\gamma\gamma}^{\text{Thy}} - R_{\gamma\gamma}^{\text{Cen}}\right)^2}{\left(\delta R_{\gamma\gamma}^{\text{Dev}}\right)^2} \\ & + \frac{\left(\Delta a_\mu^{\text{Thy}} - \Delta a_\mu^{\text{Cen}}\right)^2}{\left(\delta \Delta a_\mu^{\text{Dev}}\right)^2} + \frac{\left(\Delta a_e^{\text{Thy}} - \Delta a_e^{\text{Cen}}\right)^2}{\left(\delta \Delta a_e^{\text{Dev}}\right)^2}, \end{aligned} \quad (79)$$

where the superscripts Thy, Cen and Dev mean theoretical prediction, central value of experimental bound and deviation from the central value at one of $1, 2, 3\sigma$, respectively. The parameters used in this fitting function are defined as below (the integer number multiplied in delta terms means σ):

$$\begin{aligned} m_h^{\text{Cen}} &= 125.38 \text{ GeV}, & \delta m_h^{\text{Dev}} &= 3 \times 0.14 \text{ GeV}, \\ a_{hWW}^{\text{Cen}} &= 0.59, & \delta a_{hWW}^{\text{Dev}} &= 1 \times 0.35, \\ R_{\gamma\gamma}^{\text{Cen}} &= \frac{1}{2} (R_{\gamma\gamma}^{\text{CMS}} + R_{\gamma\gamma}^{\text{ATLAS}}) = 1.07, & \delta R_{\gamma\gamma}^{\text{Dev}} &= 1 \times 0.14, \\ \Delta a_\mu^{\text{Cen}} &= 26.1 \times 10^{-10}, & \delta \Delta a_\mu^{\text{Dev}} &= 1 \times (8.0 \times 10^{-10}) \\ \Delta a_e^{\text{Cen}} &= -0.88 \times 10^{-12}, & \delta \Delta a_e^{\text{Dev}} &= 2 \times (0.36 \times 10^{-12}) \end{aligned} \quad (80)$$

For an initial scan, we set up the starting parameter region as below:

Parameter	Value/Scanned Region(GeV)
$v_u = v_1$	$\frac{\tan \beta}{\sqrt{1+\tan^2 \beta}} \times 246$
$v_d = v_2$	$\frac{1}{\sqrt{1+\tan^2 \beta}} \times 246$
$v_\phi = v_3$	$\pm[0.01, 1.00] \times 1000$
$\tan \beta = v_u/v_d$	$[5, 50]$
λ_1	$\left(m_h^2 + \frac{v_2 v_3^2 \lambda_5}{2v_1}\right) / (4v_1^2)$
λ_2	$\pm [0.50, 12.00]$
λ_3	$\pm [0.50, 12.00]$
λ_4	$\pm [0.50, 12.00]$
λ_5	$-4v_1 v_2 \lambda_3 / (v_3)^2$
λ_6	$\pm [0.50, 12.00]$
λ_7	$-v_2 \lambda_5 / v_1$
λ_8	$\pm [0.50, 12.00]$
M_{44}^e	$[2 \times 10^2, 2 \times 10^3]$
M_{55}^L	$[2 \times 10^2, 2 \times 10^3]$
μ_{sb}	$i^{[0,1]} \times [300, 500]$
y_e	$\sqrt{2}m_e/v_2$
y_μ	$\sqrt{2}m_\mu/v_2$
y_{24}^e	$\pm [1.0, 3.5]$
y_{51}^e	$\pm [1.0, 3.5]$
x_{42}^e	$ y_\mu M_{44}^e / (y_{24}^e v_3) $
x_{15}^L	$ y_e M_{55}^L / (y_{51}^e v_3) $

Table II: Initial parameter setup

1. For the Higgs vevs, we are interested in the range of $\tan \beta$ from 5 to 50 as in the W boson exchange in Figure 9
2. For λ_1 , we fixed mass of the SM physical Higgs h to be 125 GeV to save time and to make the calculation faster. For $\lambda_{5,7}$, the assumption that no mixing between the SM Higgs h and non-SM Higgses $H_{1,2}$ arise is reflected on these parameters. The other quartic coupling constants $\lambda_{2,3,4,6,8}$ are set up not to go over 4π for perturbativity.
3. For the vector-like masses M_{44}^e and M_{55}^L , there is a constraint that the lightest should be greater than 200 GeV [84].
4. In our numerical analysis we consider solutions where the non SM scalar masses are larger than about 200 GeV as done in [85].
5. The soft-breaking mass term μ_{sb} is a free parameter, which does not generate any problem and appropriate values of this parameters yields masses for scalars and vector-like fermions consistent with the experimental constraints.
6. The diagonal Yukawa constants appearing in Equation 56 should be the Yukawa constant for electron, muon and tau, respectively. The Yukawa constants $y_{24,51}$ and $x_{42,15}$ interacting with vector-like families are defined under this consideration. For perturbativity, the Yukawa constants $y_{24,51}$ are considered not to go over $\sqrt{4\pi}$.

After saturating value of the χ^2 function less than or nearly 2 which we believe it is converged enough, we find a best peaked value for each free parameter. For the given parameters, we rename them by adding an index “p” to the end of subscript of each parameter like $\tan \beta_p$ and then the expansion factor κ is multiplied to find a correlation between

the observables and the mass parameters. Then, the parameter region is refreshed by both the specific value of each parameter and the expansion factor κ as per Table III.

Parameter	Value/Scanned Region(GeV)
$v_u = v_1$	$\frac{\tan \beta_p}{\sqrt{1+\tan^2 \beta_p}} \times 246$
$v_d = v_2$	$\frac{1}{\sqrt{1+\tan^2 \beta_p}} \times 246$
$v_\phi = v_3$	$[(1-\kappa), (1+\kappa)] \times v_{3p}$
$\tan \beta = v_u/v_d$	$[(1-\kappa), (1+\kappa)] \times \tan \beta_p$
λ_1	$\left(m_h^2 + \frac{v_2 v_3^2 \lambda_5}{2v_1}\right) / (4v_1^2)$
λ_2	$[(1-\kappa), (1+\kappa)] \times \lambda_{2p}$
λ_3	$[(1-\kappa), (1+\kappa)] \times \lambda_{3p}$
λ_4	$[(1-\kappa), (1+\kappa)] \times \lambda_{4p}$
λ_5	$-4v_1 v_2 \lambda_3 / (v_3)^2$
λ_6	$[(1-\kappa), (1+\kappa)] \times \lambda_{6p}$
λ_7	$-v_2 \lambda_5 / v_1$
λ_8	$[(1-\kappa), (1+\kappa)] \times \lambda_{8p}$
M_{44}^e	$[(1-\kappa), (1+\kappa)] \times M_{44p}^e$
M_{55}^L	$[(1-\kappa), (1+\kappa)] \times M_{55p}^L$
μ_{sb}	$[(1-\kappa), (1+\kappa)] \times \mu_{sbp}$
y_e	$\sqrt{2}m_e/v_2$
y_μ	$\sqrt{2}m_\mu/v_2$
y_{24}^e	$[(1-\kappa), (1+\kappa)] \times y_{24p}^e$
y_{51}^e	$[(1-\kappa), (1+\kappa)] \times y_{51p}^e$
x_{42}^e	$y_\mu M_{44}^e / (y_{24}^e v_3)$
x_{15}^L	$y_e M_{55}^L / (y_{51}^e v_3)$
κ	0.1

Table III: Next parameter setup after the initial scan result

B. A scanned result on the free parameters as well as observables across over the first and second scan

The best peaked value for each parameter is listed in Table IV and energy scale is in unit of GeV. Note that all cases are carried out independently and all points of plots in each case are collected within 1σ constraint of each anomaly.

Parameter	case A	case B	case C	case D
$v_u = v_1$	245.925	245.936	245.951	245.917
$v_d = v_2$	6.086	5.595	4.921	6.387
$v_\phi = v_3$	-57.761	-36.470	-57.919	-30.746
$\tan \beta = v_u/v_d$	40.410	43.957	49.977	38.503
λ_1	0.063	0.064	0.066	0.064
λ_2	-7.978	8.414	-2.000	2.948
λ_3	6.344	2.675	-6.242	1.724
λ_4	1.859	2.158	-3.633	10.837
λ_5	-11.384	-11.070	-9.009	-11.460
λ_6	2.888	1.228	0.866	1.351
λ_7	0.282	0.252	-0.180	0.298
λ_8	-1.363	-1.346	-10.845	-11.510
M_{44}^e	1475.010	1355.470	1495.770	1134.340
M_{55}^L	279.386	211.263	204.706	323.292
μ_{sb}	424.618 <i>i</i>	443.435 <i>i</i>	480.993	480.062 <i>i</i>
$y_e [10^{-4}]$	1.135	1.234	1.403	1.081
$y_\mu [10^{-2}]$	2.391	2.600	2.956	2.278
y_{24}^e	-3.161	-3.101	-2.942	-1.548
y_{51}^e	2.315	2.164	2.050	1.352
x_{42}^e	0.193	0.312	0.260	0.543
$x_{15}^L [10^{-4}]$	2.371	3.304	2.419	8.408
m_{H_1}	213.390	222.924	212.147	238.523
m_{H_2}	911.585	614.516	891.413	518.147
m_{A_1}	741.343	537.111	807.268	435.887
m_{A_2}	1003.790	939.553	1035.800	1006.240
m_{H^\pm}	938.259	674.054	987.625	929.786
$\Delta a_\mu [10^{-9}]$	2.734	2.688	2.935	2.891
$\Delta a_e [10^{-13}]$	-5.073	-8.310	-5.543	-6.365
a_{hWW}	1.000	1.000	1.000	1.000
$R_{\gamma\gamma}$	0.999	0.999	0.999	0.999
χ^2	1.794	1.516	1.870	1.740

Table IV: A best peaked value for each parameter at each case. All energy scale is in unit of GeV

Here, we put two constraints on the lightest vector-like mass and the lightest non-SM scalar mass; the vector-like mass should be greater than 200 GeV as well as the non-SM scalar mass[84, 85]. After we carry out second parameter scan based on the first scan result of Table IV, range of the parameters are given in Table V.

Parameter	case A	case B	case C	case D
$v_u = v_1$	[245.907 \rightarrow 245.938]	[245.921 \rightarrow 245.947]	[245.939 \rightarrow 245.959]	[245.898 \rightarrow 245.931]
$v_d = v_2$	[5.533 \rightarrow 6.761]	[5.087 \rightarrow 6.216]	[4.474 \rightarrow 5.468]	[5.807 \rightarrow 7.096]
$v_\phi = v_3$	[-63.525 \rightarrow -51.985]	[-40.117 \rightarrow -32.823]	[-63.706 \rightarrow -52.128]	[-33.820 \rightarrow -27.671]
$\tan \beta = v_u/v_d$	[36.371 \rightarrow 44.451]	[39.561 \rightarrow 48.353]	[44.980 \rightarrow 54.975]	[34.653 \rightarrow 42.354]
m_{H_1}	[200.000 \rightarrow 242.653]	[201.520 \rightarrow 246.046]	[200.000 \rightarrow 230.754]	[215.523 \rightarrow 261.920]
m_{H_2}	[752.061 \rightarrow 1088.130]	[516.289 \rightarrow 724.997]	[735.831 \rightarrow 1059.900]	[441.371 \rightarrow 604.981]
m_{A_1}	[638.813 \rightarrow 853.637]	[442.527 \rightarrow 640.705]	[670.550 \rightarrow 945.705]	[357.697 \rightarrow 516.760]
m_{A_2}	[892.847 \rightarrow 1141.780]	[847.825 \rightarrow 1032.140]	[927.768 \rightarrow 1154.640]	[907.576 \rightarrow 1105.770]
m_{H^\pm}	[783.823 \rightarrow 1111.600]	[580.316 \rightarrow 779.945]	[842.585 \rightarrow 1143.880]	[856.237 \rightarrow 1007.360]
M_{44}^e	[1327.510 \rightarrow 1622.510]	[1219.930 \rightarrow 1491.020]	[1346.190 \rightarrow 1645.330]	[1029.900 \rightarrow 1247.770]
M_{55}^L	[251.447 \rightarrow 307.323]	[200.000 \rightarrow 232.389]	[200.000 \rightarrow 225.176]	[290.963 \rightarrow 355.621]
$ \mu_{sb} $	[382.158 \rightarrow 467.079]	[399.091 \rightarrow 487.777]	[432.895 \rightarrow 529.091]	[432.059 \rightarrow 528.067]
$\Delta a_\mu [10^{-9}]$	[1.811 \rightarrow 3.410]	[1.810 \rightarrow 3.410]	[1.810 \rightarrow 3.410]	[1.810 \rightarrow 3.410]
$\Delta a_e [10^{-13}]$	[-6.730 \rightarrow -5.200]	[-11.142 \rightarrow -5.985]	[-7.207 \rightarrow -5.200]	[-8.721 \rightarrow -5.200]
a_{hWW}	[1.000 \rightarrow 1.000]	[1.000 \rightarrow 1.000]	[0.999 \rightarrow 1.000]	[1.000 \rightarrow 1.000]
$R_{\gamma\gamma}$	[0.999 \rightarrow 0.999]	[0.999 \rightarrow 0.999]	[0.999 \rightarrow 1.000]	[1.000 \rightarrow 1.000]
χ^2	[1.604 \rightarrow 2.750]	[1.501 \rightarrow 2.635]	[1.580 \rightarrow 2.761]	[1.509 \rightarrow 2.749]

Table V: A scanned range of each parameter at case A, B, C and D. $H_{1,2}$ mean non SM CP-even scalars and $A_{1,2}$ are non SM CP-odd scalars and H^\pm stand for non SM charged scalars in this model. All data of $\Delta a_{\mu,e}$ are collected within the 1σ constraint of each anomaly.

C. The muon and electron anomalous magnetic moments

In order to confirm that our theoretical prediction for both anomalies can accommodate their constraints at 1σ and to analyze correlations between both anomalies and mass parameters, we take a case B in Table IV since this benchmark point has the lowest value of the χ^2 function when compared to other cases. The reason that the case B has the lowest value of the χ^2 function arises from the obtained value of the electron anomaly, which is very close to the central experimental value. The four cases revealed the nearly central value of muon anomaly constraint at 1σ , whereas the other cases except B revealed the nearly edge value of electron anomaly constraint at 1σ . Therefore, the reason why the case B is most converged is related to whether our theoretical prediction for both anomalies can gain access to their central value of each anomaly constraint at 1σ . For this reason, we take the case B in Table V to study the correlations. The relevant parameter spaces are listed in Figure 11 and 12.

To begin with, we consider the parameter spaces for the muon anomaly versus electron anomaly with a mass parameter which attends both anomalies ($H_{1,2}, A_{1,2}$) and does not (H^\pm) in Figure 11. Even though the non-SM charged scalar does not attend both anomalies, the similar pattern which the other scalars implement in Figure 11 is also appeared. We confirmed that mass of H_2 is nearly proportional to that of H^\pm , which causes the correlation identified in plots of the other non-SM scalars in Figure 11 is still maintained for the non-SM charged scalar. Interestingly, the case A, B and C in Table V reported m_{H_2} is nearly proportional to m_{H^\pm} one-to-one ratio, whereas the case D revealed a fat proportion between them and still maintained the correlation.

As mentioned at the beginning of this section, we take the case B for the plots in Figure 11 and 12 and a main distinction between the case B and others arises from the value of electron anomaly. If we take other cases instead of the case B to investigate the parameter spaces, the darker region appeared in top-left plot of Figure 11 will be shifted upward by locating at the value of -5 or -6×10^{-13} for the electron anomaly. In other words, the whole colored region in Figure 11 is shifted upwards to meet the scanned value of electron anomaly constraint at 1σ , holding the correlations. Therefore, the white region appeared in Figure 11 is not strictly excluded region and affected by how

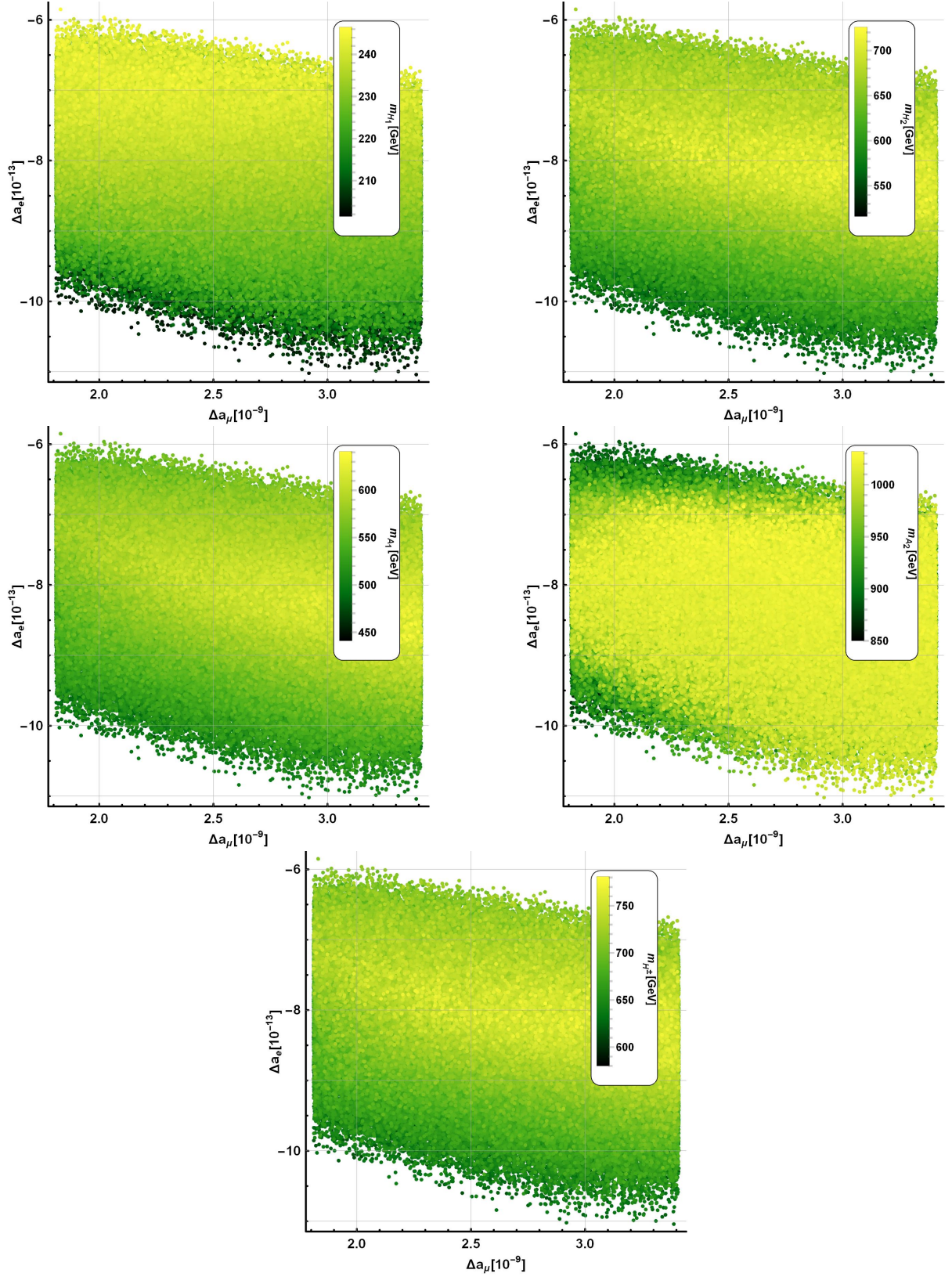


Figure 11: Available parameter spaces for the muon anomaly versus electron anomaly with a mass parameter which attends the both anomalies($H_{1,2}, A_{1,2}$) and does not(H^\pm). $H_{1,2}$ are non-SM CP even scalars, $A_{1,2}$ are non-SM CP odd scalars and H^\pm are non-SM charged scalars. All points in each plot are collected within 1σ constraint of each anomaly.

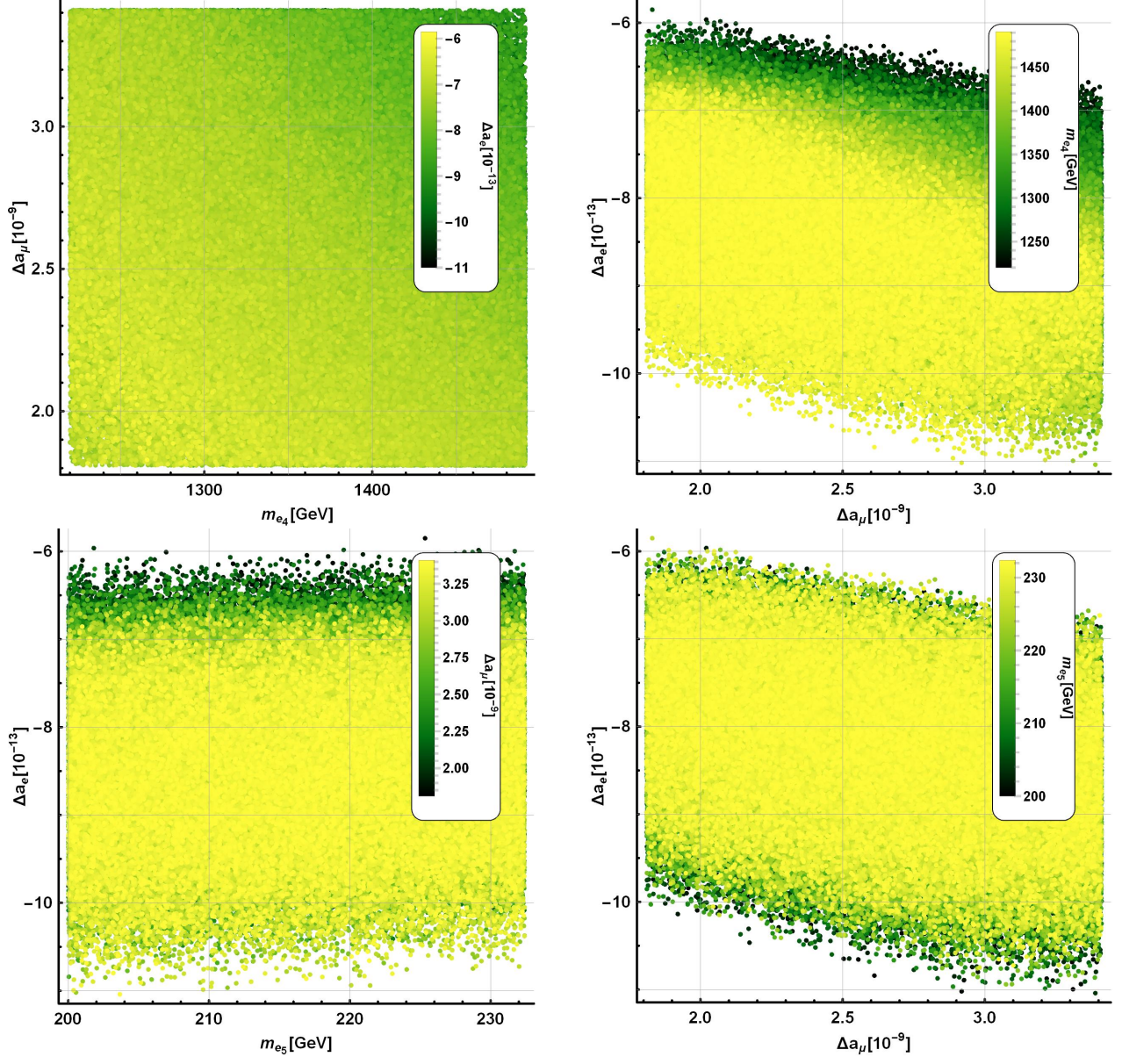


Figure 12: Available parameter spaces for the muon anomaly(electron anomaly) versus a relevant vector-like mass $m_{e_4}(m_{e_5})$ with another anomaly(two left plots) in bar where $m_{e_4}(m_{e_5})$ is simplified notation for $M_{44}^e(M_{55}^L)$, while the two right plots for the muon anomaly versus electron anomaly with a vector-like mass $m_{e_4}(m_{e_5})$

well a benchmark point is converged and by a factor of κ . However, these plots still tells a correlation between both anomalies and a tendency that the lighter mass of H_1 is located at lower region of the parameter space. Mass of the lightest non-SM scalar H_1 implied in top-left plot of Figure 11 is ranged from 201 to 246 GeV[85] and the cross section for this light non-SM scalar will be compared to that for SM Higgs in appendix. As for mass range of the other non-SM scalars confirmed in rest of other plots in Figure 11, they all implied heavier mass than that of H_1 which can be flexible depending on how the parameters are converged as seen in each case of Table V.

We investigate a correlation for an anomaly versus a relevant mass parameter with another anomaly in bar in Figure 12. Note that the fourth vector-like mass is relevant only for the muon anomaly, whereas the fifth is only for the electron anomaly. Even though the fourth(fifth) is irrelevant to the electron(muon) anomaly, it is good to express them together since we rearrange the mass parameter and the anomaly in bar for comparison. The top-left plot in Figure 12 just fills in whole parameter region, thus no any correlation between the fourth vector-like mass and the muon anomaly is identified. After we rearranged the order of m_{e_4} and $\Delta a_{\mu,e}$ from the top-left plot, we can

confirm the similar correlation identified in Figure 11 from the top-right plot in Figure 12. The bottom-left plot identifies some correlation between the fifth vector-like mass and the electron anomaly contrary to the top-left plot. For the fifth vector-like mass, we put the constraint that the lightest vector-like mass should be greater than 200 GeV [84] and the mass region below 200 GeV is all excluded. After rearranging the order of m_{e5} and Δa_μ as in the above plot, we confirmed the similar correlation appeared in the bottom-right plot. Interestingly, the top-right and the bottom-right plots checked the similar correlation.

We confirmed that the muon and electron anomalous magnetic moments with vector-like particles can be explained to within 1σ constraint of each anomaly in a unified way, which is based on two attributes; the first one is the extended scalar sector and the second one is related with the contributions of the vector-like leptons. The first one which is reflected in our prediction for both anomalies, consists of four non-SM scalars and these contributions play a crucial role for determining the magnitude of each anomaly. The second one is seen by two vertices of both anomaly diagrams. The other Yukawa interactions can take place at each vertex since the vector-like leptons come in the loop, which is differentiated by the case where the normal SM particles enter in the loop. To be more specific, the helicity flip mass caused by the vector-like fermions in the CP-even and CP-odd basis couples the initial particle inside the loop to another particle of different chirality, thus allowing different interactions at each vertex. This means that the different sign problem can be solved by only considering multiplication of the Yukawa constants of each vertex and this property will be covered in detail in next subsection.

1. How is the scalar exchange possible to accommodate both anomalies at 1σ constraint analytically?

In order to analyze how the scalar exchange is able to explain both anomalies within the 1σ range, we revisit the analytic expressions for both muon and electron anomalous magnetic moments:

$$\begin{aligned}\Delta a_\mu &= y_{24}^e x_{42}^e \frac{m_\mu^2}{8\pi^2} \left[(R_e^T)_{22} (R_e^T)_{32} I_S^{(\mu)}(m_{e4}, m_{H_1}) + (R_e^T)_{23} (R_e^T)_{33} I_S^{(\mu)}(m_{e4}, m_{H_2}) \right. \\ &\quad \left. - (R_o^T)_{22} (R_o^T)_{32} I_P^{(\mu)}(m_{e4}, m_{A_1}) - (R_o^T)_{23} (R_o^T)_{33} I_P^{(\mu)}(m_{e4}, m_{A_2}) \right], \\ \Delta a_e &= y_{51}^e x_{15}^L \frac{m_e^2}{8\pi^2} \left[(R_e^T)_{22} (R_e^T)_{32} I_S^{(e)}(m_{e5}, m_{H_1}) + (R_e^T)_{23} (R_e^T)_{33} I_S^{(e)}(m_{e5}, m_{H_2}) \right. \\ &\quad \left. - (R_o^T)_{22} (R_o^T)_{32} I_P^{(e)}(m_{e5}, m_{A_1}) - (R_o^T)_{23} (R_o^T)_{33} I_P^{(E)}(m_{e5}, m_{A_2}) \right],\end{aligned}\tag{81}$$

where

$$I_{S(P)}^{(e,\mu)}(m_{E_{4,5}}, m_S) = \int_0^1 \frac{x^2 \left(1 - x \pm \frac{m_{E_{4,5}}}{m_{e,\mu}}\right)}{m_{e,\mu}^2 x^2 + \left(m_{E_{4,5}}^2 - m_{e,\mu}^2\right) x + m_{S,P}^2 (1 - x)} dx\tag{82}$$

with $S(P)$ corresponding to scalar (pseudoscalar) and $E_{4,5}$ standing for the vector-like family. Furthermore, E_4 and E_5 only contribute to the muon and electron anomalous magnetic moments, respectively.

First of all, we focus on the sign of each anomaly. The different signs of each anomaly indicated by the 1σ experimentally allowed range can be understood at the level of Yukawa constants apart from the loop structures. As seen in Table II, the Yukawa coefficient y can be either positive or negative, while x only remains positive since we take the absolute value to the x . We also considered the case where the coefficients x, y are purely positive, assuming v_3 is positive, without taking absolute value and the multiplication of the Yukawa coefficients $x \times y$ cannot change the sign of each anomaly since the denominator of x includes y and they are cancel out. Then, the sign problem depends on summing over loop functions and we found that the order of the muon anomaly prediction is suitable, whereas the corresponding to the electron anomaly is about 10^{-16} which is too small to be accommodated within the 1σ experimentally allowed range. Therefore, we found that taking an absolute value to one of the Yukawa coefficients is an appropriate strategy for the sign and allows to reproduce the correct order of magnitude of each anomaly allowed by the 1σ experimentally allowed range, for an appropriate choice of the model parameters. This feature is a crucial difference compared with the W or Z' gauge boson exchange[26]. The W gauge boson exchange covered in the main body of this work keeps the same coupling constant at each vertex, therefore it is completely different from the scalar exchange with vector-like leptons. For the Z' exchange covered in [26], it has the common

property that the coupling constant of each vertex is different to each other, whereas the coupling constants of the Z' are more constrained by the mixing angle between i th chiral family and fourth vector-like family, so it is impossible to explain both anomalies at the same time. As a result, allowing different Yukawa constants with appropriate signs enables both anomalies to be explained in a unified way.

Next we turn our attention to the order of magnitude of our predictions for both anomalies. Considering that the sign problem is solved by having each Yukawa constant y either positive or negative, it can be easily understood that inside the structure in parentheses of Equation 81 should imply the same direction, which is determined by the contribution of all loop functions in parentheses. Since the mass difference among non-SM scalars and vector-like particles is not so big, we have to consider their masses in the computation of muon and electron anomalous magnetic moments, as follows from Equation 81. For an easy analysis, we take the case B reported in Table IV and suppose that

$$\begin{aligned} (R_e^T)_{22}(R_e^T)_{32} &= c_1, & (R_e^T)_{23}(R_e^T)_{33} &= -c_1, & (R_o^T)_{22}(R_o^T)_{32} &= c_2, & (R_o^T)_{23}(R_o^T)_{33} &= -c_2, \\ I_S^\mu(m_{e_4}, m_{H_1}) &= d_1, & I_S^\mu(m_{e_4}, m_{H_2}) &= d_2, & I_P^\mu(m_{e_4}, m_{A_1}) &= -d_3, & I_P^\mu(m_{e_4}, m_{A_2}) &= -d_4, \\ I_S^e(m_{e_5}, m_{H_1}) &= e_1, & I_S^e(m_{e_5}, m_{H_2}) &= e_2, & I_P^e(m_{e_5}, m_{A_1}) &= -e_3, & I_P^e(m_{e_5}, m_{A_2}) &= -e_4, \\ d_1 > d_3 > d_2 > d_4, & e_1 > e_3 > e_2 > e_4 \end{aligned} \quad (83)$$

where $c_{1,2}$ are arbitrary constant between 0 and 1 either positive or negative and mass ordering among $d(e)_i$, ($i = 1, 2, 3, 4$) can be easily understood by considering mass difference between non-SM scalars and vector-like particles. The muon and electron anomaly prediction can be rewritten in terms of these redefined constants:

$$\begin{aligned} \Delta a_\mu &= y_2 x_2 \frac{m_\mu^2}{8\pi^2} [c_1 d_1 - c_1 d_2 + c_2 d_3 - c_2 d_4] = y_2 x_2 \frac{m_\mu^2}{8\pi^2} [c_1 (d_1 - d_2) + c_2 (d_3 - d_4)] = y_2 x_2 \frac{m_\mu^2}{8\pi^2} [c_1 d_{12} + c_2 d_{34}] \\ \Delta a_e &= y_1 x_1 \frac{m_e^2}{8\pi^2} [c_1 e_1 - c_1 e_2 + c_2 e_3 - c_2 e_4] = y_1 x_1 \frac{m_e^2}{8\pi^2} [c_1 (e_1 - e_2) + c_2 (e_3 - e_4)] = y_1 x_1 \frac{m_e^2}{8\pi^2} [c_1 e_{12} + c_2 e_{34}] \end{aligned} \quad (84)$$

where y_2, x_2, y_1, x_1 are simplified notation for $y_{24}^e, x_{42}^e, y_{51}^e, x_{15}^L$, respectively, and $d(e)_{ij} \equiv d(e)_i - d(e)_j$ and $d(e)_{ij}$ are positive. Since the inside structure in parentheses depends on relative magnitude of both $c_{1,2}$ and $d(e)_{ij}$ at this stage where no more analytic simplification is possible, it is good to implement a specific value for them. Referring the values used to derive the result of case B, they are

$$\begin{aligned} y_2 x_2 \frac{m_\mu^2}{8\pi^2} c_1 d_1 &= 1.494 \times 10^{-7}, & y_1 x_1 \frac{m_e^2}{8\pi^2} c_1 e_1 &= -2.237 \times 10^{-12} \\ -y_2 x_2 \frac{m_\mu^2}{8\pi^2} c_1 d_2 &= -1.338 \times 10^{-7}, & -y_1 x_1 \frac{m_e^2}{8\pi^2} c_1 e_e &= 1.028 \times 10^{-12} \\ y_2 x_2 \frac{m_\mu^2}{8\pi^2} c_2 d_3 &= -9.839 \times 10^{-8}, & y_1 x_1 \frac{m_e^2}{8\pi^2} c_2 e_3 &= 8.406 \times 10^{-13} \\ -y_2 x_2 \frac{m_\mu^2}{8\pi^2} c_2 d_4 &= 8.541 \times 10^{-8}, & -y_1 x_1 \frac{m_e^2}{8\pi^2} c_2 e_4 &= -4.631 \times 10^{-13} \end{aligned} \quad (85)$$

and summing over all values in left or right column of Equation 85 yields the prediction for muon and electron anomaly at 1σ

$$\begin{aligned} \Delta a_\mu &= y_2 x_2 \frac{m_\mu^2}{8\pi^2} [c_1 d_1 - c_1 d_2 + c_2 d_3 - c_2 d_4] = 2.688 \times 10^{-9} \\ \Delta a_e &= y_1 x_1 \frac{m_e^2}{8\pi^2} [c_1 e_1 - c_1 e_2 + c_2 e_3 - c_2 e_4] = -8.310 \times 10^{-13}. \end{aligned} \quad (86)$$

VII. CONCLUSION

We have proposed a model to account for the hierarchical structure of the SM Yukawa couplings. In our approach the SM is an effective theory arising from a theory with extended particle spectrum and symmetries. The considered

model includes an extension of the 2HDM where the particle spectrum is enlarged by the inclusion of two vector-like fermion families, right handed Majorana neutrinos and a gauge singlet scalar field, together with the inclusion of a global $U(1)'$ symmetry spontaneously broken at the TeV scale. Since the $U(1)'$ symmetry is global, this model does not feature a Z' boson and it is softly broken in the 2HDM potential to avoid a Goldstone boson. Its main effect is to forbid SM Yukawa interactions due to the $U(1)'$ charge conservation. Besides that, this model has the property of the 2HDM type II where one Higgs doublet couples with the up-type fermions whereas the remaining one has Yukawa interactions with down-type fermions, where such couplings are allowed between chiral fermions and vector-like fermions due to the choice of $U(1)'$ charges (chiral fermions having zero charges while vector-like fermions, Higgs and flavons have charges ± 1). Below the mass scale of the vector-like fermions, such couplings result in effective Yukawa couplings suppressed by a factor $\langle \phi \rangle / M$ where the numerator is the vev of the flavon and the denominator is the vector-like mass. This factor naturally determines the magnitude of SM interactions and the mass scale for the vector-like fermions under a suitable choice of the flavon vev. We have developed a mixing formalism based on 7×7 mass matrices to describe the mixing of the three chiral families with the two vector-like families.

Within the above proposed model, we have focused on accommodating the long-established muon and less established electron anomalous magnetic moments at one-loop level. A main difficulty arises from the sign of each anomalous deviation of the experimental value from its SM prediction. Generally, the Feynman diagrams for the muon and electron anomalous magnetic moments have the same structure except from the fact that the external particles are different, which makes it difficult to flip the sign of each contribution. Specifically we have required that both deviations in Equation 1) at one-loop should be accommodated within the 1σ experimentally allowed range, which is a challenging requirement.

We first considered in detail the W boson exchange contributions to the muon and electron anomalous magnetic moments at one-loop. The relevant sector for the W boson exchange is that of the neutrino and we analyzed a novel operator that generates the masses of the light active neutrinos in this model. The well-known five dimensional Weinberg operator which we refer as type Ia seesaw mechanism does not work in this model since it is forbidden by the $U(1)$ symmetry due to the fact that both $SU(2)$ scalar doublets are negatively charged under this symmetry. For this reason, we made use of the Weinberg-like operator known as type Ib seesaw mechanism allowed in this model. With the type Ib seesaw mechanism, we built the neutrino mass matrix with two vector-like neutrinos and ignored fifth vector-like neutrinos since they are too heavy to contribute to the phenomenology. The deviation of unitarity η derived from the heavy vector-like neutrinos plays a crucial role for enhancing the sensitivity of the CLFV $\mu \rightarrow e\gamma$ decay to the observable level. Furthermore, the Yukawa constants of Dirac neutrino mass matrix can be connected to the observables measured in neutrino oscillation experiments. One of the neutrino Yukawa constants is defined with a suppression factor ϵ . Therefore, the effective 3×3 neutrino mass matrix tells that the tiny masses of the light active neutrinos depend on the mass scale of vector-like neutrinos as well as on the suppression factor ϵ . This implies that mass scale of vector-like neutrinos is not required to be of the order of 10^{14} GeV, as in the conventional type Ia seesaw mechanism. In our proposed model, the vector-like neutrinos can have masses at the TeV scale, thus allowing to test our model at colliders. Those vector-like neutrinos can be pair produced at the LHC via Drell-Yan annihilation mediated by a virtual Z gauge boson. They can also be produced in association with a SM charged lepton via Drell-Yan annihilation mediated by a W gauge boson. These heavy vector like sterile neutrinos can decay into a SM charged lepton and light active neutrinos. Thus, the heavy neutrino pair production at a proton-proton collider will give rise to an opposite sign dilepton final state, which implies that the observation of an excess of events in this final state over the SM background can be a smoking gun signature of this model, whose observation will be crucial to assess its viability. It is confirmed that the branching ratio of $\mu \rightarrow e\gamma$ decay can be expressed in terms of the deviation of unitarity η as shown in [5, 72] and our prediction for the muon and electron anomalous magnetic moments can also be written in terms of non-unitarity. We derived the analytic expression for the anomalies and found that the order of magnitude of these predictions is too small to accommodate the experimental bound within the 1σ range and the sign of each prediction also points out in the same direction. Therefore, we concluded that the W boson exchange at one-loop is not enough to explain both anomalies at 1σ and this conclusion has been a good motivation to search for another possibility such as scalar exchange, which is one of the main purposes of this work.

We then turned our attention to the 2HDM contributions (inclusion also of the singlet scalar ϕ) to the muon and electron anomalous magnetic moments, assuming by a choice of parameters a diagonal charged lepton mass matrix to suppress the branching ratio of $\mu \rightarrow e\gamma$. In our analysis we considered in detail the scalar sector of our model, which is composed of two $SU(2)$ scalar doublets H_u and H_d and one electrically neutral complex scalar ϕ by studying the corresponding scalar potential, deriving the squared mass matrices for the CP-even, CP-odd neutral and electrically charged scalars and determining the resulting scalar mass spectrum. We have restricted to the scenario corresponding to the decoupling limit where no mixing between the physical SM Higgs h and the physical non-SM

scalars $H_{1,2}$ arise and within this scenario we have imposed the restrictions arising from the Higgs diphoton decay rate, the hWW coupling, the 125 GeV mass of the SM-like Higgs and the experimental lower bounds on non SM scalar masses, to determine the allowed parameter space consistent with the muon and electron anomalous magnetic moments. To this end, we have constructed a χ^2 fitting function, which measures the deviation of the values of the physical observables obtained in the model, i.e., $(g-2)_{e,\mu}$, the 125 GeV SM-like Higgs mass, the Higgs diphoton signal strength, the hWW coupling, with respect to their experimental values. Its minimization allows to determine the values of the model parameters consistent with the measured experimental values of these observables. After saturating the χ^2 value less than or nearly 2, we obtained four independent benchmark points and carried out second scan with the benchmark points to find a correlation between observables and mass parameters. For the plots, we took a case most converged when compared to other ones. We found that our prediction for both anomalies can be explained within the 1σ constraint of each anomaly and a correlation inversely proportional for muon versus electron anomaly is appeared in Figure 11 and 12. Here, we put two constraints on mass of the lightest non-SM scalar and of the lightest vector-like family; $m_{H_1}, m_{e_5} > 200$ GeV based on references. The second scan result tells that the available parameter space is not significantly constrained by current experimental results on non-SM scalar mass and vector-like mass, while keeping perturbativity for quartic couplings and Yukawa constants. Lastly, we discussed how we were able to explain both $(g-2)_{e,\mu}$ anomalies at 1σ constraint and impact of the light non-SM scalar H_1 . For the former, we first simplified the prediction for both anomalies and used some numerical values at the stage where no more analytic simplification is possible. For the latter, we compared the cross section for the SM process $pp \rightarrow h$ and BSM process $pp \rightarrow H_1$ and included this comparison in Appendix B.

We conclude that the proposed model of fermion mass hierarchies is able to successfully accommodate both the muon and electron anomalous magnetic moments within the 1σ experimentally allowed ranges, with the dominant contributions arising from one loop diagrams involving the 2HDM scalars and vector-like leptons. The resulting model parameter space consistent with the $(g-2)_{e,\mu}$ anomalies requires masses of non-SM scalars and vector-like particles in the sub TeV and TeV ranges, thus making these particles accessible at the LHC and future colliders.

Acknowledgements

We would like to thank Simon King for discussions. This research has received funding from Fondecyt (Chile), Grants No. 1170803, CONICYT PIA/Basal FB0821. SFK acknowledges the STFC Consolidated Grant ST/L000296/1 and the European Union's Horizon 2020 Research and Innovation programme under Marie Skłodowska-Curie grant agreements Elusives ITN No. 674896, HIDDEN European ITN project (H2020-MSCA-ITN-2019//860881-HIDDEN) and InvisiblesPlus RISE No. 690575.

Appendix A: Quark mass matrices in two bases

As the lepton mass matrix is constructed in main body of this work, the quark sector can be built in a similar way. Like the lepton sector, we make use of two approaches to an effective lepton mass matrix, one of which is a convenient basis and the other is a decoupling basis.

1. A convenient basis for quarks

Consider the 7×7 quark mass matrix rotated as in the lepton sector.

$$\begin{aligned}
M^u &= \begin{pmatrix} & u_{1R} & u_{2R} & u_{3R} & u_{4R} & u_{5R} & \tilde{Q}_{4R} & \tilde{Q}_{5R} \\ \overline{Q}_{1L} & 0 & 0 & 0 & 0 & y_{15}^u v_u & 0 & x_{15}^Q v_\phi \\ \overline{Q}_{2L} & 0 & 0 & 0 & y_{24}^u v_u & y_{25}^u v_u & 0 & x_{25}^Q v_\phi \\ \overline{Q}_{3L} & 0 & 0 & 0 & y_{34}^u v_u & y_{35}^u v_u & x_{34}^Q v_\phi & x_{35}^Q v_\phi \\ \overline{Q}_{4L} & 0 & 0 & y_{43}^u v_u & 0 & 0 & M_{44}^Q & M_{45}^Q \\ \overline{Q}_{5L} & y_{51}^u v_u & y_{52}^u v_u & y_{53}^u v_u & 0 & 0 & 0 & M_{55}^Q \\ \tilde{u}_{4L} & 0 & x_{42}^u v_\phi & x_{43}^u v_\phi & M_{44}^u & 0 & 0 & 0 \\ \tilde{u}_{5L} & x_{51}^u v_\phi & x_{52}^u v_\phi & x_{53}^u v_\phi & M_{54}^u & M_{55}^u & 0 & 0 \end{pmatrix} \\
M^d &= \begin{pmatrix} & d_{1R} & d_{2R} & d_{3R} & d_{4R} & d_{5R} & \tilde{Q}_{4R} & \tilde{Q}_{5R} \\ \overline{Q}_{1L} & 0 & 0 & 0 & y_{14}^d v_d & y_{15}^d v_d & 0 & x_{15}^Q v_\phi \\ \overline{Q}_{2L} & 0 & 0 & 0 & y_{24}^d v_d & y_{25}^d v_d & 0 & x_{25}^Q v_\phi \\ \overline{Q}_{3L} & 0 & 0 & 0 & y_{34}^d v_d & y_{35}^d v_d & x_{34}^Q v_\phi & x_{35}^Q v_\phi \\ \overline{Q}_{4L} & 0 & 0 & y_{43}^d v_d & 0 & 0 & M_{44}^Q & M_{45}^Q \\ \overline{Q}_{5L} & y_{51}^d v_d & y_{52}^d v_d & y_{53}^d v_d & 0 & 0 & 0 & M_{55}^Q \\ \tilde{d}_{4L} & 0 & x_{42}^d v_\phi & x_{43}^d v_\phi & M_{44}^d & 0 & 0 & 0 \\ \tilde{d}_{5L} & x_{51}^d v_\phi & x_{52}^d v_\phi & x_{53}^d v_\phi & M_{54}^d & M_{55}^d & 0 & 0 \end{pmatrix}
\end{aligned} \tag{A1}$$

Notice that the same rotations operated in the lepton sector is applied to both up- and down-type quark sector except for y_{14}^d since quark doublet rotation is already used in the up-type quark sector. These two mass matrices clearly tells that this model is an extended 2HDM in that the up-type SM Higgs H_u corresponds to up-type quark sector, while the down-type SM Higgs H_d corresponds for down-type quark sector. After developing vev of the flavon ϕ , the effective 3×3 Yukawa matrices for the up- and down-type quarks, $y_{ij}^u \overline{Q}_{iL} \tilde{H}_u u_{jR}$ and $y_{ij}^d \overline{Q}_{iL} \tilde{H}_d d_{jR}$, read:

$$\begin{aligned}
y_{ij}^u &= \begin{pmatrix} 0 & -\frac{y_{15}^u x_{42}^u M_{54}^u}{M_{55}^u} & -\frac{y_{15}^u x_{43}^u M_{54}^u}{M_{55}^u} \\ 0 & -\frac{y_{25}^u x_{42}^u M_{54}^u}{M_{55}^u} + y_{24}^u x_{42}^u & -\frac{y_{25}^u x_{43}^u M_{54}^u}{M_{55}^u} + y_{24}^u x_{43}^u \\ 0 & -\frac{y_{35}^u x_{42}^u M_{54}^u}{M_{55}^u} + y_{34}^u x_{42}^u & -\frac{y_{35}^u x_{43}^u M_{54}^u}{M_{55}^u} + y_{34}^u x_{43}^u \end{pmatrix} \frac{\langle \phi \rangle}{M_{44}^u} + \begin{pmatrix} y_{15}^u x_{51}^u & y_{15}^u x_{52}^u & y_{15}^u x_{53}^u \\ y_{25}^u x_{51}^u & y_{25}^u x_{52}^u & y_{25}^u x_{53}^u \\ y_{35}^u x_{51}^u & y_{35}^u x_{52}^u & y_{35}^u x_{53}^u \end{pmatrix} \frac{\langle \phi \rangle}{M_{55}^u} \\
&+ \begin{pmatrix} y_{51}^u x_{15}^Q & y_{52}^u x_{15}^Q & y_{53}^u x_{15}^Q \\ y_{51}^u x_{25}^Q & y_{52}^u x_{25}^Q & y_{53}^u x_{25}^Q \\ y_{51}^u x_{35}^Q & y_{52}^u x_{35}^Q & y_{53}^u x_{35}^Q \end{pmatrix} \frac{\langle \phi \rangle}{M_{55}^Q} + \begin{pmatrix} 0 & 0 & 0 \\ 0 & 0 & 0 \\ -\frac{y_{51}^u x_{34}^Q M_{45}^Q}{M_{55}^Q} & -\frac{y_{52}^u x_{34}^Q M_{45}^Q}{M_{55}^Q} & -\frac{y_{53}^u x_{34}^Q M_{45}^Q}{M_{55}^Q} + x_{34}^Q y_{43}^u \end{pmatrix} \frac{\langle \phi \rangle}{M_{44}^Q} \\
y_{ij}^d &= \begin{pmatrix} 0 & -\frac{y_{15}^d x_{42}^d M_{54}^d}{M_{55}^d} + y_{14}^d x_{42}^d & -\frac{y_{15}^d x_{43}^d M_{54}^d}{M_{55}^d} + y_{14}^d x_{43}^d \\ 0 & -\frac{y_{25}^d x_{42}^d M_{54}^d}{M_{55}^d} + y_{24}^d x_{42}^d & -\frac{y_{25}^d x_{43}^d M_{54}^d}{M_{55}^d} + y_{24}^d x_{43}^d \\ 0 & -\frac{y_{35}^d x_{42}^d M_{54}^d}{M_{55}^d} + y_{34}^d x_{42}^d & -\frac{y_{35}^d x_{43}^d M_{54}^d}{M_{55}^d} + y_{34}^d x_{43}^d \end{pmatrix} \frac{\langle \phi \rangle}{M_{44}^d} + \begin{pmatrix} y_{15}^d x_{51}^d & y_{15}^d x_{52}^d & y_{15}^d x_{53}^d \\ y_{25}^d x_{51}^d & y_{25}^d x_{52}^d & y_{25}^d x_{53}^d \\ y_{35}^d x_{51}^d & y_{35}^d x_{52}^d & y_{35}^d x_{53}^d \end{pmatrix} \frac{\langle \phi \rangle}{M_{55}^d} \\
&+ \begin{pmatrix} y_{51}^d x_{15}^Q & y_{52}^d x_{15}^Q & y_{53}^d x_{15}^Q \\ y_{51}^d x_{25}^Q & y_{52}^d x_{25}^Q & y_{53}^d x_{25}^Q \\ y_{51}^d x_{35}^Q & y_{52}^d x_{35}^Q & y_{53}^d x_{35}^Q \end{pmatrix} \frac{\langle \phi \rangle}{M_{55}^Q} + \begin{pmatrix} 0 & 0 & 0 \\ 0 & 0 & 0 \\ -\frac{y_{51}^d x_{34}^Q M_{45}^Q}{M_{55}^Q} & -\frac{y_{52}^d x_{34}^Q M_{45}^Q}{M_{55}^Q} & -\frac{y_{53}^d x_{34}^Q M_{45}^Q}{M_{55}^Q} + x_{34}^Q y_{43}^d \end{pmatrix} \frac{\langle \phi \rangle}{M_{44}^Q}
\end{aligned} \tag{A2}$$

With the mass hierarchy assumption $M_{54}^{u,d}, M_{45}^Q \ll M_{44}^Q, M_{44}^d, M_{44}^u, M_{55}^{Q,u,d}$, we can recover much simpler form of hierarchy in the quark sector and it can explain the stronger mass hierarchy in the up quark sector than the down sector due to the presence of top quark.

$$\begin{aligned}
y_{ij}^u &= \begin{pmatrix} 0 & 0 & 0 \\ 0 & y_{24}^u x_{42}^u & y_{24}^u x_{43}^u \\ 0 & y_{34}^u x_{42}^u & y_{34}^u x_{43}^u \end{pmatrix} \frac{\langle \phi \rangle}{M_{44}^u} + \begin{pmatrix} y_{15}^u x_{51}^u & y_{15}^u x_{52}^u & y_{15}^u x_{53}^u \\ y_{25}^u x_{51}^u & y_{25}^u x_{52}^u & y_{25}^u x_{53}^u \\ y_{35}^u x_{51}^u & y_{35}^u x_{52}^u & y_{35}^u x_{53}^u \end{pmatrix} \frac{\langle \phi \rangle}{M_{55}^u} \\
&+ \begin{pmatrix} y_{51}^u x_{15}^Q & y_{52}^u x_{15}^Q & y_{53}^u x_{15}^Q \\ y_{51}^u x_{25}^Q & y_{52}^u x_{25}^Q & y_{53}^u x_{25}^Q \\ y_{51}^u x_{35}^Q & y_{52}^u x_{35}^Q & y_{53}^u x_{35}^Q \end{pmatrix} \frac{\langle \phi \rangle}{M_{55}^Q} + \begin{pmatrix} 0 & 0 & 0 \\ 0 & 0 & 0 \\ 0 & 0 & x_{34}^Q y_{43}^u \end{pmatrix} \frac{\langle \phi \rangle}{M_{44}^Q} \\
y_{ij}^d &= \begin{pmatrix} 0 & y_{14}^d x_{42}^d & y_{14}^d x_{43}^d \\ 0 & y_{24}^d x_{42}^d & y_{24}^d x_{43}^d \\ 0 & y_{34}^d x_{42}^d & y_{34}^d x_{43}^d \end{pmatrix} \frac{\langle \phi \rangle}{M_{44}^d} + \begin{pmatrix} y_{15}^d x_{51}^d & y_{15}^d x_{52}^d & y_{15}^d x_{53}^d \\ y_{25}^d x_{51}^d & y_{25}^d x_{52}^d & y_{25}^d x_{53}^d \\ y_{35}^d x_{51}^d & y_{35}^d x_{52}^d & y_{35}^d x_{53}^d \end{pmatrix} \frac{\langle \phi \rangle}{M_{55}^d} \\
&+ \begin{pmatrix} y_{51}^d x_{15}^Q & y_{52}^d x_{15}^Q & y_{53}^d x_{15}^Q \\ y_{51}^d x_{25}^Q & y_{52}^d x_{25}^Q & y_{53}^d x_{25}^Q \\ y_{51}^d x_{35}^Q & y_{52}^d x_{35}^Q & y_{53}^d x_{35}^Q \end{pmatrix} \frac{\langle \phi \rangle}{M_{55}^Q} + \begin{pmatrix} 0 & 0 & 0 \\ 0 & 0 & 0 \\ 0 & 0 & x_{34}^Q y_{43}^d \end{pmatrix} \frac{\langle \phi \rangle}{M_{44}^Q}
\end{aligned} \tag{A3}$$

2. A basis for decoupling heavy fourth and fifth vector-like family

In this section, we treat the decoupling basis with quarks holding an assumption $\langle \phi \rangle \approx M_{44}^Q$. As in the charged lepton mass matrix, we can read off the Yukawa matrix from the 5×5 upper block of Equation A3

$$\tilde{y}_{\alpha\beta}^u = \begin{pmatrix} 0 & 0 & 0 & 0 & y_{15}^u \\ 0 & 0 & 0 & y_{24}^u & y_{25}^u \\ 0 & 0 & 0 & y_{34}^u & y_{35}^u \\ 0 & 0 & y_{43}^u & 0 & 0 \\ y_{51}^u & y_{52}^u & y_{53}^u & 0 & 0 \end{pmatrix}, \quad \tilde{y}_{\alpha\beta}^d = \begin{pmatrix} 0 & 0 & 0 & y_{14}^d & y_{15}^d \\ 0 & 0 & 0 & y_{24}^d & y_{25}^d \\ 0 & 0 & 0 & y_{34}^d & y_{35}^d \\ 0 & 0 & y_{43}^d & 0 & 0 \\ y_{51}^d & y_{52}^d & y_{53}^d & 0 & 0 \end{pmatrix} \tag{A4}$$

where α and β run from 1 to 5. The Yukawa matrices $\tilde{y}_{\alpha\beta}^{u,d}$ can be diagonalized by the unitary rotations V

$$V_Q = V_{45}^Q V_{35}^Q V_{25}^Q V_{15}^Q V_{34}^Q V_{24}^Q V_{14}^Q, \quad V_u = V_{45}^u V_{35}^u V_{25}^u V_{15}^u V_{34}^u V_{24}^u V_{14}^u, \quad V_d = V_{45}^d V_{35}^d V_{25}^d V_{15}^d V_{34}^d V_{24}^d V_{14}^d \tag{A5}$$

where each of the unitary matrices $V_{i4,5}$ are parameterized by a single angle $\theta_{i4,5}$ featuring the mixing between the i th SM chiral quark and the 4, 5th vector-like quark. In the rotated mass matrix, we need (3, 4), (1, 5), (2, 5), (3, 5) mixing in the Q sector and (2, 4), (3, 4), (1, 5), (2, 5), (3, 5) mixing in the u, d sectors to go to the decoupling basis therefore the unitary mixing matrices V are defined to be

$$\begin{aligned}
V_Q &= V_{35}^Q V_{25}^Q V_{15}^Q V_{34}^Q \\
&= \begin{pmatrix} 1 & 0 & 0 & 0 & 0 \\ 0 & 1 & 0 & 0 & 0 \\ 0 & 0 & c_{35}^Q & 0 & s_{35}^Q \\ 0 & 0 & 0 & 1 & 0 \\ 0 & 0 & -s_{35}^Q & 0 & c_{35}^Q \end{pmatrix} \begin{pmatrix} 1 & 0 & 0 & 0 & 0 \\ 0 & c_{25}^Q & 0 & 0 & s_{25}^Q \\ 0 & 0 & 1 & 0 & 0 \\ 0 & 0 & 0 & 1 & 0 \\ 0 & -s_{25}^Q & 0 & 0 & c_{25}^Q \end{pmatrix} \begin{pmatrix} c_{15}^Q & 0 & 0 & 0 & s_{15}^Q \\ 0 & 1 & 0 & 0 & 0 \\ 0 & 0 & 1 & 0 & 0 \\ 0 & 0 & 0 & 1 & 0 \\ -s_{15}^Q & 0 & 0 & 0 & c_{15}^Q \end{pmatrix} \begin{pmatrix} 1 & 0 & 0 & 0 & 0 \\ 0 & 1 & 0 & 0 & 0 \\ 0 & 0 & c_{34}^Q & s_{34}^Q & 0 \\ 0 & 0 & -s_{34}^Q & c_{34}^Q & 0 \\ 0 & 0 & 0 & 0 & 1 \end{pmatrix}, \\
&\approx \begin{pmatrix} 1 & 0 & 0 & 0 & s_{15}^Q \\ 0 & 1 & 0 & 0 & s_{25}^Q \\ 0 & 0 & 1 & s_{34}^Q & s_{35}^Q \\ 0 & 0 & -s_{34}^Q & 1 & 0 \\ -s_{15}^Q & -s_{25}^Q & -s_{15}^Q & 0 & 1 \end{pmatrix}, \\
s_{34}^Q &= \frac{x_{34}^Q \langle \phi \rangle}{\sqrt{(x_{34}^Q \langle \phi \rangle)^2 + (M_{44}^Q)^2}}, \quad s_{15}^Q = \frac{x_{15}^Q \langle \phi \rangle}{\sqrt{(x_{15}^Q \langle \phi \rangle)^2 + (M_{55}^Q)^2}}, \\
s_{25}^Q &= \frac{x_{25}^Q \langle \phi \rangle}{\sqrt{(x_{25}^Q \langle \phi \rangle)^2 + (M_{55}^Q)^2}}, \quad s_{35}^Q = \frac{x_{35}^Q \langle \phi \rangle}{\sqrt{(x_{35}^Q \langle \phi \rangle)^2 + (M_{55}^Q)^2}}, \\
x_{35}^Q \langle \phi \rangle &= c_{34}^Q x_{35}^Q \langle \phi \rangle + s_{34}^Q M_{45}^Q, \quad M_{45}^Q = -s_{34}^Q x_{35}^Q \langle \phi \rangle + c_{34}^Q M_{45}^Q \\
\widetilde{M}_{44}^Q &= \sqrt{(x_{34}^Q \langle \phi \rangle)^2 + (M_{44}^Q)^2}, \\
M_{55}^Q &= \sqrt{(x_{15}^Q \langle \phi \rangle)^2 + (M_{55}^Q)^2}, \quad M_{55}^{\prime Q} = \sqrt{(x_{25}^Q \langle \phi \rangle)^2 + (M_{55}^Q)^2}, \quad \widetilde{M}_{55}^Q = \sqrt{(x_{35}^Q \langle \phi \rangle)^2 + (M_{55}^Q)^2}
\end{aligned} \tag{A6}$$

$$\begin{aligned}
V_u &= V_{35}^u V_{25}^u V_{15}^u V_{34}^u V_{24}^u \\
&= \begin{pmatrix} 1 & 0 & 0 & 0 & 0 \\ 0 & 1 & 0 & 0 & 0 \\ 0 & 0 & c_{35}^u & 0 & s_{35}^u \\ 0 & 0 & 0 & 1 & 0 \\ 0 & 0 & -s_{35}^u & 0 & c_{35}^u \end{pmatrix} \begin{pmatrix} 1 & 0 & 0 & 0 & 0 \\ 0 & c_{25}^u & 0 & 0 & s_{25}^u \\ 0 & 0 & 1 & 0 & 0 \\ 0 & 0 & 0 & 1 & 0 \\ 0 & -s_{25}^u & 0 & 0 & c_{25}^u \end{pmatrix} \begin{pmatrix} c_{15}^u & 0 & 0 & 0 & s_{15}^u \\ 0 & 1 & 0 & 0 & 0 \\ 0 & 0 & 1 & 0 & 0 \\ 0 & 0 & 0 & 1 & 0 \\ -s_{15}^u & 0 & 0 & 0 & c_{15}^u \end{pmatrix} \\
&\times \begin{pmatrix} 1 & 0 & 0 & 0 & 0 \\ 0 & 1 & 0 & 0 & 0 \\ 0 & 0 & c_{34}^u & s_{34}^u & 0 \\ 0 & 0 & -s_{34}^u & c_{34}^u & 0 \\ 0 & 0 & 0 & 0 & 1 \end{pmatrix} \begin{pmatrix} 1 & 0 & 0 & 0 & 0 \\ 0 & c_{24}^u & 0 & s_{24}^u & 0 \\ 0 & 0 & 1 & 0 & 0 \\ 0 & -s_{24}^u & 0 & c_{24}^u & 0 \\ 0 & 0 & 0 & 0 & 1 \end{pmatrix} \approx \begin{pmatrix} 1 & 0 & 0 & 0 & \theta_{15}^u \\ 0 & 1 & 0 & \theta_{24}^u & \theta_{25}^u \\ 0 & 0 & 1 & \theta_{34}^u & \theta_{35}^u \\ 0 & -\theta_{24}^u & -\theta_{34}^u & 1 & 0 \\ -\theta_{15}^u & -\theta_{25}^u & -\theta_{35}^u & 0 & 1 \end{pmatrix}, \\
s_{24}^u &\approx \frac{x_{42}^u \langle \phi \rangle}{M_{44}^u}, \quad s_{34}^u \approx \frac{x_{43}^u \langle \phi \rangle}{M_{44}^u}, \quad s_{15}^u \approx \frac{x_{51}^u \langle \phi \rangle}{M_{55}^u}, \quad s_{25}^u \approx \frac{x_{52}^u \langle \phi \rangle}{M_{55}^u}, \quad s_{35}^u \approx \frac{x_{53}^u \langle \phi \rangle}{M_{55}^u}, \\
x_{52}^u \langle \phi \rangle &= c_{24}^u x_{52}^u \langle \phi \rangle + s_{24}^u M_{54}^u, \quad M_{54}^u = -s_{24}^u x_{52}^u \langle \phi \rangle + c_{24}^u M_{54}^u, \\
x_{53}^u \langle \phi \rangle &= c_{34}^u x_{53}^u \langle \phi \rangle + s_{34}^u M_{54}^u, \quad M_{54}^u = -s_{34}^u x_{53}^u \langle \phi \rangle + c_{34}^u M_{54}^u, \\
M_{44}^u &= \sqrt{(x_{42}^u \langle \phi \rangle)^2 + (M_{44}^u)^2}, \quad \widetilde{M}_{44}^u = \sqrt{(x_{43}^u \langle \phi \rangle)^2 + (M_{44}^u)^2}, \\
M_{55}^u &= \sqrt{(x_{51}^u \langle \phi \rangle)^2 + (M_{55}^u)^2}, \quad M_{55}^{\prime u} = \sqrt{(x_{52}^u \langle \phi \rangle)^2 + (M_{55}^u)^2}, \quad \widetilde{M}_{55}^u = \sqrt{(x_{53}^u \langle \phi \rangle)^2 + (M_{55}^u)^2}.
\end{aligned} \tag{A7}$$

With the defined unitary mixing matrices in place, the 5×5 Yukawa matrices in a mass basis (primed) are transformed by

$$\widetilde{y}_{\alpha\beta}^{\prime u} = V_Q \widetilde{y}_{\alpha\beta}^u V_u^\dagger, \quad \widetilde{y}_{\alpha\beta}^{\prime d} = V_Q \widetilde{y}_{\alpha\beta}^d V_d^\dagger, \tag{A8}$$

where tilde with prime means interaction basis whereas tilde alone corresponds to the mass basis. The effective SM Yukawa couplings for the quarks then correspond to the 3×3 upper block of $\widetilde{y}_{\alpha\beta}^{\prime u}, \widetilde{y}_{\alpha\beta}^{\prime d}$, namely

$$y_{ij}^u \tilde{H}_u \bar{Q}_{iL} u_{jR}, \quad y_{ij}^d \tilde{H}_d \bar{Q}_{iL} d_{jR}, \quad \text{with } y_{ij}^u \equiv \tilde{y}_{ij}^u, \quad y_{ij}^d \equiv \tilde{y}_{ij}^d, \quad (i, j = 1, 2, 3). \quad (\text{A9})$$

The 3×3 SM Yukawa matrices for up- and down-type quark sector read:

$$y_{ij}^u = \begin{pmatrix} s_{15}^Q y_{51}^u + y_{15}^u \theta_{15}^u & s_{15}^Q y_{52}^u + y_{15}^u \theta_{25}^u & s_{15}^Q y_{53}^u + y_{15}^u \theta_{35}^u \\ s_{25}^Q y_{51}^u + y_{25}^u \theta_{15}^u & s_{25}^Q y_{52}^u + y_{24}^u \theta_{24}^u + y_{25}^u \theta_{25}^u & s_{25}^Q y_{53}^u + y_{24}^u \theta_{34}^u + y_{25}^u \theta_{35}^u \\ s_{35}^Q y_{51}^u + y_{35}^u \theta_{15}^u & s_{35}^Q y_{52}^u + y_{34}^u \theta_{24}^u + y_{35}^u \theta_{25}^u & s_{34}^Q y_{43}^u + s_{35}^Q y_{53}^u + y_{34}^u \theta_{34}^u + y_{35}^u \theta_{35}^u \end{pmatrix} \\ y_{ij}^d = \begin{pmatrix} s_{15}^Q y_{51}^d + y_{15}^d \theta_{15}^d & s_{15}^Q y_{52}^d + y_{14}^d \theta_{24}^d + y_{15}^d \theta_{25}^d & s_{15}^Q y_{53}^d + y_{14}^d \theta_{34}^d + y_{15}^d \theta_{35}^d \\ s_{25}^Q y_{51}^d + y_{25}^d \theta_{15}^d & s_{25}^Q y_{52}^d + y_{24}^d \theta_{24}^d + y_{25}^d \theta_{25}^d & s_{25}^Q y_{53}^d + y_{24}^d \theta_{34}^d + y_{25}^d \theta_{35}^d \\ s_{35}^Q y_{51}^d + y_{35}^d \theta_{15}^d & s_{35}^Q y_{52}^d + y_{34}^d \theta_{24}^d + y_{35}^d \theta_{25}^d & s_{34}^Q y_{43}^d + s_{35}^Q y_{53}^d + y_{34}^d \theta_{34}^d + y_{35}^d \theta_{35}^d \end{pmatrix} \quad (\text{A10})$$

Appendix B: Heavy scalar production at a proton-proton collider

We have confirmed that the mass of the non-SM CP even scalar H_1 is ranged from 200 to 240 GeV in Table V and this light mass of H_1 has not been observed at CERN or other experiments so far. In order to see how big an impact of H_1 is when compared to that of SM Higgs h , we studied a total cross section for the SM process $pp \rightarrow h$ and for BSM process $pp \rightarrow H_1$. The SM cross section for $pp \rightarrow h$ process is

$$\sigma_{\text{SM}} = \frac{\alpha_S^2 m_h^2}{64\pi v^2} \left(L \left(\frac{m_h^2}{m_t^2} \right) \right)^2 \frac{1}{S} \int_{\ln \sqrt{m_h^2/S}}^{-\ln \sqrt{m_h^2/S}} \text{PDF}(0, x_1(y), m_h) \text{PDF}(0, x_2(y), m_h) dy \quad (\text{B1})$$

where L is a loop integral

$$L(a) = | [2a + (-4 + a) \text{PolyLog}(2, 1/2(-\sqrt{-4+a}\sqrt{a} + a)) \\ + (-4 + a) \text{PolyLog}(2, 1/2(\sqrt{-4+a}\sqrt{a} + a))] / a^2 |, \quad (\text{B2})$$

α_S is the strong coupling constant, v is the conventional SM Higgs vev 246.22 GeV, m_h is the Higgs mass 125 GeV, m_t is the top quark mass 173 GeV, S is the squared LHC center of mass energy (14 TeV)², PDF corresponds to the parton distribution function where 0 means 0th parton - gluon, x is the momentum fraction of the proton carried out by the gluon. Here the factorization scale has been taken to be equal to the SM like Higgs boson mass m_h and $x_{1,2}(y)$ are defined as follows:

$$x_1(y) = \frac{\sqrt{m_h^2/S}}{S} \exp(y), \quad x_2(y) = \frac{\sqrt{m_h^2/S}}{S} \exp(-y). \quad (\text{B3})$$

With these defined functions and values, the total cross section for $pp \rightarrow h$ is

$$\sigma_{\text{SM}} \simeq 18 \text{ pb}. \quad (\text{B4})$$

Next, the total cross section for $pp \rightarrow H_1$ process is

$$\sigma(pp \rightarrow H_1) = \frac{\alpha_S^2 m_{H_1}^2 a_{hbb}^2}{64\pi v^2} \left(L \left(\frac{m_{H_1}^2}{m_b^2} \right) \right)^2 \frac{1}{S} \int_{\ln \sqrt{m_{H_1}^2/S}}^{-\ln \sqrt{m_{H_1}^2/S}} \text{PDF}(0, x'_1(y), m_{H_1}) \text{PDF}(0, x'_2(y), m_{H_1}) dy \quad (\text{B5})$$

where m_{H_1} is mass of non-SM CP even scalar H_1 , and $x'_{1,2}$ are defined in a similar way:

$$x'_1(y) = \frac{\sqrt{m_{H_1}^2/S}}{S} \exp(y), \quad x'_2(y) = \frac{\sqrt{m_{H_1}^2/S}}{S} \exp(-y) \quad (\text{B6})$$

One main distinction between Equation B1 and Equation B5 is the non-SM scalar H_1 only interacts with down-type quark pair $b\bar{b}$ since it is a mixed state between h_d^0 and ϕ while the SM Higgs h can interact with top-quark pair $t\bar{t}$. According to the mass range of H_1 reported in Table V, the total cross section for $pp \rightarrow H_1$ is given in Figure 13.

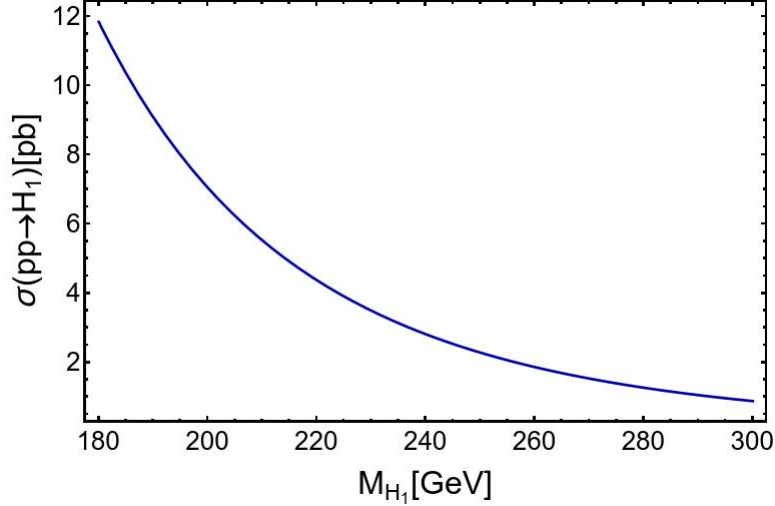


Figure 13: The total cross section for $pp \rightarrow H_1$ at 14 TeV

The total cross section for $pp \rightarrow H_1$ runs from nearly 8 pb at 200 GeV to smaller values as mass of H_1 increases. The order of magnitude of this cross section for $pp \rightarrow H_1$ is compatible to that of the SM process $pp \rightarrow h$, however the BSM process is strongly suppressed since its single LHC production via gluon fusion mechanism is dominated by the triangular bottom quark loop as mentioned in Section VI. Therefore, our prediction with the light non-SM scalar H_1 is possible to accommodate each anomaly constraint at 1σ .

-
- [1] G. W. Bennett *et al.* [Muon g-2 Collaboration], Phys. Rev. D **73**, 072003 (2006) doi:10.1103/PhysRevD.73.072003 [hep-ex/0602035].
 - [2] R. H. Parker, C. Yu, W. Zhong, B. Estey and H. Müller, Science **360**, 191 (2018) doi:10.1126/science.aap7706 [arXiv:1812.04130 [physics.atom-ph]].
 - [3] L. Morel, Z. Yao, P. Cladé and S. Guellati-Khélifa, Nature **588**, no. 7836, 61 (2020). doi:10.1038/s41586-020-2964-7
 - [4] S. F. King, JHEP **1809**, 069 (2018) doi:10.1007/JHEP09(2018)069 [arXiv:1806.06780 [hep-ph]].
 - [5] J. Hernandez-Garcia and S. F. King, JHEP **1905**, 169 (2019) doi:10.1007/JHEP05(2019)169 [arXiv:1903.01474 [hep-ph]].
 - [6] A. Crivellin, M. Hoferichter and P. Schmidt-Wellenburg, Phys. Rev. D **98**, no. 11, 113002 (2018) doi:10.1103/PhysRevD.98.113002 [arXiv:1807.11484 [hep-ph]].
 - [7] T. Appelquist, M. Piai and R. Shrock, Phys. Lett. B **593**, 175 (2004) doi:10.1016/j.physletb.2004.04.062 [hep-ph/0401114].
 - [8] G. F. Giudice, P. Paradisi and M. Passera, JHEP **1211**, 113 (2012) doi:10.1007/JHEP11(2012)113 [arXiv:1208.6583 [hep-ph]].
 - [9] A. Falkowski, S. F. King, E. Perdomo and M. Pierre, JHEP **1808**, 061 (2018) doi:10.1007/JHEP08(2018)061 [arXiv:1803.04430 [hep-ph]].
 - [10] B. Allanach, F. S. Queiroz, A. Strumia and S. Sun, Phys. Rev. D **93**, no. 5, 055045 (2016) Erratum: [Phys. Rev. D **95**, no. 11, 119902 (2017)] doi:10.1103/PhysRevD.93.055045, 10.1103/PhysRevD.95.119902 [arXiv:1511.07447 [hep-ph]].
 - [11] C. H. Chen, T. Nomura and H. Okada, Phys. Rev. D **94**, no. 11, 115005 (2016) doi:10.1103/PhysRevD.94.115005 [arXiv:1607.04857 [hep-ph]].
 - [12] S. Raby and A. Trautner, Phys. Rev. D **97**, no. 9, 095006 (2018) doi:10.1103/PhysRevD.97.095006 [arXiv:1712.09360 [hep-ph]].
 - [13] C. W. Chiang, H. Okada and E. Senaha, Phys. Rev. D **96**, no. 1, 015002 (2017) doi:10.1103/PhysRevD.96.015002 [arXiv:1703.09153 [hep-ph]].

- [14] C. H. Chen, T. Nomura and H. Okada, Phys. Lett. B **774**, 456 (2017) doi:10.1016/j.physletb.2017.10.005 [arXiv:1703.03251 [hep-ph]].
- [15] H. Davoudiasl and W. J. Marciano, Phys. Rev. D **98**, no. 7, 075011 (2018) doi:10.1103/PhysRevD.98.075011 [arXiv:1806.10252 [hep-ph]].
- [16] J. Liu, C. E. M. Wagner and X. P. Wang, JHEP **1903**, 008 (2019) doi:10.1007/JHEP03(2019)008 [arXiv:1810.11028 [hep-ph]].
- [17] A. E. Cárcamo Hernández, S. Kovalenko, R. Pasechnik and I. Schmidt, Eur. Phys. J. C **79**, no. 7, 610 (2019) doi:10.1140/epjc/s10052-019-7101-0 [arXiv:1901.09552 [hep-ph]].
- [18] T. Nomura and H. Okada, Phys. Rev. D **101**, no. 1, 015021 (2020) doi:10.1103/PhysRevD.101.015021 [arXiv:1903.05958 [hep-ph]].
- [19] J. Kawamura, S. Raby and A. Trautner, Phys. Rev. D **100**, no. 5, 055030 (2019) doi:10.1103/PhysRevD.100.055030 [arXiv:1906.11297 [hep-ph]].
- [20] M. Bauer, M. Neubert, S. Renner, M. Schnubel and A. Thamm, Phys. Rev. Lett. **124**, no. 21, 211803 (2020) doi:10.1103/PhysRevLett.124.211803 [arXiv:1908.00008 [hep-ph]].
- [21] X. F. Han, T. Li, L. Wang and Y. Zhang, Phys. Rev. D **99**, no. 9, 095034 (2019) doi:10.1103/PhysRevD.99.095034 [arXiv:1812.02449 [hep-ph]].
- [22] B. Dutta and Y. Mimura, Phys. Lett. B **790**, 563 (2019) doi:10.1016/j.physletb.2018.12.070 [arXiv:1811.10209 [hep-ph]].
- [23] M. Badziak and K. Sakurai, JHEP **1910**, 024 (2019) doi:10.1007/JHEP10(2019)024 [arXiv:1908.03607 [hep-ph]].
- [24] M. Endo and W. Yin, JHEP **1908**, 122 (2019) doi:10.1007/JHEP08(2019)122 [arXiv:1906.08768 [hep-ph]].
- [25] G. Hiller, C. Hormigos-Feliu, D. F. Litim and T. Steudtner, Phys. Rev. D **102**, no. 7, 071901 (2020) doi:10.1103/PhysRevD.102.071901 [arXiv:1910.14062 [hep-ph]].
- [26] A. E. Cárcamo Hernández, S. F. King, H. Lee and S. J. Rowley, Phys. Rev. D **101**, no. 11, 115016 (2020) doi:10.1103/PhysRevD.101.115016 [arXiv:1910.10734 [hep-ph]].
- [27] A. E. Cárcamo Hernández, D. T. Huang and H. N. Long, Phys. Rev. D **102**, no. 5, 055002 (2020) doi:10.1103/PhysRevD.102.055002 [arXiv:1910.12877 [hep-ph]].
- [28] J. Kawamura, S. Raby and A. Trautner, Phys. Rev. D **101**, no. 3, 035026 (2020) doi:10.1103/PhysRevD.101.035026 [arXiv:1911.11075 [hep-ph]].
- [29] A. E. Cárcamo Hernández, Y. Hidalgo Velásquez, S. Kovalenko, H. N. Long, N. A. Pérez-Julve and V. V. Vien, arXiv:2002.07347 [hep-ph].
- [30] C. Arbeláez, R. Cepedello, R. M. Fonseca and M. Hirsch, Phys. Rev. D **102**, no. 7, 075005 (2020) doi:10.1103/PhysRevD.102.075005 [arXiv:2007.11007 [hep-ph]].
- [31] G. Hiller, C. Hormigos-Feliu, D. F. Litim and T. Steudtner, Phys. Rev. D **102**, no. 9, 095023 (2020) doi:10.1103/PhysRevD.102.095023 [arXiv:2008.08606 [hep-ph]].
- [32] S. Jana, V. P. K. and S. Saad, Phys. Rev. D **101**, no. 11, 115037 (2020) doi:10.1103/PhysRevD.101.115037 [arXiv:2003.03386 [hep-ph]].
- [33] Á. S. de Jesus, S. Kovalenko, C. A. de S. Pires, F. S. Queiroz and Y. S. Villamizar, Phys. Lett. B **809**, 135689 (2020) doi:10.1016/j.physletb.2020.135689 [arXiv:2003.06440 [hep-ph]].
- [34] A. S. De Jesus, S. Kovalenko, F. S. Queiroz, C. Siqueira and K. Sinha, Phys. Rev. D **102**, no. 3, 035004 (2020) doi:10.1103/PhysRevD.102.035004 [arXiv:2004.01200 [hep-ph]].
- [35] C. Hati, J. Kriewald, J. Orloff and A. M. Teixeira, JHEP **2007**, 235 (2020) doi:10.1007/JHEP07(2020)235 [arXiv:2005.00028 [hep-ph]].
- [36] F. J. Botella, F. Cornet-Gomez and M. Nebot, Phys. Rev. D **102**, no. 3, 035023 (2020) doi:10.1103/PhysRevD.102.035023 [arXiv:2006.01934 [hep-ph]].
- [37] I. Doršner, S. Fajfer and S. Saad, Phys. Rev. D **102**, no. 7, 075007 (2020) doi:10.1103/PhysRevD.102.075007 [arXiv:2006.11624 [hep-ph]].
- [38] L. Calibbi, M. L. López-Ibañez, A. Melis and O. Vives, JHEP **2006**, 087 (2020) doi:10.1007/JHEP06(2020)087 [arXiv:2003.06633 [hep-ph]].
- [39] L. T. Hue, P. N. Thanh and T. D. Tham, Commun. in Phys. **30**, no. 3, 221 (2020). doi:10.15625/0868-3166/30/3/14963
- [40] S. Jana, P. K. Vishnu, W. Rodejohann and S. Saad, Phys. Rev. D **102**, no. 7, 075003 (2020) doi:10.1103/PhysRevD.102.075003 [arXiv:2008.02377 [hep-ph]].
- [41] E. J. Chun and T. Mondal, JHEP **2011**, 077 (2020) doi:10.1007/JHEP11(2020)077 [arXiv:2009.08314 [hep-ph]].
- [42] C. K. Chua, Phys. Rev. D **102**, no. 5, 055022 (2020) doi:10.1103/PhysRevD.102.055022 [arXiv:2004.11031 [hep-ph]].
- [43] Y. Daikoku and H. Okada, arXiv:2011.10374 [hep-ph].
- [44] H. Banerjee, B. Dutta and S. Roy, arXiv:2011.05083 [hep-ph].
- [45] C. H. Chen and T. Nomura, arXiv:2003.07638 [hep-ph].
- [46] I. Bigaran and R. R. Volkas, Phys. Rev. D **102**, no. 7, 075037 (2020) doi:10.1103/PhysRevD.102.075037 [arXiv:2002.12544 [hep-ph]].
- [47] J. Kawamura, S. Okawa and Y. Omura, JHEP **2008**, 042 (2020) doi:10.1007/JHEP08(2020)042 [arXiv:2002.12534 [hep-ph]].
- [48] M. Endo, S. Iguro and T. Kitahara, JHEP **2006**, 040 (2020) doi:10.1007/JHEP06(2020)040 [arXiv:2002.05948 [hep-ph]].
- [49] A. Davidson and K. C. Wali, Phys. Rev. Lett. **59**, 393 (1987). doi:10.1103/PhysRevLett.59.393
- [50] A. Davidson and K. C. Wali, Phys. Rev. Lett. **58**, 2623 (1987). doi:10.1103/PhysRevLett.58.2623
- [51] Z. G. Berezhiani and R. Rattazzi, Phys. Lett. B **279**, 124 (1992). doi:10.1016/0370-2693(92)91851-Y

- [52] I. S. Sogami and T. Shinohara, Prog. Theor. Phys. **86**, 1031 (1991). doi:10.1143/PTP.86.1031
- [53] P. H. Gu and M. Lindner, Phys. Lett. B **698**, 40 (2011) doi:10.1016/j.physletb.2011.02.042 [arXiv:1010.4635 [hep-ph]].
- [54] C. Alvarado, R. Martinez and F. Ochoa, Phys. Rev. D **86**, 025027 (2012) doi:10.1103/PhysRevD.86.025027 [arXiv:1207.0014 [hep-ph]].
- [55] A. E. Carcamo Hernandez, R. Martinez and F. Ochoa, Phys. Rev. D **87**, no. 7, 075009 (2013) doi:10.1103/PhysRevD.87.075009 [arXiv:1302.1757 [hep-ph]].
- [56] R. Kawasaki, T. Morozumi and H. Umeeda, Phys. Rev. D **88**, 033019 (2013) doi:10.1103/PhysRevD.88.033019 [arXiv:1306.5080 [hep-ph]].
- [57] R. N. Mohapatra and Y. Zhang, JHEP **1406**, 072 (2014) doi:10.1007/JHEP06(2014)072 [arXiv:1401.6701 [hep-ph]].
- [58] P. S. B. Dev, R. N. Mohapatra and Y. Zhang, JHEP **1602**, 186 (2016) doi:10.1007/JHEP02(2016)186 [arXiv:1512.08507 [hep-ph]].
- [59] D. Borah and S. Patra, Phys. Lett. B **771**, 318 (2017) doi:10.1016/j.physletb.2017.05.059 [arXiv:1701.08675 [hep-ph]].
- [60] A. Patra and S. K. Rai, Phys. Rev. D **98**, no. 1, 015033 (2018) doi:10.1103/PhysRevD.98.015033 [arXiv:1711.00627 [hep-ph]].
- [61] K. S. Babu, B. Dutta and R. N. Mohapatra, JHEP **1901**, 168 (2019) doi:10.1007/JHEP01(2019)168 [arXiv:1811.04496 [hep-ph]].
- [62] I. de Medeiros Varzielas and S. F. King, JHEP **1811**, 100 (2018) doi:10.1007/JHEP11(2018)100 [arXiv:1807.06023 [hep-ph]].
- [63] A. E. Cárcamo Hernández and S. F. King, Phys. Rev. D **99**, no. 9, 095003 (2019) doi:10.1103/PhysRevD.99.095003 [arXiv:1803.07367 [hep-ph]].
- [64] A. E. Cárcamo Hernández, Y. Hidalgo Velásquez and N. A. Pérez-Julve, Eur. Phys. J. C **79**, no. 10, 828 (2019) doi:10.1140/epjc/s10052-019-7325-z [arXiv:1905.02323 [hep-ph]].
- [65] A. E. Cárcamo Hernández, J. Marchant González and U. J. Saldaña-Salazar, Phys. Rev. D **100**, no. 3, 035024 (2019) doi:10.1103/PhysRevD.100.035024 [arXiv:1904.09993 [hep-ph]].
- [66] A. E. C. Hernández and I. Schmidt, arXiv:2101.02718 [hep-ph].
- [67] S. F. King, JHEP **1708**, 019 (2017) doi:10.1007/JHEP08(2017)019 [arXiv:1706.06100 [hep-ph]].
- [68] M. Blennow and E. Fernandez-Martinez, Phys. Lett. B **704**, 223 (2011) doi:10.1016/j.physletb.2011.09.028 [arXiv:1107.3992 [hep-ph]].
- [69] L. L. Chau and W. Y. Keung, Phys. Rev. Lett. **53**, 1802 (1984). doi:10.1103/PhysRevLett.53.1802
- [70] E. Fernandez-Martinez, M. B. Gavela, J. Lopez-Pavon and O. Yasuda, Phys. Lett. B **649**, 427 (2007) doi:10.1016/j.physletb.2007.03.069 [hep-ph/0703098].
- [71] A. Broncano, M. B. Gavela and E. E. Jenkins, Phys. Lett. B **552**, 177 (2003) Erratum: [Phys. Lett. B **636**, 332 (2006)] doi:10.1016/j.physletb.2006.04.003, 10.1016/S0370-2693(02)03130-1 [hep-ph/0210271].
- [72] L. Calibbi and G. Signorelli, Riv. Nuovo Cim. **41**, no. 2, 71 (2018) doi:10.1393/ncr/i2018-10144-0 [arXiv:1709.00294 [hep-ph]].
- [73] S. L. Glashow, J. Iliopoulos and L. Maiani, Phys. Rev. D **2**, 1285 (1970). doi:10.1103/PhysRevD.2.1285
- [74] T. P. Cheng and L. F. Li, Oxford, UK: Clarendon (1984) 536 P. (Oxford Science Publications)
- [75] M. Lindner, M. Platscher and F. S. Queiroz, Phys. Rept. **731**, 1 (2018) doi:10.1016/j.physrep.2017.12.001 [arXiv:1610.06587 [hep-ph]].
- [76] E. Fernandez-Martinez, J. Hernandez-Garcia and J. Lopez-Pavon, JHEP **1608**, 033 (2016) doi:10.1007/JHEP08(2016)033 [arXiv:1605.08774 [hep-ph]].
- [77] M. Tanabashi *et al.* [Particle Data Group], Phys. Rev. D **98**, no. 3, 030001 (2018). doi:10.1103/PhysRevD.98.030001
- [78] A. M. Sirunyan *et al.* [CMS Collaboration], JHEP **1811**, 185 (2018) doi:10.1007/JHEP11(2018)185 [arXiv:1804.02716 [hep-ex]].
- [79] G. Aad *et al.* [ATLAS Collaboration], Phys. Rev. D **101**, no. 1, 012002 (2020) doi:10.1103/PhysRevD.101.012002 [arXiv:1909.02845 [hep-ex]].
- [80] R. A. Diaz, R. Martinez and J. A. Rodriguez, Phys. Rev. D **67**, 075011 (2003) doi:10.1103/PhysRevD.67.075011 [hep-ph/0208117].
- [81] F. Jegerlehner and A. Nyffeler, Phys. Rept. **477**, 1 (2009) doi:10.1016/j.physrep.2009.04.003 [arXiv:0902.3360 [hep-ph]].
- [82] C. Kelso, H. N. Long, R. Martinez and F. S. Queiroz, Phys. Rev. D **90**, no. 11, 113011 (2014) doi:10.1103/PhysRevD.90.113011 [arXiv:1408.6203 [hep-ph]].
- [83] K. Kowalska and E. M. Sessolo, JHEP **1709**, 112 (2017) doi:10.1007/JHEP09(2017)112 [arXiv:1707.00753 [hep-ph]].
- [84] F. Z. Xu, W. Zhang, J. Li and T. Li, Phys. Rev. D **98**, no. 11, 115033 (2018) doi:10.1103/PhysRevD.98.115033 [arXiv:1809.01472 [hep-ph]].
- [85] J. Hernández-Sánchez, C. G. Honorato, S. Moretti and S. Rosado-Navarro, Phys. Rev. D **102**, no. 5, 055008 (2020) doi:10.1103/PhysRevD.102.055008 [arXiv:2003.06263 [hep-ph]].